Kondo Effect in Double Quantum Dots

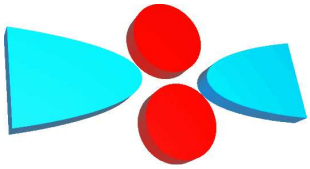

Dissertation zur Erlangung des Doktorgrades
des Fachbereichs Physik der Universität Hamburg

vorgelegt von
Frank Hellmuth
aus Kassel

Hamburg, Juni 2011

Gutachterin/Gutachter der Dissertation:	Dr. Alexander Chudnovskiy Prof. Dr. Michael Potthoff
Gutachterin/Gutachter der Disputation:	Dr. Alexander Chudnovskiy Prof. Dr. Michael Thorwart
Datum der Disputation:	6.7.2011
Vorsitzender des Prüfungsausschusses:	Dr. Georg Steinbrück
Vorsitzender des Promotionsausschusses:	Prof. Dr. Peter Hauschildt
Dekan der Fakultät für Mathematik, Informatik und Naturwissenschaften:	Prof. Dr. Heinrich Graener

Abstract

The analysis of metal-semiconductor-hybrid-systems represents an interesting task, especially the influence of spin and Coulomb interactions on the transport is an important topic, such as for the understanding and development of basic devices for spintronic circuits. Next to other systems, various arrangements of quantum dots have proven to be worthwile toy-systems for the investigation of of the fundamental transport properties of these systems.

In this work a double quantum dot system is investigated: two quantum dots are connected in parallel by tunnel to common source and drain reservoirs. The formation of Kondo correlations affects the physics of the transport through this system significantly. Both, a spin- and an orbital Kondo effect are possible in these systems, where the orbital Kondo effect depends on the existance of an orbital degenerate ground state in the quantum dot system.

The orbital fluctuations then form an SU(2) degree of freedom and thus can be described analogous to the spin by a *pseudo spin*. The fluctuation of this pseudo spin will lead to an increase in the non-resonant transport through the double quantum dot system at low temperatures due to cotunneling processes by the same mechanism as the spin-Kondo-effect. The investigation of the interplay of these two Kondo-effects respectively the impact on the resulting SU(2) vs. SU(4) symmetry and the intermediate regime of the Hamiltonian is the objective of this work, which is organized as follows.

After an introductory chapter that briefly introduces the physical basics of the Kondo effect, the used method of the renormalization group calculations and different manifestations of the Kondo effect in various systems, chapter two begins with the description of the system considered in detail. To describe the orbital Kondo effect, a mixing parameter is defined that describes how strong the different electronic modes in the reservoirs couple to each single quantum dot. In the case of strong fluctuations the common reservoir for both dots breaks into single reservoirs for each dot depending on the electronic mode in the reservoir. This is the SU(4)-point of the system, for which a significantly increased Kondo-temperature, compared to the SU(2)

situation is predicted.

In the other limiting case of perfectly symmetrical coupling to both Quantum dots, the orbital fluctuations are frozen and the orbital Kondo effect thus is suppressed. Only the SU(2) Symmetry of the spin Kondo effect remains. However, since the suppression of the orbital Kondo effect in this situation goes along with a doubling the density of states by the now common reservoir, the Kondo temperature is the same for both symmetry points.

The intermediate regime of the two symmetry points results in a decrease of the Kondo temperature. This is due to the strong destructive effect of the asymmetric mode of the occupation of quantum dots on the transport: These states have, due to their weak coupling, a long lifetime, and the Coulomb blockade suppresses the transport through the strongly coupled symmetric state. Finally, we consider the effect of an external Zeeman field, which suppresses the spin-Kondo effect. In the limit of a strong Zeeman field the transition of a pure spin-Kondo system to a system without Kondo correlations is observed via the mixing parameter.

In the third chapter, the conductivity of the double quantum dot system is determined. The results of these calculations can be interpreted by an interesting comparison to the double slit experiment: the situation of strong fluctuations (separate reservoirs) represents a double slit experiment without interference effects, the symmetrical coupling to the quantum dots a double slit experiment with interference. This behavior can clearly be verified at higher temperatures, and by means of the mixing parameter also intermediate situations can be considered. As we approach the Kondo temperature Kondo correlations more and more take over the dominant role of the transport through the system, resulting in increasing deviations from the double-slit picture. The Kondo temperature itself is not accessible, due to the breakdown of the perturbative approach of these calculations at the Kondo temperature.

Zusammenfassung

Die Untersuchung von Metall-Halbleiter-Hybridsystemen stellt eine interessante Aufgabe dar, insbesondere der Einfluss von Spin- und Ladungswechselwirkung auf den Transport ist ein wichtiges Thema, z.B. bezüglich des Verständnisses und der Entwicklung spintronischer Basiselemente. Neben anderen Systemen haben sich verschiedene Anordnungen von Quantenpunkten als für die Untersuchung der grundlegenden Transporteigenschaften lohnenswerte Modellsysteme herausgestellt.

In dieser Arbeit wird ein Doppelquantenpunktsystem untersucht: Zwei Quantenpunkte sind parallel durch Tunnelbarrieren mit gemeinsamen Source- und Drain-Reservoirs verbunden. Die Ausbildung von Kondo-Korrelationen beeinflußt die Physik des Transports durch diese Systeme wesentlich. Dabei kann es sowohl zur Ausprägung eines Spin- als auch eines orbitalen Kondoeffekts kommen, wenn der Grundzustand des Doppelquantenpunkt-Systems orbital entartet ist.

Die orbitalen Fluktuationen bilden dann einen SU(2)-Freiheitsgrad und können analog zum Spin durch einen *Pseudospin* beschrieben werden und führen, ebenso wie der Spin-Kondoeffekt durch Kotunnelprozesse zu einer Erhöhung des nichtresonanten Transports durch das Doppelquantenpunktsystem bei tiefen Temperaturen. Die Untersuchung des Wechselspiels dieser beiden Kondoeffekte bzw. der Auswirkungen der daraus resultierenden SU(2) vs. SU(4)-Symmetrie des Hamiltonoperators und der Zwischenbereich dieser ist das Ziel dieser Arbeit, die sich wie folgt gliedert.

Nach einem einleitend Kapitel, daß kurz die physikalischen Grundlagen des Kondoeffekts, die verwendete Methode der Renormierungs-Rechnungen und Manifestationen des Kondoeffekts in verschiedenen Systemen vorstellt, wird in Kapitel Zwei zunächst das konkret betrachtete System genauer erläutert. Zur Beschreibung des orbitalen Kondoeffekts wird ein Mischungsparamter definiert, der beschreibt wie stark die jeweiligen elektronischen Moden in den Reservoiren an einzelnen Quantenpunkte koppeln. Für den Fall starker orbitaler Fluktuationen zerfällt das gemeinsame Reservior in zwei getrennte Reservoirs die, je nach Mode, an nur einen der Quantenpunkte koppeln. Dies

ist der SU(4)-Punkt des Systems, für den eine stark erhöhte Kondotemperatur gegenüber der SU(2)-Situation erwartet wird.

Im anderen Grenzfall vollkommen symmetrischer Kopplung an beide Quantenpunkte, sind die orbitalen Fluktuationen eingefroren und der orbitale Kondoeffekt somit unterdrückt, es bleibt lediglich die SU(2) Symmetrie des Spin Kondoeffekts erhalten. Da jedoch die Unterdrückung des orbitalen Kondoeffekts in dieser Situation mit einer Verdoppelung der Zustandsdichte durch die nun gemeinsamen Reservoirs einhergeht, ergibt sich eine gleiche Kondotemperatur für beide Symmetriepunkte.

Zwischen den beiden Symmetriepunkten ergibt sich ein Abfall der Kondotemperatur. Dieser resultiert aus der starken destruktiven Wirkung der asymmetrischen Mode der Besetzung der Quantenpunkte für den Transport: Diese Zustände haben, aufgrund ihrer schwachen Kopplung, eine lange Lebenszeit und blockieren durch die Coulombblockade den Transport durch den stark koppelnden symmetrischen Zustand. Abschließend der Effekt eines externen Zeemann-Feldes betrachtet, welches den Spin-Kondoeffekt unterdrückt. Hier kann im Grenzfall eines starken Zemannfeldes bei Variation des Mischungsparametes der Übergang eines reinen Spin-Kondosystems zu einem System ohne Kondokorrelationen beobachtet werden.

Im dritten Kapitel wird die Leitfähigkeit des Doppelquantenpunktsystems bestimmt. Die Ergebnisse dieser Rechnungen lassen einen interessanten Vergleich zum Doppelspaltexperiment zu: Die Situation starker Fluktuation (getrennter Reservoirs) entspricht einem Doppelspaltexperiment ohne Interferenzeffekte, die der symmetrischen Kopplung an die Quantenpunkte der des Doppelspaltexperiments mit Interferenz. Dieses Verhalten läßt sich bei höheren Temperaturen eindeutig verifizieren, wobei mittels des Mischungsparameters auch intermediäre Situationen betrachtet werden können. Mit zunehmder Annäherung an die Kondotemperatur übernehmen die Kondokorrelationen immer mehr die dominante Rolle für den Transport durch das System, so daß sich immer stärkere Abweichungen vom Doppelspalt-Bild ergeben, wobei die Kondotemperatur selber durch den störungstheoretischen Ansatz dieser Rechnungen nicht erreicht werden kann.

Publikation

Teile dieser Dissertation sind bereits in folgendem Artikel veröffentlicht worden:

Publications

Parts of this thesis are already published in the following paper:

Alexander Chudnovskiy, Frank Hellmuth, and Victor Kagalovsky, *From spin and orbital SU(4) to spin SU(2) Kondo effect in double quantum dot*, HAIT Journal of Science and Engineering A **5**, 1–2, 93–111, 2008

Contents

Chapter 1

Introduction

The Kondo effect, in which the electronic state is modulated by magnetic impurities, has been the subject of many theoretical and experimental analyses since its first observation in the 1930s, where de Haas et al. found at low temperatures an unexpected non-linear increase in the resistivity with decreasing temperature in their experiments on metals containing diluted magnetic impurities [1]. Fig. 1.1 shows de Haas' original experimental data for different concentrations of iron in gold. An important characteristic of the measured increase in resistance is the logarithmic temperature dependence: $\rho \propto \ln 1/T$. A conventional theory of conductivity of metals would predict a decrease of resistance with temperature or a saturation due to defects in the lattice of the conductor.

The effect is named after Jun Kondo, who, in 1964, gave the first theoretical explanation of this effect in his work about the scattering of conduction electrons by diluted magnetic impurities [2]. Kondo assumed phenomenologically motivated a Hamiltonian for the low energy sector of the system, consisting of a part describing the electronic states in the conduction band of the metal and their exchange interaction with the magnetic impurity

$$H_{\mathrm{K}} = H_{\mathrm{metal}} + J(\mathbf{s} \cdot \mathbf{S}) \tag{1.1}$$

with $\mathbf{s}$ the spin density in the metal, $\mathbf{S}$ the spin operator of the impurity and J the coupling strength of the interaction.

In an earlier work Anderson modeled in 1961 the magnetic impurity as a localized quantum state in a metal using the Hamiltonian

$$H_{\mathrm{A}} = H_{\mathrm{metal}} + H_{\mathrm{imp}} + H_{\mathrm{T}}$$

where H_{metal}, H_{imp} and H_{T} respectively describes the conduction band of the metal, the electrons in the impurity and the tunneling processes between the

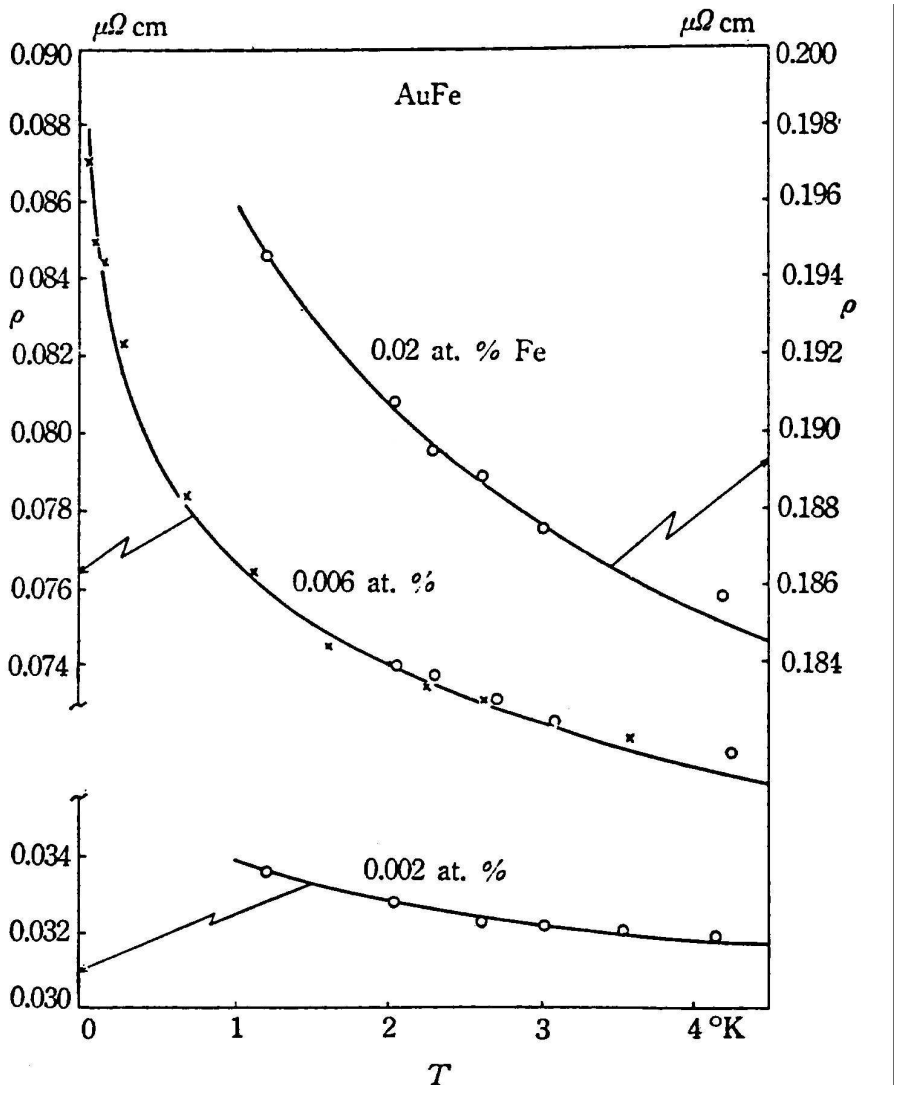

Figure 1.1: First experimental data of the Kondo effect by de Haas *et al.* [1]. Metal alloys with diluted magnetic impurities show an increase in resistivity with decreasing temperature, the amount of the increase depends on the concentration of the magnetic impurities

metal and the impurity [3]. In 1966 Schrieffer and Wolf demonstrated the equivalence of Anderson's and Kondo's models for the low energy sector and gave an explicit unitary transformation between them [4].

In 1970 Anderson introduced the idea of *scaling* into the theoretical framework of the Kondo physics [5]. This idea means that it is possible to map a physical system onto a reduced version of itself by integrating out high energy contributions. Iterating this process results in *flow equations* for the physical quantities, which still is one of the most used methods for theoretical calculations on Kondo problems today.

1.1 The Kondo effect

The basic mechanism of the Kondo effect is that the electron in the impurity can lower its energy by pairing with a delocalized electron of opposite spin of the surrounding metal, thereby building a singlet state [6]. This leads to an enhanced scattering of electrons at the impurity and therefore to an enhanced resistivity. As the binding energy of such a paired state is small compared to the thermal energy of the electrons, this effect just becomes visible for small temperatures, but becomes the dominant effect if the system is cooled down below a certain temperature T_K, the so called *Kondo temperature*.

Progresses in experimental nanotechnological methods enable physicists to realize different setups of the Kondo scenario: a localized magnetic atom in contact with a metallic environment. Thanks to new techniques it is possible to build nano structures, in which electron movement is confined to two, one or zero dimensions. A zero dimensional quantum system is called a *quantum dot* or an artificial atom, because of its similarities in the electronic structure to the quantized energy levels of an atom. Hence such a quantum dot can play the role of the magnetic impurity in the Kondo scenario.

In 1998 the groups of Goldhaber-Gordon and Kouwenhoven both verified the Kondo effect in a single electron transistor, using a quantum dot as an artificial magnetic impurity [7,8]. The schematic setup of such an experiment to measure the conductivity through a quantum dot is shown in Fig. 1.2. A quantum dot is connected via tunneling junctions to metallic source and drain reservoirs, to which a source-drain voltage V_{sd} can be applied. With an additional gate voltage V_g all energy levels in the dot can be simultaneously shifted.

In contrast to the increase in resistivity with decreasing temperature in experiments in three dimensional metals, the Kondo effect manifests in these experiments as an *increase* in the conductivity. The basic reason for this qualitative difference is that the same mechanism produces enhanced scattering

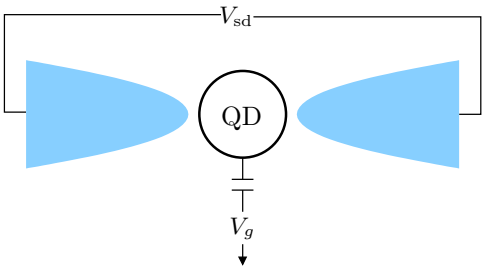

Figure 1.2: Experimental setup: A quantum dot is connected to a source and a drain reservoir via tunneling contacts. A source-drain voltage V_{sd} and a gate voltage V_g can be applied.

in the case of the three dimensional metals, but enhanced transport due to extended wave functions in the case of the tunneling junction contacted quantum dot.

Due to the possibility to tailor the parameters of these artificial atoms over a wide range, the quantum dots are excellent systems to study the many particle phenomena of todays condensed matter physics.

1.1.1 Transport Channels and Coulomb blockade

To understand how an electron can tunnel sequentially from the source reservoir to the dot and finally from the dot to the drain reservoir to give rise to a finite conductivity through the dot, let's assume that N electrons are on the dot and have a ground state energy of $E(N)$. Adding another electron to the dot will cost an additional charging energy $Q = E(N+1) - E(N)$ due to Coulomb interaction with the electrons already in the dot[1], see Fig. 1.3(b). The energy spectrum of the dot therefore is a ladder of energy levels separated by gaps of width Q.

It is important to note that all these energy levels are not single electron energy levels, but those of transitions between different states or occupation numbers in the dot. In this case the energy to change the occupation of the dot by one from N to $N+1$. These discrete levels are also called *transport channels*, because an electron tunneling through the dot has to go through one of them to contribute to the current.

Transport is only possible if a transport channel lays in the region between the Fermi energies of the left and the right Fermi reservoirs. This region is also called the *transport window*. In this case the transition $N \rightarrow N+1$ is possible and the number of electrons in the dot can fluctuate, allowing electrons to tunnel into and out of the dot, contributing to a non vanishing current through the dot. In the case of equal Fermi energies in the reservoirs

[1] strictly speaking this is only true for metallic dots, as only in these the one particle contribution is neglectable

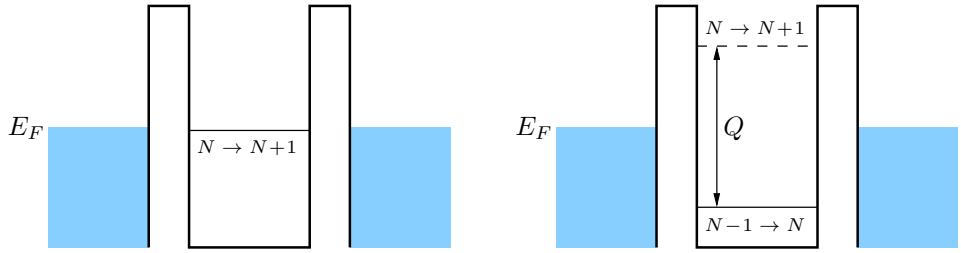

(a) transport channel in resonance (b) Coulomb blockade

Figure 1.3: Energetic situation of a quantum dot in tunneling contact with metallic reservoirs

(vanishing transport voltage V_{sd}) that means one of the transport channels has to be in resonance with the Fermi energy of that reservoirs. This situation is shown in Fig. 1.3(a).

The situation depicted in Fig. 1.3(b) is a situation where no transport is possible. The $N \to N+1$ transport channel is energetically unreachable for the electrons in the reservoir, and also a tunneling process out of the dot is impossible since there are no free states in the reservoir for the $N-1 \to N$ process. This suppression of current through the dot is called *Coulomb blockade*.

It is possible to tune the energy levels in the dot via a gate voltage V_g. Applying a gate voltage results in a simultaneous energetic shift of all levels in the dot to lower, respectively higher energies. Assuming equal Fermi energies in the reservoirs, sweeping the gate voltages from higher to lower values will therefore fill the dot one by one with electrons, when a transition energy level $E(N) \to E(N+1)$ crosses the Fermi energy of the reservoirs. In this moment transport through the dot is possible. When no transport channel is in resonance with the Fermi energies of the reservoirs, transport is suppressed by the Coulomb blockade. Measuring the differential conductivity versus the gate voltage exhibits peaks for the resonances separated by so called *Coulomb valleys*, resulting from the dot being in Coulomb blockade. This typical behavior is sketched in Fig. 1.4.

1.1.2 Spin Flip Co-Tunneling

The simple picture of the conductivity through a quantum dot experiences a drastic change when the Kondo effect plays the dominant role. At gate voltages, where previously the Coulomb blockade suppressed the conductivity,

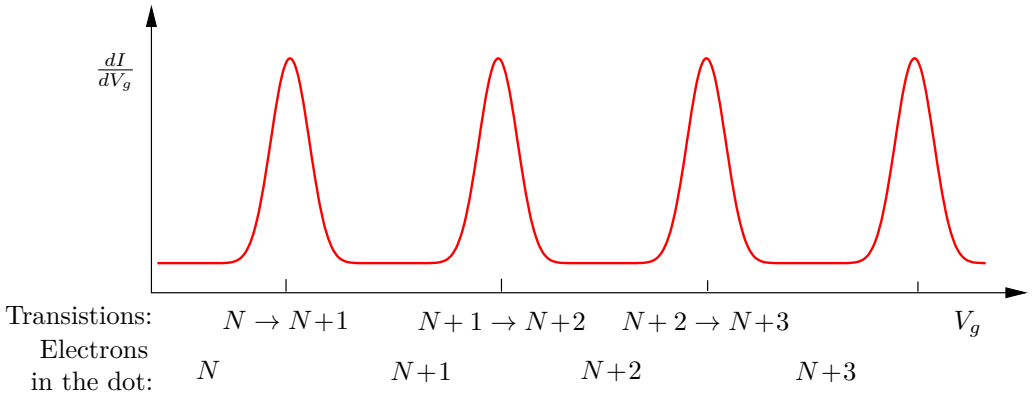

Figure 1.4: Differential conductivity through a quantum dot connected to reservoirs with equal Fermi energies: Peaks from the resonant tunneling are separated by Coulomb valleys.

so called *Kondo plateaus* arise with falling temperature, reverting the situation to its opposite: The conductivity reaches for very low temperatures its unitary limit of $2e^2/h$ and therewith doubling the value for a single resonant transport channel.

But these Kondo plateaus only appear for odd occupations of the quantum dot with electrons. For even occupations the conductivity follows the expected behavior of getting smaller with falling temperatures. See Fig. 1.5 for an illustration of this typical fingerprint of the Kondo effect.

The reason of this even-odd pattern in the $G - V_g$ diagram is the spin of the highest occupied state of the dot: If this state has a remaining spin of 1/2, correlations between the spin of the dot and a spin in the reservoirs will result in building a singlet state with a lowered energy. This extended state, involving an electron in the dot and in the reservoir leads to enhanced transport through the dot and is the basic mechanism of the Kondo effect. It will be discussed in more details in the following.

Although the dot is in Coulomb blockade for first order processes, transport through the dot is still possible via co-tunneling processes of higher order, in which electrons tunnel through the dot by means of a virtual state as illustrated in Fig. 1.6. As a result of a single co-tunneling process the spin in the dot and in the reservoir will be flipped. Conservation of energy demands equal energies before and after the co-tunneling process and therefore spin degenerate states in the dot and in the reservoirs.

The superposition of all these spin flip co-tunneling processes results in a correlated spin singlet state between the localized spin state and the electrons

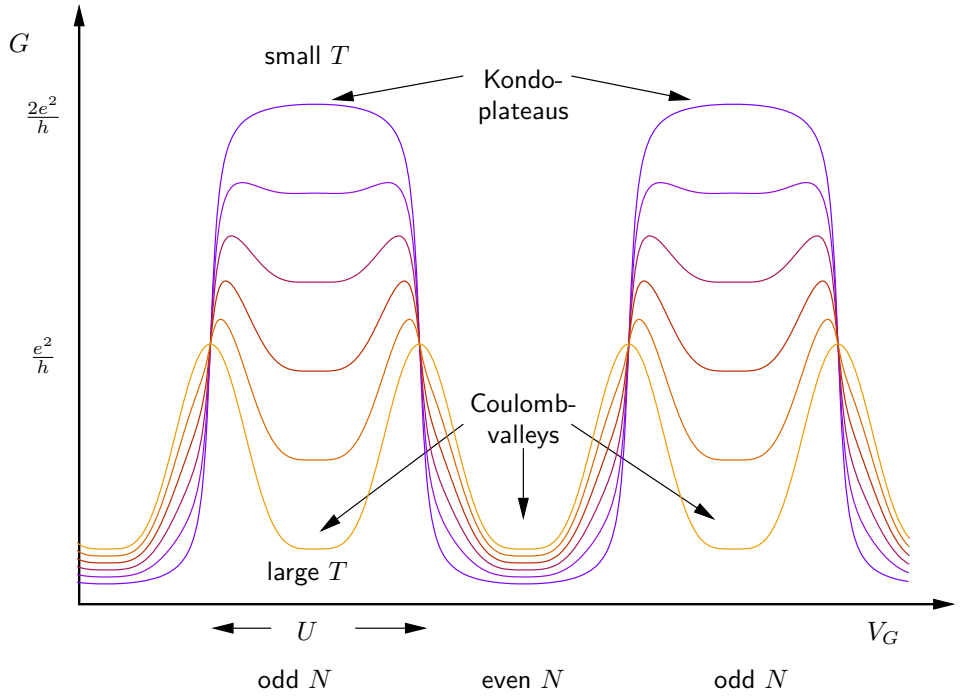

Figure 1.5: Characteristic even-odd pattern of the Kondo effect in the G-V_G diagram. Only when the localized system is occupied with an odd number of electrons, resulting in a remaining spin of $\pm 1/2$, the Coulomb valleys evolve to Kondo plateaus with decreasing temperature. These Kondo plateaus reach the conductivity of $2e^2/h$ in the unitary limit and are separated by a Coulomb valley with the width of the charging energy U.

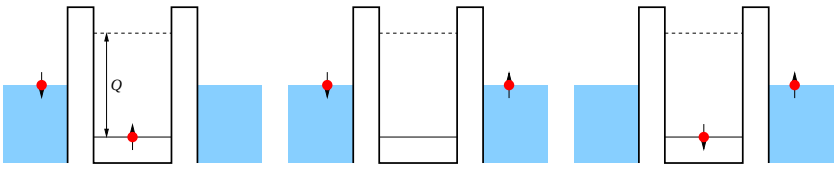

Figure 1.6: Spin flip co-tunneling through a quantum dot in the Kondo regime. Left: initial state, middle: virtual state, right: final state. Due to the Coulomb interaction energy Q the dot is blocked for transport processes in first order. But the electrons can still co-tunnel through a virtual state through the dot, leaving the spin in the dot flipped

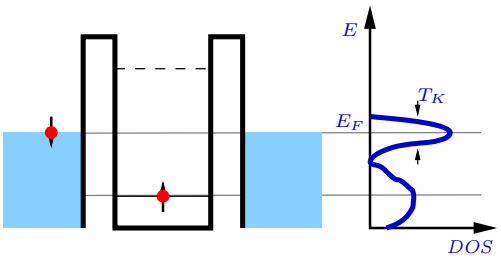

Figure 1.7: Kondo resonance in the DOS. The superposition of all tunneling processes manifests itself a sharp peak of the virtual state in the density of states exactly at the Fermi level. The width of this peak T_K determines the energy scale of the Kondo regime.

in the reservoirs. This state enhances the transport through the dot, in the unitary limit up to a fully open transport channel. This makes the Kondo effect one of the few examples in physics where higher order processes completely govern the physical properties of a system and first order perturbative descriptions completely fail.

In the density of states (DOS) picture the Kondo effect appears as a sharp resonance in the DOS of the dot exactly at the Fermi level of the reservoirs resulting from the virtual state, as sketched in Fig. 1.7. The width of the peak gives the energy scale on which the Kondo effect plays the dominant role in the behavior of the system. It is usually given in terms of a temperature T_K which is called the *Kondo temperature*.

1.2 Perturbative Calculations

We follow Abrikosov [9] to give a basic perturbative treatment of the Kondo problem. The scattering amplitude of the Kondo Hamiltonian (1.1) in first order approximation is simply

$$A^{(1)} = J(\mathbf{s} \cdot \mathbf{S})_{\sigma\sigma'}, \tag{1.2}$$

where σ and σ' are the initial and final orientation of the electron spin.

Now let us assume an electron getting scattered from a initial state $\mathbf{p}\sigma$ (where $\mathbf{p}$ denotes its momentum and σ its spin) to a final state $\mathbf{p}'\sigma'$ through an intermediate state $\mathbf{p}_1\sigma_1$. We have two possibilities for this to happen.

1. The electron first gets scattered into the intermediate state $\mathbf{p}\sigma \to \mathbf{p}_1\sigma_1$ and then to the final state $\mathbf{p}_1\sigma_1 \to \mathbf{p}'\sigma'$. To calculate the scattering amplitude for this process we have to respect that the intermediate state has to be unoccupied by a factor $1-f(\mathbf{p}_1)$, where $f(\mathbf{p})$ is the Fermi distribution function. Taking the sum over all intermediate states we have

$$A_1^{(2)} = J^2 \sum \sigma_1 \int \frac{(\mathbf{s}\cdot\mathbf{S})_{\sigma'\sigma_1}(\mathbf{s}\cdot\mathbf{S})_{\sigma_1\sigma}(1-f(\mathbf{p}_1))}{\epsilon(\mathbf{p})-\epsilon(\mathbf{p}_1)} \frac{d^3\mathbf{p}_1}{(2\pi\hbar)^3} \tag{1.3}$$

   for the scattering amplitude.

2. An electron from the already occupied intermediate state could get scattered into the final state $\mathbf{p}_1\sigma_1 \to \mathbf{p}'\sigma'$ and the initial electron fills up the now free intermediate state $\mathbf{p}\sigma \to \mathbf{p}_1\sigma_1$. The scattering amplitude for this process is given by

$$A_2^{(2)} = -J^2 \sum \sigma_1 \int \frac{(\mathbf{s}\cdot\mathbf{S})_{\sigma_1\sigma}(\mathbf{s}\cdot\mathbf{S})_{\sigma'\sigma_1} f(\mathbf{p}_1)}{\epsilon(\mathbf{p}_1)-\epsilon(\mathbf{p}')} \frac{d^3\mathbf{p}_1}{(2\pi\hbar)^3}. \tag{1.4}$$

   The minus sign takes the asymmetry of the electronic wave function into account as the particles are permutated with reference to (1.3).

Since we assume elastic scattering, we have

$$\epsilon(\mathbf{p}) = \epsilon(\mathbf{p}'). \tag{1.5}$$

Using the commutator and eigenvalue relations for the spin operators, we get

$$(\mathbf{s}\cdot\mathbf{S})(\mathbf{s}\cdot\mathbf{S}) = S(S+1) - (\mathbf{s}\cdot\mathbf{S}) \tag{1.6}$$

$$\sum_{i,k} \sigma^i \sigma^k S^k S^i = S(S+1) + (\mathbf{s}\cdot\mathbf{S}). \tag{1.7}$$

With (1.5)–(1.7) scattering amplitudes (1.3) and (1.4) can be written as

$$A^{(2)} = A_1^{(2)} + A_2^{(2)} = J^2 \int \left\{ \frac{S(S+1)\delta_{\sigma'\sigma}}{\epsilon(\mathbf{p})-\epsilon(\mathbf{p}_1)} + \frac{2f(\mathbf{p}_1)-1}{\epsilon(\mathbf{p})-\epsilon(\mathbf{p}_1)} (\mathbf{s}\cdot\mathbf{S})_{\sigma'\sigma} \right\} \frac{d^3\mathbf{p}_1}{(2\pi\hbar)^3}.$$

Replacing the energies $\epsilon(\mathbf{p})$ and $\epsilon(\mathbf{p}_1)$ by their relative value to the Fermi energy $\xi(\mathbf{p}) = \epsilon(\mathbf{p}) - \mu$ and noting that $f(\mathbf{p}_1)$ only depends on ξ_1 gives

$$A^{(2)} = J^2 \int \left\{ \frac{S(S+1)}{\xi-\xi_1}\delta_{\sigma'\sigma} + \frac{2f(\xi_1)-1}{\xi-\xi_1} (\mathbf{s}\cdot\mathbf{S})_{\sigma'\sigma} \right\} \frac{\nu(\epsilon)}{2} d\xi_1, \tag{1.8}$$

where $\nu(\epsilon)$ is the density of states which is considered constant $\nu(\mu)$ in the vicinity of the Fermi energy $\epsilon \approx \mu$.

The first term in the integrand of (1.8) gives upon integration over ξ_1 a value of order ξ/μ, which can be neglected, when we are interested in electrons in the vicinity of the Fermi energy.

The second term is antisymmetric with respect to ξ_1, as

$$2f(\xi_1) - 1 = -\tanh\left(\frac{\xi_1}{2T}\right).$$

Taking the limits of the integral in the order of $\pm\mu$ and exploiting the asymmetry of the integrand the integral in (1.8) can be rewritten as

$$\begin{aligned}\int_{-\mu}^{\mu} \frac{2f(\xi_1)-1}{\xi-\xi_1} d\xi_1 &= \int_0^{\mu} (2f(\xi_1)-1)\left(\frac{1}{\xi-\xi_1} - \frac{1}{\xi+\xi_1}\right) d\xi_1 \\ &= \int_0^{\mu} (2f(\xi_1)-1)\frac{2\xi_1}{\xi^2-\xi_1^2} d\xi_1. \end{aligned} \tag{1.9}$$

For $\xi_1 \gg |\xi|$, the ξ^2 in the denominator of (1.9) may be ignored. For also $\xi_1 \gg T$ the Fermi distribution $f(\xi_1)$ vanishes and the integral becomes logarithmic. The logarithmic integral subsequently justifies the choice of the limits as $\pm\mu$, as for logarithmic integrals it is sufficient to know just the order of their limits. So we can evaluate (1.9) to

$$2\ln\left(\frac{\mu}{\max(|\xi|, T)}\right).$$

The contribution of the second Born approximation to the scattering amplitude is therefore given by

$$\nu J^2 (\mathbf{s}\cdot\mathbf{S})_{\sigma'\sigma} \ln\left(\frac{\mu}{\max(|\xi|, T)}\right).$$

Adding this to the first Born approximation (1.2) we end up with

$$J(\mathbf{s}\cdot\mathbf{S})_{\sigma'\sigma}\left[1 + \nu J \ln\left(\frac{\mu}{\max(|\xi|, T)}\right)\right].$$

Since for the physical description of the system electrons with energies $|\xi| \approx T$ are most interesting, we drop the case discrimination $\max(|\xi|, T)$ in the argument of the logarithm.

The resistance depends on the square of the scattering amplitude. Within the adopted accuracy we find a correction due to the scattering in first and second Born approximation of

$$\delta\rho \propto 1 + 2\nu J \ln\left(\frac{\mu}{T}\right).$$

It turns out that all higher orders of perturbation theory contain powers of that logarithmic dependency and summing them up results in a geometric series [10]

$$\delta\rho \propto \left\{\sum_{n=0}^{\infty}(\nu J)^n \left[\nu J \ln\left(\frac{\mu}{T}\right)\right]^{n-1}\right\}^2 = \left[\frac{\nu J}{1-\nu J \ln(\mu/T)}\right]^2 \tag{1.10}$$

Eq. (1.10) has a logarithmic divergence when T approaches the Kondo temperature

$$T_K = \mu e^{-\frac{1}{\nu J}}. \tag{1.11}$$

which signals the breakdown of perturbation theory. Due to the many body character of the Kondo effect, the coupling of the localized spin with the electrons in the reservoir is not a small perturbation anymore.

1.3 Anderson's Poor Man Scaling

In (1.9) we introduced the band width μ as a cutoff for the energy integration, resulting in a logarithmic dependency on the band width in the result (1.10). As these terms do not vanish for $\mu \to \infty$, this implies the importance of high energy excitations (e.g. those with energies close to the band width) in the Kondo problem. They can't be neglected and have to be taken into account, for which the *scaling approach* provides an elegant solution.

The basic principle of a scaling [5,11] theory is, as said in the beginning, to map a system onto a reduced version of itself by integrating out high energy contributions beginning from a cutoff energy. The cutoff may be given for example by the band width of the system. Of course the new, energetically reduced system will have different and even newly generated couplings. In this case it is necessary to rewrite the Hamiltonian in an invariant form for scaling purposes to get the relation between the old and the new coupling constants. These relations are called the *flow equations*. Analyzing them for fix points, invariants or divergences will reveal important physical properties of the studied system.

Let us illustrate this method by the analysis of the Kondo effect: Beginning with the coupling term of the Hamiltonian for the SU(2) spin 1/2 Kondo

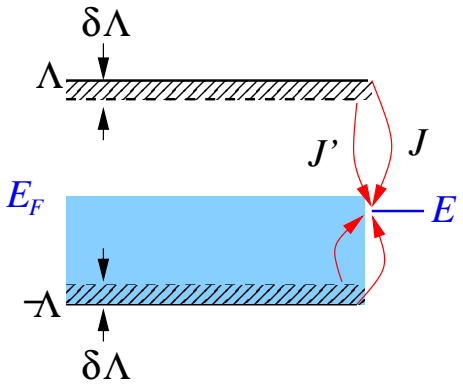

Figure 1.8: Principle of the scaling: Integrating out high energy shells from $-\Lambda$ to $-\Lambda + \delta\Lambda$ and $\Lambda - \delta\Lambda$ to Λ (hatched areas) has to be reflected in renormalizing the coupling constants $J \to J'$

effect (1.1),

$$H_K = J\,(\mathbf{s}\cdot\mathbf{S})$$

the reduced system is described by a new Hamiltonian

$$H'_K = H_K + \delta H_K$$

where δH_K incorporates the corrections that emerge when integrating out a high energy shell as sketched in Fig. 1.8. Carrying out the calculations for scattering processes in the high energy shell in the first non vanishing order in J gives the correction to the Kondo Hamiltonian in the form

$$\delta H_K = -\nu J^2 \frac{\delta\Lambda}{\Lambda}\,(\mathbf{s}\cdot\mathbf{S})\,. \tag{1.12}$$

The new Hamiltonian obviously has the same structure as the original one, no new interactions are generated so it is already in it's invariant form. Just the coupling constant has to be replaced by a new one

$$J \to J + \delta J$$

with

$$\delta J = -\nu J^2 \frac{\delta\Lambda}{\Lambda}. \tag{1.13}$$

Substituting J by $J + \delta J$ is called *renormalization* of the coupling constant. For infinitely small energy shells $\delta\Lambda$ becomes $d\Lambda$ in (1.13) and we get (respecting the logarithmic derivative on the right hand side of (1.13)) the flow equation for the coupling constant

$$\frac{dJ}{d\ln(\nu\Lambda)} = -\nu J^2 \tag{1.14}$$

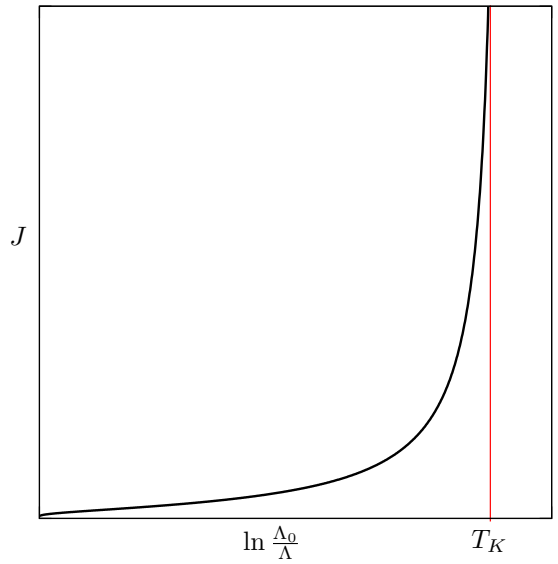

Figure 1.9: Flow of the coupling constant J during the scaling as a function of the reduced band width Λ of the system. As J approaches T_K a logarithmic divergence in J appears.

Integrating the flow equation from an initial band width Λ_0 and coupling constant J_0 gives

$$J = \frac{J_0}{1 - J_0 \nu \ln(\Lambda_0/\Lambda)}. \tag{1.15}$$

Also in the scaling calculation the Kondo temperature marks the end of the validity of the results, as the coupling constant diverges when Λ reaches T_K.

It may be worth noting, that the expression

$$T_K = \Lambda e^{-\frac{1}{\nu J}}$$

is a constant during the scaling, where $J = J(\Lambda)$ as given by 1.15. Values with this property are called *scaling invariants*. This underlines the role of the Kondo temperature as the important energy scale for the Kondo effect. Systems characterized by the same $T_K(J, \nu)$ lay on the same trajectories and show therefore the same low energy behavior.

In summary the scaling method provides a way to include contributions of high energy processes in first order calculations by summing them up leading to new coupling constants J for a system with reduced bandwidth, characterized by the energy scale T_K. Higher order contributions could be taken into account, but it turns out that are irrelevant as these behave like $1/\Lambda$ rather then $\ln \Lambda$ and therefore are neglectable for the high energy region.

This remapping of the system on itself comes to an end when the band width of the new system becomes of the order T_K, which corresponds to the breakdown of the perturbative approach: The assumption of a small pertur-

bation isn't justifiable anymore in this case, which is reflected by diverging coupling constants in the scaling[2].

1.4 Realizations of the Kondo Effect

Goldhaber-Gordon [7] and Kouwenhoven [8] both experimentally verified the predictions of the Kondo model on quantum dots made of GaAs/GaAlAs heterostructures. They measured the zero bias conductance through a dot in dependence of the gate voltage. Varying the gate voltage results in adding or removing an electron to the dot, as the energy spectrum of the dot gets shifted. The conductance shows coulomb peaks, which arise when a transport channel is in resonance with the reservoirs. The measured peaks formed pairs separated by valleys, which reflect the odd or even number of electrons in the dot. The peaks became better resolved with increasing temperature from 90 mK to 400 mK, suggesting that the range of increased conductivity between the pairs of peaks results from a Kondo resonance.

In a similar way Nygard [12] could show the Kondo effect using carbon nanotubes. These Kondo systems differ in several ways from the quantum dots. Carbon nanotubes show a discrete spectrum like the quantum dots but are geometrically 2D systems. In contrast to electrostatically defined semiconductor quantum dots the carbon nano tubes are geometrically fixed. While geometry and contact transmission probabilities of semiconductor quantum dots depend on the gate voltages these properties are fixed geometrical qualities for carbon nano tubes. These Kondo systems thus enabled the observation over a wider range of V_G, making several hundred Coulomb oscillations experimentally accessible. The latter enabled measurements on Kondo systems with very high occupation numbers and the conductivity to be driven almost to it's theoretical maximum, the unitary limit. An example of the results of such an experiment is shown in Fig. 1.10.

The Kondo effect has also been observed in single molecule transistors, where divanadium molecules play the role of the magnetic impurity [13], see Fig. 1.11. These systems show very high Kondo temperatures, but the underlying physics is more complicated. The orbital degrees of freedom play a role here, as discussed later in this section.

A crucial prerequisite for the Kondo effect is the existence of a degenerate state in the localized system. In the above mentioned systems this degeneracy is related to the occupation of the highest occupied orbital. A single electron in this state leads to a degeneracy with respect to the possible spin

[2]For ferromagnetic systems the scaling can be continued down to $\Lambda \to 0$ giving $J \to 0$. The impurity spin becomes uncoupled and asymptotically free.

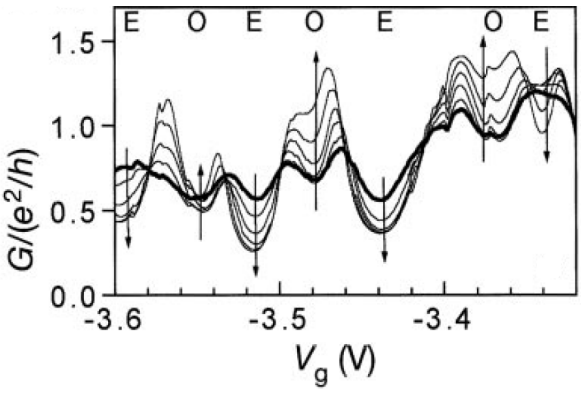

Figure 1.10: Experimental results of conductivity measurements of a carbon nano tube at different temperatures. E and O indicate even and odd numbers of electrons in the nano tube, arrows indicate the direction of the change with decreasing temperature. For high temperatures the Coulomb oscillations are visible. With decreasing temperatures the Coulomb valleys for odd numbers of electrons evolve into Kondo plateaus, those for even numbers deepen. From [12], compare Fig. 1.5

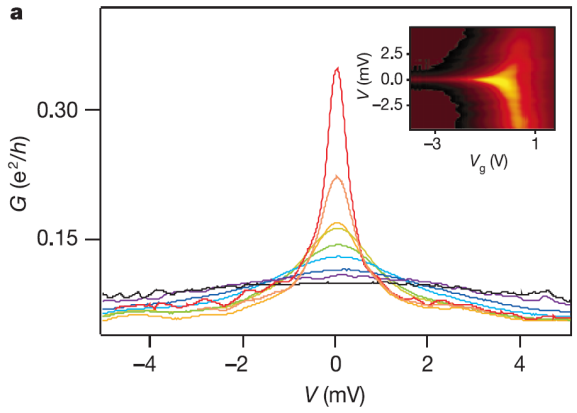

Figure 1.11: Experimental results of conductivity measurements of a single molecule transistor at different temperatures. This graph shows V_{sd} vs. G at V_g fixed in a Coulomb valley. With decreasing temperatures the Kondo peak arises at zero bias between source and drain. From [13]

orientations. A double occupation of the highest occupied orbital, forming a spinless singlet state of the highest occupied orbital obviously shows no degeneracy regarding the spin orientations. If the occupation number in the localized system can be varied with a gate voltage V_g, this change from the spin $\pm 1/2$ to a spinless ground state of the localized system leads to the well known even-odd pattern in the dI/dV_g characteristics of the Kondo effect as shown in Fig. 1.10 and schematically illustrated in Fig. 1.5.

But experimental results also show the typical zero bias resonance with logarithmic T dependency, resulting from the enhanced density of states at the Fermi energy in the Kondo effect for quantum dots with *even* occupation numbers [14]. Here it is not a single electron but a two electron ground state that is the key for understanding the Kondo physics. Two electrons can form a singlet or a triplet state. With these states again possible degeneracies can be constructed that generate a Kondo effect:

- First, the triplet could be split up energetically using a magnetic field. The Zeeman energy can bring one of the components of the triplet into resonance with the singlet state [15]. This gives rise to a $S = 1/2$ Kondo effect.

- Second, the singlet state can be brought into resonance with a threefold degenerate triplet state via magnetic fields in a way that the triplet state is still nearly degenerate. A fourfold degeneracy arises and all four states contribute to the Kondo effect, this situation will be discussed later in details[3].

Eto and Nazarov gave theoretical calculations for the enhancement of the Kondo effect due to competition between singlet and triplet states and its dependency on the energy differences between them for both limiting cases [16].

1.4.1 Spinless Kondo Effects

Spin degeneracy is not the only way to realize the Kondo scenario, and actually other kinds of degeneracy can also cause a Kondo effect and can be treated theoretically in a similar way as the spin Kondo effect. U. Wilhelm et al. demonstrated such a spinless Kondo system by using two vertically stacked quantum dots [17]. In this system the spin degeneracy of the original Kondo effect is replaced by the orbital degeneracy of the double quantum

[3]Because of the $s = 1/2$ degeneracy of the spins in the reservoirs the localized spin can not get fully screened, this is called an *under-screened* Kondo effect

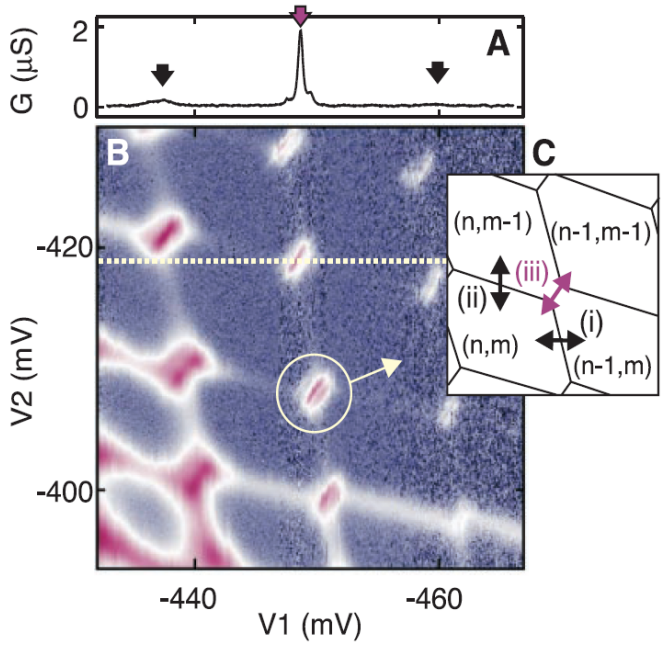

Figure 1.12: Charging diagram of a double quantum dot system for small fixed source drain voltage with the characteristical Coulomb diamonds. V_1 and V_2 are the gate voltages for dot 1 resp. 2. Inside the hexagonal Coulomb diamonds the transport is blocked through Coulomb blockade, along the lines one electron is transferred into one of the dots and the total occupation number changes by one. In the red marked region one electron is transferred from one dot to the other without any energy costs

dot system: The states, which differ in the occupation numbers of the dots by one, as $(n, m-1)$ and $(n-1, m)$, are energetically degenerate. That means an electron can be transferred from one dot to the other without any energy costs (Fig. 1.12). Capacitive coupling of the dots separates these states energetically from those with different total occupation numbers, so that the system can be described in terms of a pseudo spin. Pseudo spin up means an electron in the upper dot and pseudo spin down an electron in the lower dot. Consequently the low energy sector of these systems is described by a Hamiltonian obeying the SU(2) symmetry, like ordinary spin systems. A very similar system will be the subject of this thesis.

Another spinless Kondo system can be realized using carbon nano tubes. An orbital degree of freedom will also take the role of the degenerate ground state here. It is easy to see from the cylindrical geometry of the nano tubes that electrons rotating clockwise or anticlockwise with the same angular momentum are degenerate. The obvious choice of using these states as a basis

of a Kondo effect will be discussed in the next paragraph. Their fourfold degeneracy according to spin and orbit needs a more subtle analysis. Beside from this it is also possible to use a parallel magnetic field to create a crossing of states with the same spin polarization. These twofold degenerate states create a purely orbital Kondo effect, since spin flip would break the degeneracy of the states, as experimentally verified in [18].

1.4.2 SU(4) Kondo Effects

In these orbital Kondo systems both spin and orbital degeneracies of the electrons are possible. The Kondo effects in the spin and orbital sector develop independently and are characterized by different Kondo temperatures T_K^{Spin} and T_K^{Orbit} [19, 20]. In the special case that these two energy scales coincide, a greatly enhanced Kondo temperature has been predicted and experimentally observed in carbon nanotubes [18, 21, 22]. Also the limiting cases of SU(2) and SU(4) Kondo effects have been investigated and a four-peak splitting in the non-linear conductance in the SU(4) point in presence of an axial magnetic field has been predicted [23].

Concerning quantum dot systems, the double dot systems are obvious candidates to show a SU(4) Kondo effect. There are different geometrical setups for such a configuration. In [22] the dots are attached to separate leads in serial geometry. Another possible geometry for the double dot system are parallel dots. Pseudo-spin correlations have been detected in such a geometry [24, 25]. In [26] such a device is used as a Aharonov Bohm interferometer to investigate the transition form an SU(2) Kondo effect to an SU(2) Kondo effect due to ground state crossing. A similar geometry of a double dot system connected in parallel to the leads will be described in detail in the next chapter.

Chapter 2

Renormalization Group Analysis of the Double Dot System

2.1 Setup

In this thesis a double dot system will be considered, in which two single level quantum dots are coupled in parallel via tunnel junctions to two reservoirs. The quantum dots are coupled capacitively to separate gate electrodes, so that the occupation numbers of the dots and the position of the energy levels can be controlled via gate voltages V_1 and V_2. A transport voltage V_{sd} can be applied to the source (left) and the drain (right) reservoir (see Fig. 2.1 A, from [24]). An experimental realization of such a setup can be seen in Fig. 2.1 B. The Hamiltonian of this system consists of three terms, describing the isolated quantum dots including their inter-dot interaction, the reservoirs and the tunneling between the reservoirs and the dots

$$H = H_{QD} + \sum_{\nu=s,d} H_\nu^{res} + H^t. \tag{2.1}$$

The Hamiltonian of the isolated quantum dots reads

$$H_{QD} = \sum_{i=1,2} \left[\sum_{\sigma=\uparrow\downarrow} E_i \hat{n}_{i\sigma} + U \hat{n}_{i\uparrow} \hat{n}_{i\downarrow} \right] + U_{12} \hat{n}_1 \hat{n}_2. \tag{2.2}$$

The term inside the square brackets is the Hamiltonian of the isolated single quantum dot i with energy level E_i and occupation operator $\hat{n}_{i\sigma} = \hat{c}_{i\sigma}^\dagger \hat{c}_{i\sigma}$ of electrons with spin projection σ. $\hat{c}_{i\sigma}$ annihilates one electron with spin projection σ in dot i. U is the coupling constant for the Coulomb interaction,

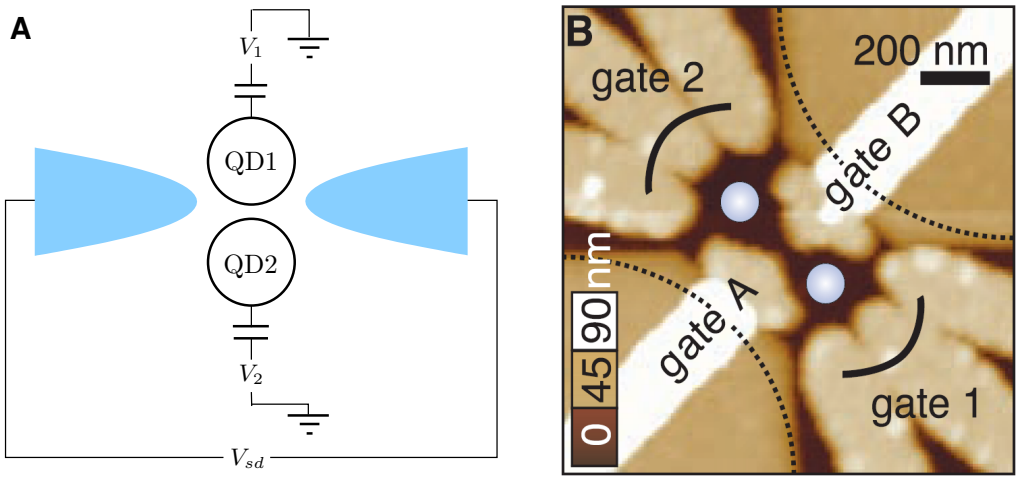

Figure 2.1: **(A)** Setup of a parallel double dot experiment. Two quantum dots QD1 and QD2 are connected via tunneling junctions to source and drain reservoirs, to which a voltage V_{sd} can be applied. The electronic levels in the dots can be shifted with separate gate voltages V_1 and V_2. **(B)** Experimental realization of such a setup in an atomic force microscopy picture. Quantum dots (indicated by blue circles) are formed below the surface in a two dimensional electron gas of a GaAs/AlGaAs heterostructure by applying negative voltages to the gate electrodes 1, 2, A and B. Source and drain contacts are formed by an additional layer (dotted lines), which prevents the electron gas from depletion below the gates A and B, from [24].

and therefore the second term inside the square brackets describes the intra-dot Coulomb interaction and the last term of Eq. (2.2) the inter-dot Coulomb interaction.

The low energy sector of the model consists of states with a total of one electron in the double dot. The inter-dot Coulomb interaction provides a strong electrostatic coupling between the dots. Then U_{12} and U separate the double occupied states from those with one electron in the double dot. Also inter-dot tunneling is excluded in this model, e.g. it is not possible for an electron to tunnel directly from one dot to the other.

An orbital SU(2) Kondo effect can arise if the single electron in the double dot can be transferred between the dots without energy costs[1], that is if $E_1 = E_2 = E$. The tunneling Hamiltonian is given by

$$H^t = \sum_{\substack{i=1,2 \\ r=s,d \\ k\sigma}} T^r_{i,k}\, \hat{a}^\dagger_{rk\sigma} \hat{c}_{i\sigma} + \text{h.c.} \tag{2.3}$$

where $\hat{a}_{rk\sigma}$ annihilates an electron with wave number k and spin σ in reservoir r and $T^r_{i,k}$ is the tunneling matrix element for this electron to tunnel into dot i.

2.1.1 The tunneling angle η

Since we are interested in describing the dynamics of the orbital motion, it is useful to introduce a tunneling angle by

$$\cos\eta^r_k = \frac{|T^r_{1k}|}{T^r_k}, \qquad \sin\eta^r_k = \frac{|T^r_{2k}|}{T^r_k} \qquad \text{with} \qquad T^r_k = \sqrt{|T^r_{1k}|^2 + |T^r_{2k}|^2}. \tag{2.4}$$

The geometric meaning of the tunneling angle η^r_k is illustrated in Fig. 2.2. Tunneling matrix elements for wave vectors k that just allow tunneling between reservoir r and dot 1, $T^r_{1k} = T^r_k$ and $T^r_{2k} = 0$, are described by $\eta^r_k = 0$, those that restrict tunneling to and from dot 2 by $\eta^r_k = \pi/2$. In these cases a mode couples explicitly to one dot of the double dot system. Modes that couple equally to both dots are described by a tunneling angle of $\eta^r_k = \pi/4$ as sketched in Fig. 2.2 (c).

In an alternative, but equivalent picture, the tunneling angle describes different physical setups concerning the reservoirs. For the extreme cases of modes with $\eta^r_k = 0, \pi/2$ the reservoir can be considered as two separate

[1] A possible inter-dot tunneling would lift this degeneracy: In that case the previous degenerate states in each dot would couple to a symmetric and an anti-symmetric state, energetically separated by a splitting Δ_{SAS}

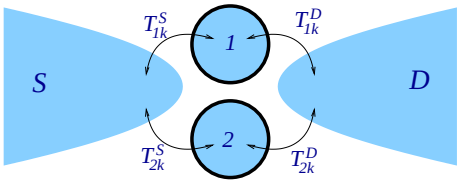

(a) Possible tunneling processes in the model

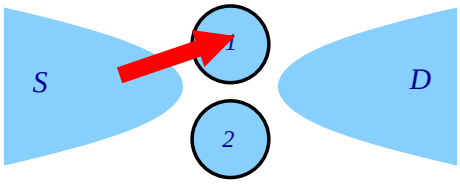

(b) Tunneling angle $\eta^s_k = 0$

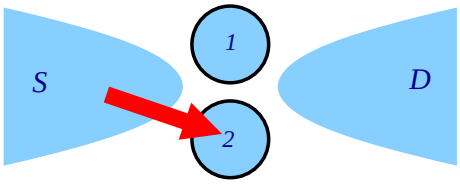

(c) Tunneling angle $\eta^s_k = \pi/2$

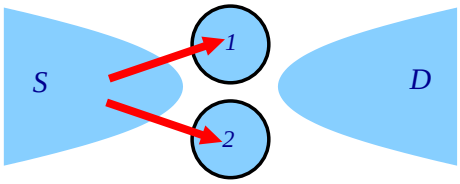

(d) Tunneling angle $\eta^s_k = \pi/4$

Figure 2.2: Tunneling processes considered in the model of the double dot with their tunneling rates and illustration of the tunneling angle η^r_k

reservoirs which each just couple do dot 2 respectively dot 1, as sketched in Fig. 2.3(a) and (b). Between these limiting cases the dots couple to one common reservoir reaching balance in the couplings for modes with $T^s_{1k} = T^s_{2k} = 1/\sqrt{2}T^s_k$, see Fig. 2.3(c).

In the case of a perpendicular magnetic field the tunneling matrix elements carry a complex Aharonov-Bohm phase ϕ. We chose a symmetric gauge to take ϕ into account

$$\begin{aligned} T^s_{1k} &= e^{i\frac{\phi}{4}}\,|T^s_{1k}|, & T^s_{2k} &= e^{-i\frac{\phi}{4}}\,|T^s_{2k}|, \\ T^d_{1k} &= e^{-i\frac{\phi}{4}}\,|T^d_{1k}|, & T^d_{2k} &= e^{i\frac{\phi}{4}}\,|T^d_{2k}|. \end{aligned} \tag{2.5}$$

Since the coupling matrix elements crucially decide about the orbital motion of the electrons, it's natural to introduce a pseudo spin notation by combining them to a vector which components describe the relative coupling to dot 1 and dot 2

$$\begin{pmatrix} \frac{T^r_{1k}}{T^r_k} \\ \frac{T^r_{2k}}{T^r_k} \end{pmatrix} = \begin{pmatrix} e^{\mp i\frac{\phi}{4}}\cos\eta^r_k \\ e^{\pm i\frac{\phi}{4}}\sin\eta^r_k \end{pmatrix}$$

The upper signs relate to the source reservoir, $r = s$, the lower ones to the drain reservoir $r = d$.

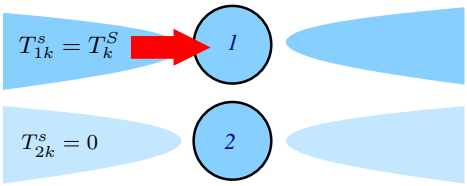

(a) Tunneling angle $\eta^s_k = 0$

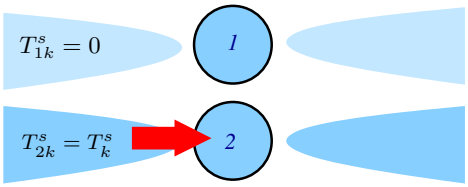

(b) Tunneling angle $\eta^s_k = \pi/2$

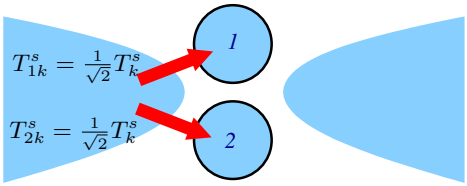

(c) Tunneling angle $\eta^s_k = \pi/4$

Figure 2.3: Alternative, equivalent description of the system: (a) modes with $T^s_{2k} = 0$ can be considered coming from an own reservoir, which just couples to dot 1, (b) modes with $T^s_{1k} = 0$ respectively as coming from another, separated reservoir, which just couples to dot 2, (c) modes with $T^s_{1k} = T^s_{2k}$ couple to a common reservoir for both dots. Other values of T^r_{ik} describe the intermediate region between these limiting cases

It is important to note that η_k^r is not a dynamical degree of freedom, but just determines the coupling of the states in the reservoir r in dependence of their wave vector k to the different dots. The tunneling matrix elements T_{ik}^r are fixed properties of the setup of the double dot system and the reservoirs.

The angle η_k is not dynamical. Yet this angle can fluctuate with wave vector k. The magnitude of those fluctuations determines whether the pseudo-spin in the reservoirs is promoted to a dynamical degree of freedom. For example, if the reservoirs for two quantum dots are strictly separated, the angle η_k assumes two possible values 0 and $\pi/2$, which results in strong fluctuations of η_k with k, and eventually leads to the pseudo-spin Kondo effect. In contrast, if there is only a single common reservoir for both dots, then the tunneling amplitudes to both dots are equal $T_{1k} = T_{2k}\ \forall k$. In that case, the angle η_k is frozen at the value $\pi/4$ for any k, and the orbital Kondo effect is suppressed.

2.1.2 Operators in the dots and the reservoirs

Using the vector of the coupling angle as a pseudo spin it is possible to introduce a formal bi-spinor notation for the operators in the reservoir by taking the outer product of the above tunneling vector and the fermionic operators in the reservoirs

$$\hat{\Psi}_{kr} = \begin{pmatrix} e^{\mp i\frac{\phi}{4}} \cos\eta_k^r \\ e^{\pm i\frac{\phi}{4}} \sin\eta_k^r \end{pmatrix} \otimes \begin{pmatrix} \hat{a}_{rk\uparrow} \\ \hat{a}_{rk\downarrow} \end{pmatrix}. \tag{2.6}$$

Also the operators in the dot can be formally combined into one bi-spinor

$$\hat{\Phi} = \begin{pmatrix} \hat{c}_{1\uparrow} \\ \hat{c}_{1\downarrow} \\ \hat{c}_{2\uparrow} \\ \hat{c}_{2\downarrow} \end{pmatrix}.$$

In this notation the tunneling Hamiltonian (2.3) reads

$$H^t = \sum_k T_k \left(\frac{T_k^s}{T_k} \hat{\Psi}_{sk}^\dagger + \frac{T_k^d}{T_k} \hat{\Psi}_{dk}^\dagger \right) \hat{\Phi} + \text{h.c.} \tag{2.7}$$

The form of the tunneling Hamiltonian (2.7) suggests to use the linear combination of operators in the source and drain reservoirs

$$\hat{\Psi}_k = \frac{T_k^s}{T_k} \hat{\Psi}_{sk} + \frac{T_k^d}{T_k} \hat{\Psi}_{dk} \tag{2.8}$$

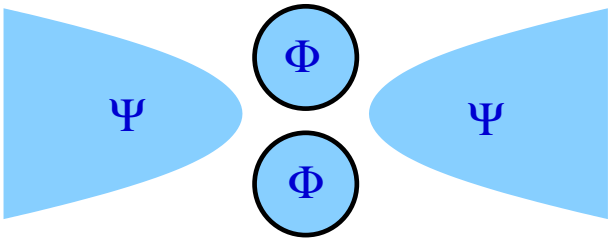

Figure 2.4: Description of the model by the operators $\hat{\Psi}$ and $\hat{\Phi}$

and it's orthogonal mode

$$\hat{\Xi}_k = \frac{T_k^d}{T_k}\hat{\Psi}_{sk} - \frac{T_k^s}{T_k}\hat{\Psi}_{dk}, \tag{2.9}$$

where

$$T_k = \sqrt{T_k^{s\,2} + T_k^{d\,2}}$$

as a new basis. If one expresses the tunneling Hamiltonian (2.7) in these new modes, it becomes

$$\sum_k T_k \hat{\Psi}_k^\dagger \hat{\Phi}$$

Since $\hat{\Xi}_k$ doesn't contribute to the tunneling Hamiltonian, this mode doesn't couple to the double dot.

2.2 The SU(4) Kondo Hamiltonian

Performing the Schrieffer Wolff-transformation in the basis given by (2.8) for the Hamiltonian (2.1) we derive the effective Kondo Hamiltonian

$$H_K = \sum_{\mu,\nu=0}^{3} \sum_{k,k'} J_{\mu\nu}^{kk'} \left[\hat{\Phi}^\dagger \left(\hat{\tau}^\mu \otimes \hat{\tau}^\nu\right) \hat{\Phi}\right] \left[\hat{\Psi}_k^\dagger \left(\hat{\sigma}^\mu \otimes \hat{\sigma}^\nu\right) \hat{\Psi}_{k'}\right] + H_{\text{res.}} \tag{2.10}$$

where σ^μ and τ^μ are Pauli matrices and $J_{\mu\nu}^{kk'}$ are the Kondo coupling constants generated during the Schrieffer-Wolff transformation. For more details on deriving the Kondo-Hamiltonian for this system, see [27].

The SU(4) symmetry point is achieved when $E_1 = E_2 = E$ and $U_{12} = U$. In this regime the Kondo couplings read

$$J_{\mu\nu}^{kk'} = T_k T_{k'} \left(\frac{1}{E+U} - \frac{1}{E}\right) \qquad \forall \quad \mu = \overline{0,3}$$

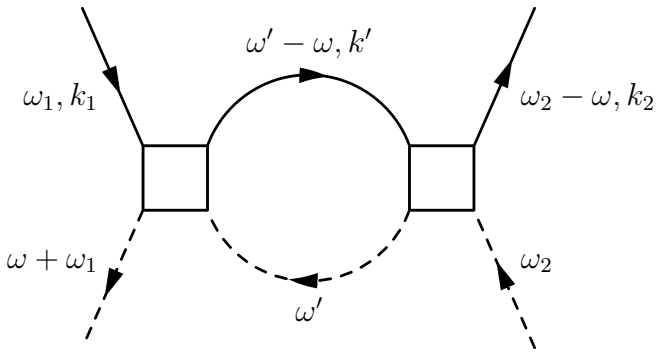

Figure 2.5: One loop renormalization of the Kondo couplings. Solid lines indicate the propagators for the electrons in the reservoirs $G(\omega, k)$, dashed the spin propagators in the dots $D(\omega)$, squares indicate non-perturbative renormalization vertices

except for $J_{00}^{kk'}$.

This Hamiltonian shows the possible SU(4) symmetry for the hyper-spins in the dots $\hat{\Phi}^\dagger \left(\hat{\tau}^\mu \otimes \hat{\tau}^\nu\right) \hat{\Phi}$ and in the reservoirs $\Psi_k^\dagger \left(\hat{\sigma}^\mu \otimes \hat{\sigma}^\nu\right) \hat{\Psi}_{k'}$. The hyper-spins in the double dot and the reservoirs are described employing a semi-fermionic representation [28, 29].

2.3 Renormalization Group Analysis

In the following the total tunneling probabilities $|T_k^r|^2$ from a given reservoir into the double dot are assumed to be k-independent for energies close to the Fermi level of the reservoirs $T_k^r = T_r$. Then the Kondo coupling constants $J_{\mu\nu}^{kk'}$ are independent of the wave vectors k and k'. Their indices are therefore omitted: $J_{\mu\nu}^{kk'} \to J_{\mu\nu}$. We also consider the case of symmetric coupling to both reservoirs $\eta_k^s = \eta_k^d$ and omit the reservoir's index of the tunneling angle.

To calculate the renormalization corrections to the coupling constants in first non-vanishing order one has to evaluate one loop diagrams, like the typical diagram shown in Fig. 2.5.

Using the propagators of the Fermi liquid in the reservoir

$$G(i\omega_n) = \frac{1}{i\omega_n - \xi_k},$$

and combining them with the definition of the bi-spinor fields (2.6) one obtains the propagators of the fields $\hat{\Psi}_k$

$$\mathsf{G}(i\omega, k) = \langle \Psi_k^\dagger \Psi_k \rangle = \frac{1}{i\omega - \xi_k} \mathsf{P} \tag{2.11}$$

with the matrix

$$\mathsf{P} = \begin{pmatrix} \cos^2\eta_k & \cos\eta_k \sin\eta_k \\ \cos\eta_k \sin\eta_k & \sin^2\eta_k \end{pmatrix} \otimes 1_2 \tag{2.12}$$

describing the non-trivial part of the coupling between the reservoirs and the dots. The propagator of the fields $\hat{\Phi}$ in the double dot reads

$$\mathsf{D}(i\omega_n, k) = \frac{1}{i\omega_n} 1_2 \otimes 1_2. \tag{2.13}$$

Evaluating the diagram shown in Fig. 2.5 gives the following correction to the Kondo Hamiltonian (2.10)

$$\begin{aligned} \delta H_K^1 &= \int \frac{d^d k'}{(2\pi)^d} \int \frac{d\omega'}{2\pi} (\sigma^\mu \otimes \sigma^\nu) \mathsf{G}(\omega' - \omega, k') (\sigma^{\mu'} \otimes \sigma^{\nu'}) (\tau^{\mu'} \otimes \tau^{\nu'}) \mathsf{D}(\omega') (\tau^\mu \otimes \tau^\nu) \\ &= \int \frac{d^d k'}{(2\pi)^d} \int \frac{d\omega'}{2\pi} (\sigma^\mu \otimes \sigma^\nu) \mathsf{P} (\sigma^{\mu'} \otimes \sigma^{\nu'}) (\tau^{\mu'} \otimes \tau^{\nu'}) (\tau^\mu \otimes \tau^\nu) \times \\ &\qquad \times \frac{1}{\omega' - \omega - \xi_k + i\,0\,\mathrm{sgn}(\omega' - \omega)} \frac{1}{\omega' + i\,0\,\mathrm{sgn}\,\omega'} \end{aligned} \tag{2.14}$$

Since $\xi_k = \xi_k(|\vec{k}|)$ only depends on the absolute value of $\vec{k}$ and P only depends on the angle of $\vec{k}$ it is useful to split the integration over the wave vector k in two parts by

$$\int d^d k = \int d\Omega \int k^{d-1} dk$$

where $d\Omega$ denotes the $d-1$ dimensional solid angle element. Then 2.14 becomes

$$\begin{aligned} \delta H_K^1 &= \int d\Omega (\sigma^\mu \otimes \sigma^\nu) \mathsf{P} (\sigma^{\mu'} \otimes \sigma^{\nu'}) (\tau^{\mu'} \otimes \tau^{\nu'}) (\tau^\mu \otimes \tau^\nu) \times \\ &\quad \times \int \frac{d^d k' k'^{d-1}}{(2\pi)^d} \int \frac{d\omega'}{2\pi} \frac{1}{\omega' - \omega - \xi_k + i\,0\,\mathrm{sgn}(\omega' - \omega)} \frac{1}{\omega' + i\,0\,\mathrm{sgn}\,\omega'} \end{aligned} \tag{2.15}$$

2.3.1 Integrating out the energy shell

The first integral gives the matrix structure of the correction and will be discussed later. To integrate out an upper energy shell from $\Lambda - \delta\Lambda$ to Λ one has to perform the ω integration in the second integral of Eq. (2.14). Substituting $\delta\Lambda$ by Λl to keep the relative size $\delta\Lambda/\Lambda$ of the energy shell constant all over the scaling and assuming $\Lambda \gg |\omega|$ the integral can be

approximated by

$$\begin{aligned}&\int_{\Lambda-\delta\Lambda}^{\Lambda}\frac{d\omega'}{2\pi}\frac{1}{\omega'-\omega-\xi_k+i\,0\,\mathrm{sgn}\,(\omega'-\omega)}\frac{1}{\omega'+i\,0\,\mathrm{sgn}\,\omega'}\\ \approx&\frac{\Lambda l}{2\pi}\frac{1}{\Lambda-\xi_k+i\,0}\frac{1}{\Lambda+i\,0}.\end{aligned}$$

For the remaining k integration the density of states is assumed to be constant at the Fermi level $\frac{d^dk'}{(2\pi)^d}\to\nu_0 d\xi_k$. Using the principle value theorem one gets

$$\begin{aligned}&\int\frac{d^dk'}{(2\pi)^d}\frac{\Lambda l}{2\pi}\frac{1}{\Lambda-\xi_k+i\,0}\frac{1}{\Lambda+i\,0}\\ =&\frac{l}{2\pi}\int\frac{\nu_0 d\xi_k}{\Lambda-\xi_k+i\,0}=\frac{l}{2\pi}(-2\pi i)\nu_0\\ =&-il\nu_0.\end{aligned}$$

An analogous calculation for the lower energy shell from $-\Lambda+\delta\Lambda$ to $-\Lambda$ contributes also $-il\nu_0$.

Evaluating all other possible one loop diagrams one gets the following results for the integrals over ω and ξ_k

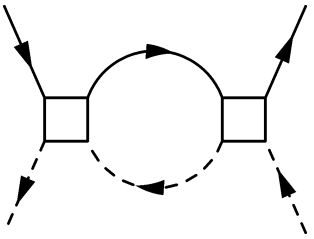

$-2il\nu_0$

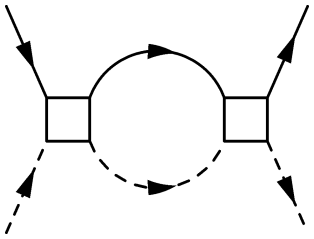

$2il\nu_0$

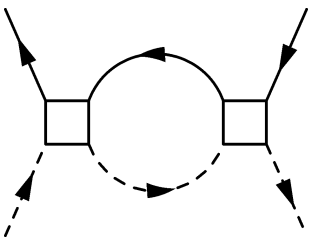

$-2il\nu_0$

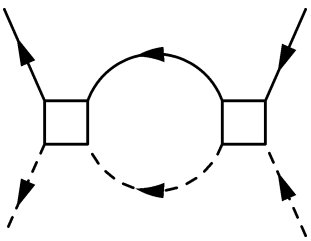

$2il\nu_0$

2.3.2 Integrating over the solid angle of the wave vector

The matrix structure P (2.12) of the propagator depends on the tunneling angle η_k which in turn depends only on the angular part of the wave vector k. To integrate over k in (2.14) therefore involves averaging over all possible angles.

$$\langle \mathsf{P} \rangle = \left\langle \begin{pmatrix} \cos\eta_k^2 & \cos\eta_k \sin\eta_k \\ \cos\eta_k \sin\eta_k & \sin^2\eta_k \end{pmatrix} \right\rangle \otimes 1_2 \tag{2.16}$$

$$= \begin{pmatrix} \langle\cos\eta_k^2\rangle & \langle\cos\eta_k \sin\eta_k\rangle \\ \langle\cos\eta_k \sin\eta_k\rangle & \langle\sin^2\eta_k\rangle \end{pmatrix} \otimes 1_2 \tag{2.17}$$

Decomposing (2.17) in the set of the Pauli matrices σ^i and the unity matrix gives

$$\langle \mathsf{P} \rangle = \left[\frac{1}{2}\langle\sin^2\eta_k + \cos^2\eta_k\rangle 1_2 + \langle\sin\eta_k\cos\eta_k\rangle\sigma^1 + \frac{1}{2}\langle\cos^2\eta_k - \sin^2\eta_k\rangle\sigma^3\right] \otimes 1_2 \tag{2.18}$$

$$= \left(b_0 1_2 + \sum_{i=1}^{3} b_i \sigma^i\right) \otimes 1_2$$

with

$$b_0 = \frac{1}{2} \tag{2.19}$$

$$b_1 = \langle\sin\eta_k\cos\eta_k\rangle \tag{2.20}$$

$$b_2 = 0 \tag{2.21}$$

$$b_3 = \frac{1}{2}\langle\cos^2\eta_k - \sin^2\eta_k\rangle \tag{2.22}$$

In the case of symmetric dots, which is assumed in this work, b_3 also vanishes. The fluctuations of the tunneling angle are now described by a single parameter b_1. The limiting values for b_1 can be interpreted in the following way:

- In the case of strictly separated reservoirs the tunneling angle is either $\eta_k = 0$ or $\eta_k = \pi/2$ for the different modes. In both cases either the sine or the cosine in the definition of b_1 is zero and therefore $b_1 = 0$. The strong fluctuations of the tunneling angle will enable an SU(4) Kondo effect for this value of b_1.

- If all modes couple equally to both dots, which means one common reservoir for the double dot, the tunneling angle is fixed to $\eta_k = \pi/4$. This results in $b_1 = 1/2$. The orbital Kondo effect is suppressed and the system will be in a spin SU(2) Kondo regime.

Because of this interpretation of the parameter b_1 it will be called *mixing parameter* in what follows. Summing up all diagrams results in a commutator like structure of the correction to the Kondo-Hamiltonian H_K

$$\begin{aligned}\delta H_K =& \pi\nu_0 \left(\delta\Lambda/\Lambda\right) J_{\mu\nu} J_{\mu'\nu'} \\ & \times \Phi^\dagger \left[\left(\tau^\mu \otimes \tau^\nu\right) \left(\tau^{\mu'} \otimes \tau^{\nu'}\right) - \left(\tau^{\mu'} \otimes \tau^{\nu'}\right) \left(\tau^\mu \otimes \tau^\nu\right) \right] \Phi \\ & \times \Psi^\dagger \left[\left(\sigma^\mu \otimes \sigma^\nu\right) \mathsf{P} \left(\sigma^{\mu'} \otimes \sigma^{\nu'}\right) - \left(\sigma^{\mu'} \otimes \sigma^{\nu'}\right) \mathsf{P} \left(\sigma^\mu \otimes \sigma^\nu\right) \right] \Psi \end{aligned} \tag{2.23}$$

This correction obviously has another structure than the original Hamiltonian (2.10)

The reason for this difference is that the original Hamiltonian is not general enough to hold during the scaling process. Differently from the scaling calculations in section 1.3 for the SU(2) spin Kondo effect new interactions are generated by the renormalization of the coupling constants.

The choice of our basis (2.8), (2.9) determines the matrix structure of the propagator in the reservoirs P, Eq. (2.19). The basis is chosen in a way that the non-trivial part of P just operates on σ^μ and $\sigma^{\mu'}$ in the tensor products of the Pauli matrices in (2.23). Therefore the indices μ, μ' of the tensor product will be called *orbital indices* and ν, ν' *spin indices*. It is just the non trivial mixing of the orbital indices that generates new interactions in the renormalization process. With this consideration in mind, one can suppose that not all four μ, μ' and ν, ν' indices are needed to describe the correction to the Kondo Hamiltonian, but just three are enough to reflect the physical structure of the system.

This motivates the trial to re-write the original Kondo Hamiltonian (2.10) for the double dot system in a more general form using *two independent* orbital indices and one spin index:

$$H_K = \sum_{\mu,\lambda,\nu=0}^{3} J_{\mu\lambda\nu} \left[\Phi^\dagger(\tau^\mu \otimes \tau^\nu)\Phi\right] \left[\Psi^\dagger(\sigma^\lambda \otimes \tau^\nu)\Psi\right] \tag{2.24}$$

and hope that this form is general enough to respect the newly generated interactions during the scaling.

To get the flow equations for the correction to the Kondo Hamiltonian one has to redo the calculations leading to correction in the first place, but this time taking the more general "three index" variant of the Kondo Hamiltonian (2.24) as starting point. If no new interactions are generated for this

generalized Kondo Hamiltonian, the assumption of three independent indices is justified and the flow equations for the coupling constants $J_{\mu\lambda\nu}$ can be read off the correction to the Hamiltonian.

2.3.3 Decomposition of the commutator into the generators of the SU(4)

Redoing the calculations for the generalized Kondo Hamiltonian (2.24) one ends up with a commutator like structure, similar to (2.23). To find the flow equations for the coupling constants $J_{\mu\lambda\nu}$ the correction to the Hamiltonian has to be expanded into a direct product of Pauli matrices. To do this we use the relation for the product of the Pauli matrices σ^i extended by $\sigma^0 = \mathbf{1}_2$

$$\sigma^n\sigma^m = \delta_{mn}\sigma^0 + \delta_{n0}\beta_{m0}\sigma^m + \delta_{m0}\beta_{n0}\sigma^n + i\epsilon_{nmk}\sigma^k, \tag{2.25}$$

where

$$\beta_{ij} = 1 - \delta_{ij}$$

and the Levi-Civita tensor ϵ_{ijk} are utilized. First, we rewrite (2.23) into a tensor product of matrix products by

$$(\sigma^\mu \otimes \sigma^\nu)(\sigma^{\mu'} \otimes \sigma^{\nu'}) = (\sigma^\mu\sigma^{\mu'}) \otimes (\sigma^\nu\sigma^{\nu'})$$

and apply identity (2.25) to the result. This gives for the commutator (2.23)

$$\begin{aligned}&(\tau^\mu\otimes\tau^\nu)(\tau^{\mu'} \otimes \tau^{\nu'}) - (\tau^{\mu'} \otimes \tau^{\nu'})(\tau^\mu \otimes \tau^\nu) = \\ &-2i\Big[(\tau^\lambda \otimes \tau^{\nu'})\beta_{0\nu'}\delta_{0\nu}\epsilon_{\mu\lambda\mu'} + (\tau^\lambda \otimes \tau^\nu)\beta_{0\nu}\delta_{0\nu'}\epsilon_{\mu\lambda\mu'} + (\tau^\lambda \otimes \tau^0)\delta_{\nu\nu'}\epsilon_{\mu\lambda\mu'} \\ &\quad+(\tau^{\mu'} \otimes \tau^\lambda)\beta_{0\mu'}\delta_{0\mu}\epsilon_{\nu\lambda\nu'} + (\tau^\mu \otimes \tau^\lambda)\beta_{0\mu}\delta_{0\mu'}\epsilon_{\nu\lambda\nu'} + (\tau^0 \otimes \tau^\lambda)\delta_{\mu\mu'}\epsilon_{\nu\lambda\nu'}\Big],\end{aligned} \tag{2.26}$$

where λ is a summation index.

The non trivial part of the correction to the Kondo Hamiltonian (2.23) is given by the commutator resulting from the propagator in the reservoirs. It

expands to

$$
\begin{aligned}
&(\sigma^{\mu}\otimes\sigma^{\nu})\mathsf{P}(\sigma^{\mu'}\otimes\sigma^{\nu'})-(\sigma^{\mu'}\otimes\sigma^{\nu'})\mathsf{P}(\sigma^{\mu}\otimes\sigma^{\nu})= \qquad (2.27)\\
&-2ib_0\Big[(\sigma^{\lambda}\otimes\sigma^{\nu'})\beta_{0\nu'}\delta_{0\nu}\epsilon_{\mu\lambda\mu'}+(\sigma^{\lambda}\otimes\sigma^{\nu})\beta_{0\nu}\delta_{0\nu'}\epsilon_{\mu\lambda\mu'}+(\sigma^{\lambda}\otimes\sigma^{0})\delta_{\nu\nu'}\epsilon_{\mu\lambda\mu'}\\
&\quad+(\sigma^{\mu'}\otimes\sigma^{\lambda})\beta_{0\mu'}\delta_{0\mu}\epsilon_{\nu\lambda\nu'}+(\sigma^{\mu}\otimes\sigma^{\lambda})\beta_{0\mu}\delta_{0\mu'}\epsilon_{\nu\lambda\nu'}+(\sigma^{0}\otimes\sigma^{\lambda})\delta_{\mu\mu'}\epsilon_{\nu\lambda\nu'}\Big]\\
&+2ib_1\Big[(\sigma^{0}\otimes\sigma^{0})\delta_{\nu\nu'}\epsilon_{1\mu'\mu}+(\sigma^{0}\otimes\sigma^{\nu})\beta_{0\nu}\delta_{0\nu'}\epsilon_{1\mu'\mu}+(\sigma^{0}\otimes\sigma^{\nu'})\beta_{0\nu'}\delta_{0\nu}\epsilon_{1\mu'\mu}\\
&\quad+(\sigma^{0}\otimes\sigma^{\lambda})(\delta_{0\mu}\delta_{1\mu'}\epsilon_{\nu\nu'\lambda}+\delta_{0\mu'}\delta_{1\mu}\epsilon_{\nu\nu'\lambda})\\
&\quad+(\sigma^{1}\otimes\sigma^{\lambda})(2\delta_{0\mu'}\delta_{0\mu}\epsilon_{\nu\nu'\lambda}-\delta_{\mu'\mu}\epsilon_{\nu\nu'\lambda})\\
&\quad+(\sigma^{\mu'}\otimes\sigma^{\lambda})\beta_{0\mu'}\delta_{1\mu}\epsilon_{\nu\nu'\lambda}+(\sigma^{\mu}\otimes\sigma^{\lambda})\beta_{0\mu}\delta_{1\mu'}\epsilon_{\nu\nu'\lambda}\\
&\quad+(\sigma^{\lambda}\otimes\sigma^{0})(\delta_{0\mu}\delta_{\nu\nu'}\epsilon_{1\mu'\lambda}-\delta_{0\mu'}\delta_{\nu\nu'}\epsilon_{1\mu\lambda})\\
&\quad+(\sigma^{\lambda}\otimes\sigma^{\nu})(\beta_{0\nu}\delta_{0\mu}\delta_{0\nu'}\epsilon_{1\mu'\lambda}-\beta_{0\nu}\delta_{0\mu'}\delta_{0\nu'}\epsilon_{1\mu\lambda})\\
&\quad+(\sigma^{\lambda}\otimes\sigma^{\nu'})(\beta_{0\nu'}\delta_{0\mu}\delta_{0\nu}\epsilon_{1\mu'\lambda}-\beta_{0\nu'}\delta_{0\mu'}\delta_{0\nu}\epsilon_{1\mu\lambda})\Big].
\end{aligned}
$$

Exploiting these identities for all indices and sorting them by the direct product of Pauli matrices one can read off the flow equations for the coupling constants. The full set of these is shown in appendix B. Since no disambiguations in the corrections to the coupling constants appear the generalized Kondo Hamiltonian (2.24) has proven to hold during the scaling.

2.3.4 The flow equations

The flow of the coupling constants differs for spin index $\nu = 0$ and $\nu = \overline{1,3}$. The scaling equations reduce consistently to two sets of equations for these cases as shown in appendix C. In the following notation the value of the index ν is therefore restricted to $\nu = \overline{1,3}$ and the case $\nu = 0$ is explicitly denoted by a zero as spin index.

Assuming that coupling constants with non diagonal orbital indices start to flow with zero as starting value, it turns out that $J_{10\nu}$, $J_{01\nu}$ and J_{100} are the only non-diagonal coupling constants generated during the scaling. Further, the coupling constants with diagonal orbital indices $J_{\mu\mu\nu}, \mu = \overline{2,3}$ have the same flow and will be denoted by $J_{\perp 0}$ respective $J_{\perp\nu}$. This eventually results

in the following set of flow equations:

$$\frac{dJ_{00\nu}}{d\Lambda} = 8\left[b_1(2J_{00\nu}J_{01\nu} + 2J_{11\nu}J_{10\nu}) + b_0(J_{00\nu}^2 + J_{11\nu}^2 + 2J_{\perp\nu}^2 + J_{01\nu}^2 + J_{10\nu}^2)\right]$$
$$\frac{J_{110}}{d\Lambda} = 8b_0\left[J_{\perp 0}^2 + 3J_{\perp\nu}^2\right]$$
$$\frac{J_{11\nu}}{d\Lambda} = 8\left[b_1(2J_{11\nu}J_{01\nu} + 2J_{00\nu}J_{10\nu}) + b_0(2J_{00\nu}J_{11\nu} + 2J_{\perp 0}J_{\perp\nu} + 2J_{01\nu}J_{10\nu})\right]$$
$$\frac{J_{\perp 0}}{d\Lambda} = 8\left[b_0(J_{10}J_{\perp 0} + 3J_{11\nu}J_{\perp\nu}) + b_1(J_{\perp 0}J_{100} + 3J_{\perp\nu}J_{10\nu})\right]$$
$$\frac{dJ_{\perp\nu}}{d\Lambda} = 8\left[b_0(J_{11\nu}J_{\perp 0} + 2J_{00\nu}J_{\perp\nu} + J_{10}J_{\perp\nu}) + b_1(2J_{\perp\nu}J_{01\nu} + J_{\perp\nu}J_{100} + J_{\perp 0}J_{10\nu})\right]$$
$$\frac{J_{01\nu}}{d\Lambda} = 8\left[b_0(2J_{00\nu}J_{01\nu} + 2J_{11\nu}J_{10\nu}) + b_1(J_{00\nu}^2 + J_{11\nu}^2 - 2J_{\perp\nu}^2 + J_{01\nu}^2 + J_{10\nu}^2)\right]$$
$$\frac{dJ_{100}}{d\Lambda} = -8b_1\left[J_{\perp 0}^2 + 3J_{\perp\nu}^2\right]$$
$$\frac{dJ_{10\nu}}{d\Lambda} = 8\left[b_0(2J_{11\nu}J_{01\nu} + 2J_{00\nu}J_{10\nu}) + b_1(2J_{00\nu}J_{11\nu} - 2J_{\perp 0}J_{\perp\nu} + 2J_{01\nu}J_{10,\nu})\right]$$

This coupled set of differential equations is integrated numerically from the starting values

$$J_{00\nu} = J_0, \quad J_{110} = J_0, \quad J_{11\nu} = J_0, \quad J_{\perp 0} = J_0,$$
$$J_{\perp\nu} = J_0, \quad J_{01\nu} = 0, \quad J_{100} = 0, \quad J_{10\nu} = 0.$$

This assumes all non-diagonal coupling constants start to flow as zero, as they are just generated by the renormalization process. J_0 is assumed to be a small constant, which depends on the properties of the considered metal of the reservoirs.

The result of the numerical integration is that all coupling constants are monotonically increasing and diverge all at the same critical value Λ_c. An example of this behavior is shown in Fig. 2.6

Integrating the flow equations for different values of the mixing parameters b_1 gives the dependence of Λ_c of b_1. The Kondo temperature T_K is proportional to $\exp(-J_0\Lambda_c)$. The resulting dependency $T_K(b_1)$, normalized to the SU(4) point at $b_1 = 0$ is shown in Fig. 2.7

2.4 Discussion of the results

Fig. 2.7 shows two characteristic features.

- The Kondo temperature is exactly equal for both limiting situations with a definite symmetry: $T_K^{SU(4)} = T_K^{SU(2)}$.

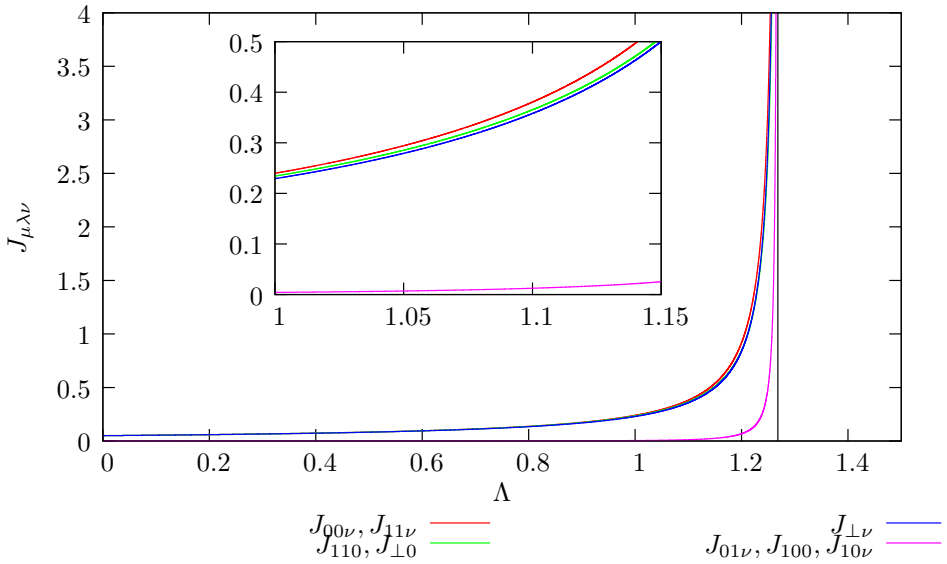

Figure 2.6: Example of the flow of the coupling constants $J_{\mu\lambda\nu}$ for an arbitrary but fixed value of b_1 during the renormalization process. At a critical length Λ_c all coupling constants diverge. In contrast to the simple spin Kondo effect (see Fig. 1.9 for comparison) new interactions $J_{01\nu}$, J_{100} and J_{10_ν} are generated during the renormalization. The inset shows that also the coupling constants which start from the same initial value J_0 split up.

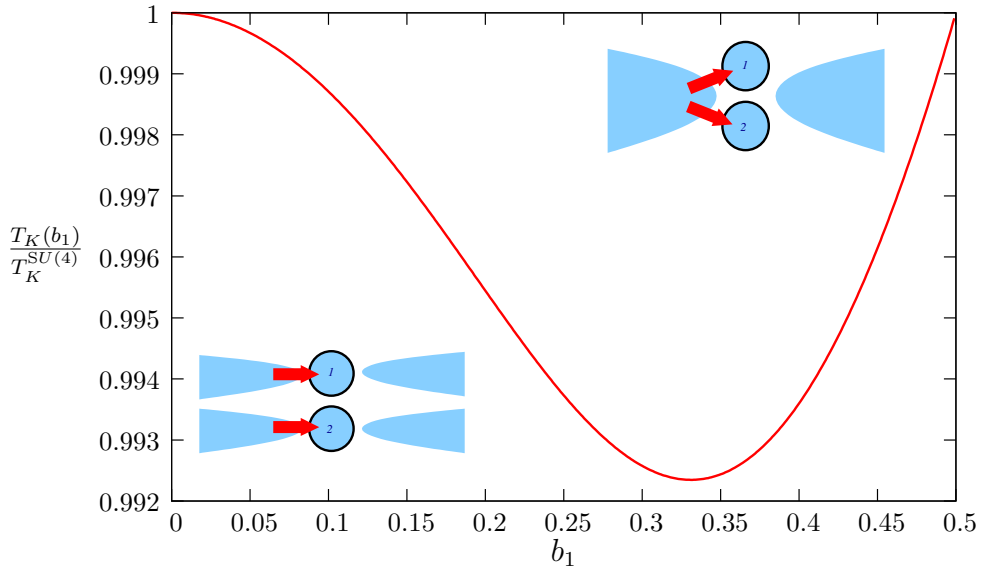

Figure 2.7: Dependence of the Kondo temperature T_K on the mixing parameter b_1, normalized to the Kondo temperature of the SU(4) point $T_K^{SU(4)}$, $b_1 = 0$. With increasing mixing of the reservoirs the Kondo temperature first drops, reaches a minimum at $b_1 \approx 0.33$ to raise again to the original value at the SU(2) point $b_1 = 0.5$

- In the intermediate regime, increasing b_1 first pushes the Kondo temperature monotonously to a minimal value at $b_{1,\min} \approx 0.33$. For even larger values $b_1 > b_{1,\min}$ the Kondo temperature rises again to its original value.

Both features can be understood in terms of transport channel blocking, a common phenomena in the transport through quantum dots [30].

2.4.1 Equality of the Kondo temperature in the limiting cases

The two transport channels through the double dot the system correspond to the projection of the pseudo-spin. The wave functions in the channels are given by the symmetric and anti-symmetric combinations of the wave functions of each dot, as sketched in Fig. 2.8.

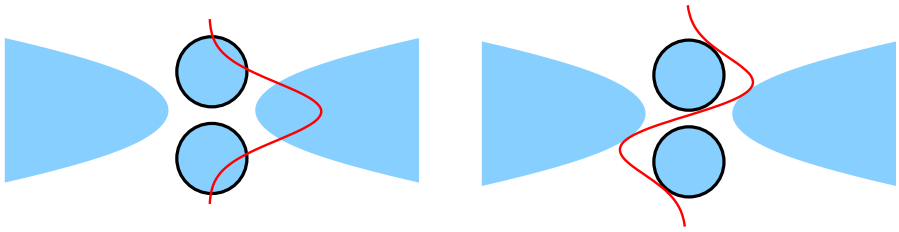

Figure 2.8: Symmetric and anti-symmetric combination of the states in each dot

In the SU(2) point of completely symmetric tunneling from each mode to both quantum dots, $b_1 = 0.5$, the Kondo effect in the orbital sector is completely suppressed. The channel through the antisymmetric combination of wave functions is completely decoupled, because of the fixed tunneling angle. All modes of the unified reservoir couple to a single electron state given by the symmetric combination of the states in each dot. This results in the doubling of the density of states in the reservoir for the spin Kondo effect, compared to the other limit $b_1 = 0$. In the case $b_1 = 0$, which corresponds to the SU(4) symmetry, each dot couples to its own reservoir, resulting in just half the density of states, though both transport channels are open.

In the end, the Kondo temperatures for the two symmetry points, the SU(4) one and the SU (2) one, are equal [21]. The doubling of the density of states for the spin Kondo effect exactly compensates the suppression of the orbital Kondo effect.

2.4.2 Non-monotonous behavior of the Kondo temperature in the intermediate regime

As stated above increasing b_1 from zero to 0.5 progressively decouples the antisymmetric combination of wave function from the reservoirs. Let's assume we drive the system a bit out of the SU(2) point, that is b_1 is just below 0.5. Now the antisymmetric state is still almost decoupled from the reservoirs, yet not completely. The Kondo correlations still occur only in the strongly coupled symmetric channel leading to the spin Kondo effect.

But as the system is not exactly in the SU(2) point there is a small probability that an electron tunnels into the anti-symmetric combination of wave functions, occupying this transport channel. These events have a huge destructive effect on the spin Kondo effect, resulting from three factors:

1. The weak coupling of this state to the reservoirs, leading to a low Kondo temperature, suppresses the spin Kondo effect in this channel.

2. The Coulomb blockade suppresses the transport through the strong coupling symmetric state.

3. The antisymmetric state, if occupied, has a long lifetime because of the weak coupling of the reservoirs to it, although the probability to occupy it by tunneling from a reservoir is small.

The combination of blocking and spin Kondo effect suppression causes the steep decay of the Kondo temperature for $0.5 > b_1 > b_{1,\min}$. For even lower values of b_1 the fluctuations of the asymmetric occupation of the dots, due to higher tunneling rates to them, give raise to the orbital Kondo effect. Finally for $b_1 = 0$ in the SU(4) symmetry point the Kondo temperature reaches again its original value.

2.5 External Zeeman field

An external magnetic field would certainly lift the spin degeneracy due to the Zeeman energy, and therefore destroy the spin Kondo effect. To investigate this behavior, we included the effect of an external magnetic field into the scaling calculations.

2.5.1 Adaptation of the Model

Our original Kondo Hamiltonian (2.10) does not depend on the magnetic field, but could be easily expanded by a Zeeman term. From that we could derive

the scaling equations and treat the effects of the magnetic field completely analogous to all other quantities in the renormalization formalism.

However, since we're just interested in the destruction of the spin Kondo effect by freezing out the spin fluctuation, we chose a much simpler effective approach: We compare the Zeeman energy h to the energy scales of the renormalization calculations. From a certain logarithmic energy scale $l_h(h)$ the Zeeman energy becomes the dominant energy scale and therefore freezes out spin fluctuations for $l > l_h$, for $l < l_h$ the Zeeman field is neglected.

Without loss of generality we take the direction of the Zeeman field along the z-axis. In this case the coupling constants $J_{\mu\lambda\nu}$ with spin-index $\nu = 1, 2$ stop abruptly to flow for $l > l_h$.

This can be understood in two equivalent pictures:

- In the first we scale the Zeeman energy scale, resulting in a running Zeeman field $h(l) = h_0 e^l$. The switch-over condition then is the running Zeeman reaching the high energy cutoff $h(l_h) = \Lambda$.

- We also could think of keeping the Zeeman energy constant and switch over to the new set of scaling equations with fixed couplings when we have integrated out enough high-energy shells to have our system scaled down to the energy scale of the Zeeman field.

Simply switching the scaling equations during the scaling may be figuratively obvious, but the results are to be taken with care when switching is done abruptly[2]. Nevertheless the simple method of switching the scaling equation gives results good enough to illustrate the breakdown of the spin Kondo effect with increasing external magnetic field and to differ between different energy regimes.

2.5.2 Discussion of the energy regimes

The results of such a calculation can be seen in Fig. 2.9. The graph shows in light blue the dependence of the Kondo temperature T_K on the mixing parameter b_1 without an external Zeeman-field, compare Fig. 2.7. The black line shows the crossover of the energy regimes $h = T_K^{SU(4)}$, above it is $h < T_K^{SU(4)}$, below $h > T_K^{SU(4)}$.

[2]The problem of this approach is: We switch abruptly from the set of completely undisturbed ($h = 0$) flow equations for the coupling constants to those for utterly frozen spins ($h \gg T_K^{SU(4)}$) even for intermediate Zeeman energies $0 < h < T_K^{SU(4)}$. While this is correct in the extremal cases, it is certainly a rough approximation in the intermediate regime.

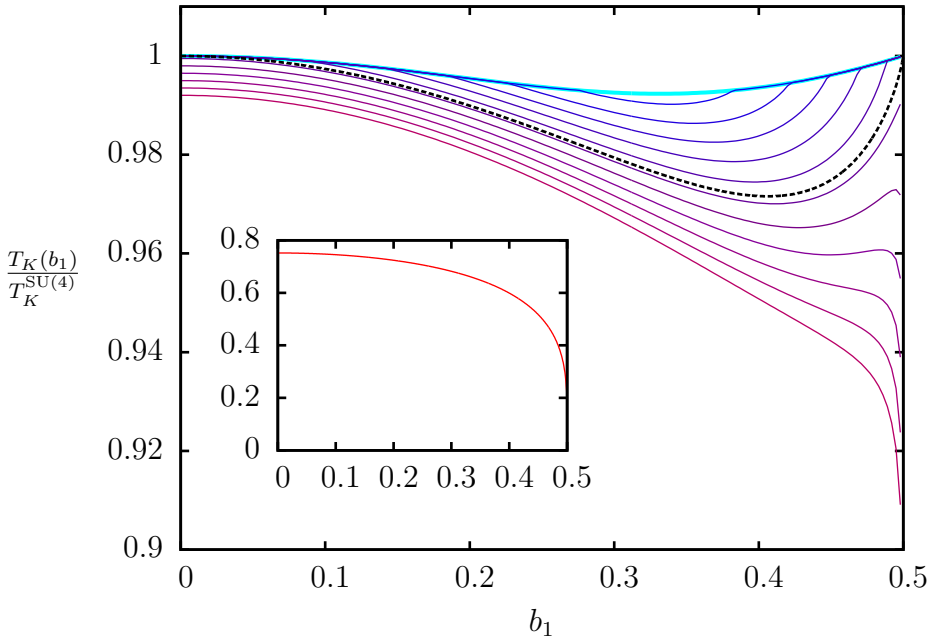

Figure 2.9: Dependence of the Kondo temperature T_K on the mixing parameter b_1 in presence of a Zeeman field, normalized to the Kondo temperature of the SU(4) point $T_K^{\mathrm{SU}(4)}$ with zero Zeeman field. The light blue curve marks the Kondo temperature without the Zeeman field (see Fig. 2.7). The Zeeman field h increases from blue ($h/T_K^{\mathrm{SU}(4)} = 0.993$) to red ($h/T_K^{\mathrm{SU}(4)} = 1.008$). The black curve shows the Kondo temperature for $h = T_K^{\mathrm{SU}(4)}$. The inset shows the Kondo temperature for large Zeeman fields ($h/T_K^{\mathrm{SU}(4)} \gg 1$).

$h < T_K^{SU(4)}$**:** In this case there exist ranges of b_1 in which the Zeeman field has no effect, the Kondo temperature is identical to the case of no Zeeman field at all. No switching of the flow equations occurred in the calculations for these values of b_1.

Just in the parameter regime of b_1, where the mixing lowered the Kondo temperature (and therefore the corresponding energy scale) to values of $h > T_K(b_1)$ the Zeeman energy becomes the dominant energy scale. Then the suppression of the spin Kondo effect lowers the Kondo Temperature even further.

With increasing h the regions where the Zeeman field lowers the Kondo temperature expand naturally to a broader range of b_1, since now even less mixing lowers the Kondo energy scale enough to let the Zeeman field become effective.

$h = T_K^{SU(4)}$**:** This is the limiting case, where the graphs of the Kondo temperature with and without external Zeeman field separate totally from each other. Just for the extremal cases $b_1 = 0$ and $b_1 = 0.5$ the Kondo temperatures still match. The slightest other value of the mixing parameter lowers the Kondo temperature below h, leading to a further decrease by the suppression of the spin Kondo effect be freezing out the spin fluctuation.

$h > T_K^{SU(4)}$**:** In this regime there exists no mixing parameter b_1 anymore, where we could see an undisturbed system. For each value of b_1 the Zeeman field freezes out the spin fluctuations. As these are more important for larger values of b_1 (meaning closer to the SU(2) point, where the orbital Kondo effect is suppressed by the fixed tunneling angle) the Kondo temperature drops drastically for large values of b_1 and should destroy the Kondo effect completely for large Zeeman fields.

The inset in Fig. 2.9 shows the Kondo temperature for large values of the Zeeman field $h \gg T_K^{SU(4)}$. In this case all values of $T_K(b_1)$ were derived from the flow equations for fixed spin, which means that the system only shows the orbital Kondo effect.

It is clearly visible that the Kondo temperature drops to zero, as b_1 approaches 0.5, which means fixed tunneling angles, and therefore no Kondo effect at all. In the other limiting case of free orbital fluctuations, $b_1 = 0$, the graph shows a reduced Kondo temperature compared to the SU(4) case without Zeeman field. This decline started when h exceeded $T_K^{SU(4)}(h = 0)$ as explained above and reaches a finite limiting value given by the full suppression of the spin Kondo effect. In the picture of transport channels half

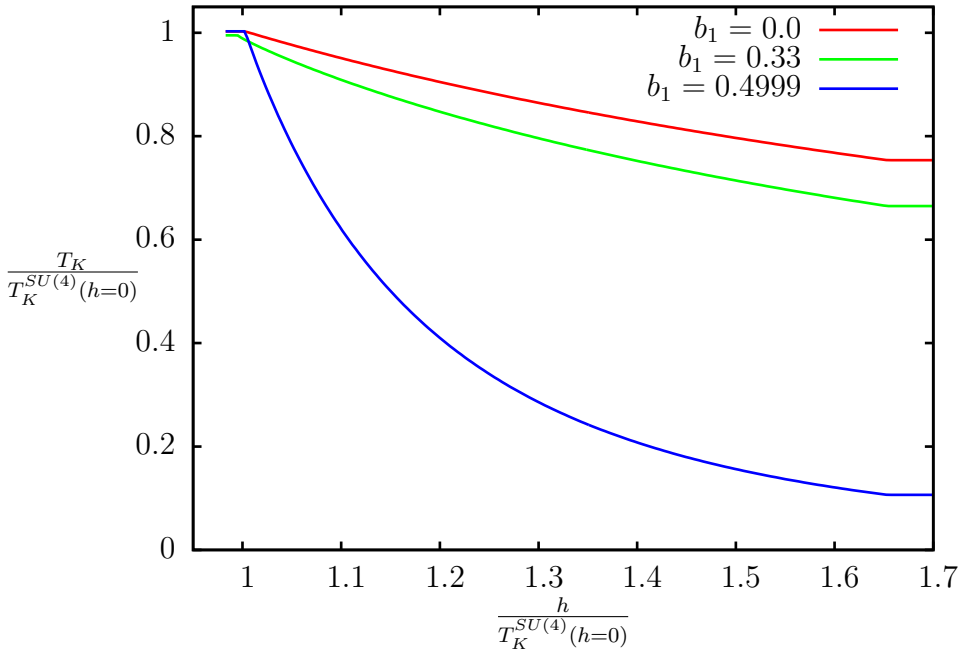

Figure 2.10: Kondo temperature as function of the Zeeman field h for different values of the mixing parameters b_1, normalized to the Kondo temperature at the SU(4) point without Zeeman field.

of the transport channels are blocked. The diminished density of states in the separate reservoirs for each dot in this situation is not compensated by a second open transport channel. The quantitive result of the numerical calculation for the lowering of the Kondo temperature from SU(4) to SU(2) is in good agreement with the expected value for half of the channels of $\exp(1/2)/\exp(1/4) \approx 0.78$.

The dependence of the Kondo temperature on the Zeeman field h for different values of the mixing parameters b_1 is shown in Fig. 2.10. b_1 was chosen for both limiting cases, the SU(2) and the SU(4) Kondo effect[3], and for the minimal Kondo temperature without Zeeman field, $b_1 = 0.33$. The spin fluctuations are frozen out completely for $h \approx 1.65\, T_K^{SU(4)}(h = 0)$. Higher values of the Zeeman field do not decrease the Kondo temperature anymore, as the double dot system just shows the orbital Kondo effect in this regime in the case of $b_1 = 0$ and no Kondo effect at all for $b_1 = 0.5$.

[3]The exact SU(2) point, $b_1 = 0.5$, leads to convergence problems in the numerical problems in the calculations, so $b_1 = 0.4999$ was chosen as approximation.

The different regimes of h with respect to $T_K^{SU(4)}$ discussed in the beginning of this section can be found in the small features in the upper left corner of the graph: Both curves for the Kondo temperature in the SU(2) and the SU(4) situation begin to show the effect of the Zeeman field at $h = T_K^{SU(4)}$, starting from the same Kondo temperature, while the curve for the case of $b_1 = 0.33$ starts with a slightly diminished Kondo temperature, due to the mixing, and at lower magnetic fields, just because of that lowered Kondo temperature.

Chapter 3

Conductance through the Double Dot

3.1 The current operator

To calculate the current through the double dot system we start out from the generalization of the effective Kondo Hamiltonian (2.10)

$$H_K = \sum_{\mu,\lambda,\nu=0}^{3} \sum_{k,k'} J^{kk'}_{\mu\lambda\nu}\, \hat{\Phi}^\dagger \left(\hat{\tau}^\mu \otimes \hat{\tau}^\nu\right) \hat{\Phi}\, \hat{\Psi}^\dagger_k \left(\hat{\sigma}^\lambda \otimes \hat{\sigma}^\nu\right) \hat{\Psi}_{k'} \tag{3.1}$$

The current operator is defined as an electric charge flow out of the source reservoirs

$$\hat{j} = -e\frac{\partial}{\partial t} \sum_k \hat{\Psi}^\dagger_{sk} \hat{\Psi}_{sk} \tag{3.2}$$

It should be pointed out that in the effective Hamiltonian (3.1) only the mode $\hat{\Psi}_k$ appears, while in the current operator explicitly the field $\hat{\Psi}^\dagger_{sk}$ in the source reservoir enters. These fields are connected by the linear combinations (2.8) and (2.9) chosen as basis in chapter 2.1.2

$$\hat{\Psi}_k = \frac{T^s_k}{T_k}\hat{\Psi}_{sk} + \frac{T^d_k}{T_k}\hat{\Psi}_{dk},$$

$$\hat{\Xi}_k = \frac{T^d_k}{T_k}\hat{\Psi}_{sk} - \frac{T^s_k}{T_k}\hat{\Psi}_{dk}.$$

Calculating the expectation value for j by evaluating the commutator of the of the Hamiltonian (3.1) with the occupation operator in (3.2) we get

$$\begin{aligned}\hat{j} &= -ie \left[\sum_{\mu,\lambda,\nu=0}^{3} \sum_{p,p'} J^{pp'}_{\mu\lambda\nu}\, \hat{\Phi}^\dagger \left(\hat{\tau}^\mu \otimes \hat{\tau}^\nu\right) \hat{\Phi}\, \hat{\Psi}^\dagger_p \left(\hat{\sigma}^\lambda \otimes \hat{\sigma}^\nu\right) \hat{\Psi}_{p'}, \sum_k \hat{\Psi}^\dagger_{sk} \hat{\Psi}_{sk} \right] \\ &= -ie \sum_{\mu,\lambda,\nu=0}^{3} \sum_{p,p'} J^{pp'}_{\mu\lambda\nu}\, \hat{\Phi}^\dagger \left(\hat{\tau}^\mu \otimes \hat{\tau}^\nu\right) \hat{\Phi} \left[\hat{\Psi}^\dagger_p \left(\hat{\sigma}^\lambda \otimes \hat{\sigma}^\nu\right) \hat{\Psi}_{p'}, \sum_k \hat{\Psi}^\dagger_{sk} \hat{\Psi}_{sk} \right]\end{aligned} \tag{3.3}$$

since the operators of the reservoirs and the dots commute.

To calculate the commutator we need the relation between $\hat{\Psi}_k$ and $\hat{\Psi}_{sk}$ given by (2.8)

$$\begin{aligned}&\left[\hat{\Psi}^\dagger_p \left(\hat{\sigma}^\lambda \otimes \hat{\sigma}^\nu\right) \hat{\Psi}_{p'}, \sum_k \hat{\Psi}^\dagger_{sk} \hat{\Psi}_{sk} \right] \\ &\quad = \sum_k \Bigg\{ \left(\frac{T^s_p}{T_p} \hat{\Psi}^\dagger_{sp} + \frac{T^d_p}{T_p} \hat{\Psi}^\dagger_{dp} \right) \left(\hat{\sigma}^\lambda \otimes \hat{\sigma}^\nu\right) \left(\frac{T^s_{p'}}{T_{p'}} \hat{\Psi}_{sp'} + \frac{T^d_{p'}}{T_{p'}} \hat{\Psi}_{dp'} \right) \hat{\Psi}^\dagger_{sk} \hat{\Psi}_{sk} \\ &\qquad - \hat{\Psi}^\dagger_{sk} \hat{\Psi}_{sk} \left(\frac{T^s_p}{T_p} \hat{\Psi}^\dagger_{sp} + \frac{T^d_p}{T_p} \hat{\Psi}^\dagger_{dp} \right) \left(\hat{\sigma}^\lambda \otimes \hat{\sigma}^\nu\right) \left(\frac{T^s_{p'}}{T_{p'}} \hat{\Psi}_{sp'} + \frac{T^d_{p'}}{T_{p'}} \hat{\Psi}_{dp'} \right) \Bigg\} \\ &\qquad\quad = \frac{T^s_p}{T_p} \frac{T^s_{p'}}{T_{p'}} \left\{ \hat{\Psi}^\dagger_{dp} \left(\hat{\sigma}^\lambda \otimes \hat{\sigma}^\nu\right) \hat{\Psi}_{sp'} - \hat{\Psi}^\dagger_{sp} \left(\hat{\sigma}^\lambda \otimes \hat{\sigma}^\nu\right) \hat{\Psi}_{dp'} \right\}\end{aligned} \tag{3.4}$$

This result enables us to rewrite the current operator in a comprehensible form as the difference of the source-drain current and the current in the opposite direction

$$\hat{j} = \hat{j}_{sd} - \hat{j}_{ds}$$

with

$$\hat{j}_{sd} = -ie \sum_{\mu,\lambda,\nu=0}^{3} \hat{\Phi}^\dagger \left(\hat{\tau}^\mu \otimes \hat{\tau}^\nu\right) \hat{\Phi} \sum_{k,k'} J^{kk'}_{\mu\lambda\nu} \frac{T^s_k}{T_k} \frac{T^s_{k'}}{T_{k'}} \hat{\Psi}^\dagger_{dk} \left(\hat{\sigma}^\lambda \otimes \hat{\sigma}^\nu\right) \hat{\Psi}_{sk'}. \tag{3.5}$$

As in section 2.3 the Kondo coupling constants $J^{kk'}_{\mu\lambda\nu}$ are assumed independent of the wave vectors k and k' and their indices are therefore omitted again: $J^{kk'}_{\mu\lambda\nu} \to J_{\mu\lambda\nu}$.

In equation 3.5 the fields $\hat{\Psi}_{sk}$ and $\hat{\Psi}_{dk}$ in the source and drain reservoirs enter into the calculation of the current. But it has been shown in the previous chapter that it is only the field $\hat{\Psi}_k$ that couples to the double dot. Therefore only this field enters the renormalization flow of the coupling constants. To respect this we change our basis again back to the mode $\hat{\Psi}_k$ and

its orthogonal mode $\hat{\Xi}_k$, defined by (2.9)

$$\hat{\Xi}_k = \frac{T_k^d}{T_k}\hat{\Psi}_{sk} - \frac{T_k^s}{T_k}\hat{\Psi}_{dk}.$$

In this basis the current through the double dot system (3.5) reads

$$\hat{j} = -ie \sum_{\mu,\lambda,\nu=0}^{3} J_{\mu\lambda\nu}\hat{\Phi}^\dagger \left(\hat{\tau}^\mu \otimes \hat{\tau}^\nu\right)\hat{\Phi}\times \\ \times \sum_{k,k'} \frac{T_k^s}{T_k}\frac{T_{k'}^s}{T_{k'}} \left\{\hat{\Psi}_k^\dagger \left(\hat{\sigma}^\lambda \otimes \hat{\sigma}^\nu\right)\hat{\Xi}_{k'} - \hat{\Xi}_k^\dagger \left(\hat{\sigma}^\lambda \otimes \hat{\sigma}^\nu\right)\hat{\Psi}_{k'}\right\}. \quad (3.6)$$

In what follows Eq. (3.6) is used in the explicit calculations of the current.

3.2 Transport Calculations

The current at finite transport voltages is calculated in the Keldysh formalism, see [31] for a presentation of the method.

In this formalism the unperturbed Green functions in the source and the drain read

$$\hat{G}_{s,d}(\epsilon,k) = \begin{pmatrix} G_{s,d}^R(\epsilon,k) & G_{s,d}^K(\epsilon,k) \\ 0 & G_{s,d}^A(\epsilon,k) \end{pmatrix}, \quad (3.7)$$

where G^R denotes the retarded Green function, G^A the advanced and G^K the Keldysh Green function, see [31].

Analog to the propagators of the fields (2.11) the unperturbed retarded and advanced Green functions in (3.7) are

$$G_{s,d}^{R/A}(\epsilon,k) = \frac{1}{\epsilon - \xi_k^{sd} \pm i\,o}\mathsf{P}_{s,d}(k) \quad (3.8)$$

with

$$\mathsf{P}_{s,d}(k) = \begin{pmatrix} \cos^2\eta_k^{s,d} & \cos\eta_k \sin\eta_k^{s,d} \\ \cos\eta_k^{s,d}\sin\eta_k & \sin^2\eta_k^{s,d} \end{pmatrix} \otimes \mathsf{1}_2 \quad (3.9)$$

describing the matrix structure of the tunneling interaction, as in Eq. (2.12). $G_{s,d}^K$ is the Keldysh component of the Green function (3.7), parametrized by

$$G_{s,d}^K(\epsilon,k) = \tanh\left(\frac{\epsilon-\mu_{s,d}}{2T}\right)\left(G_{s,d}^R - G_{s,d}^A\right).$$

Like in section 2.3 the total tunneling probabilities $|T_k^r|^2$ from a given reservoir into the the double dot are assumed to be k-independent for energies close to

the Fermi level of the reservoir $T_k^r = T^r$. The total tunneling rate is denoted by $T_0 = (T^s)^2 + (T^d)^2$ (not to be confused with the temperature T). Using the chosen basis $\hat{\Psi}_k$ and Ξ_k, (2.8, 2.9), we can express the unperturbed Green functions as

$$\begin{aligned}
\mathcal{G}_0 &= -i\langle \Psi_k \Psi_k^\dagger \rangle_0 = -i\left(\frac{(T^s)^2}{T_0^2} \langle \Psi_{sk} \Psi_{sk}^\dagger \rangle + \frac{(T^d)^2}{T_0^2} \langle \Psi_{dk} \Psi_{dk}^\dagger \rangle \right) \\
&= \frac{(T^s)^2}{T_0^2} G_s + \frac{(T^d)^2}{T_0^2} G_d, \qquad (3.10) \\
\mathcal{K}_0 &= -i\langle \Xi_k \Psi_k^\dagger \rangle_0 \\
&= \frac{T^s T^d}{T_0^2} (G_s - G_d), \qquad (3.11) \\
g_0 &= -i\langle \Xi_k \Xi_k^\dagger \rangle_0 \\
&= \frac{(T^s)^2}{T_0^2} G_s + \frac{(T^d)^2}{T_0^2} G_d. \qquad (3.12)
\end{aligned}$$

In what follows symmetric couplings to source and drain reservoir are assumed, that is $T_{ik}^s = T_{ik}^d$. In this case the retarded and advanced components $\mathcal{K}^{R/A}$ vanish, as can be seen from (3.11). The only non-vanishing component of $\mathcal{K}_0$ is

$$\mathcal{K}^K(\epsilon, k) = -2\pi i \frac{T^s T^d}{T_0^2} \left[\tanh\left(\frac{\epsilon - \mu_s}{2T} \right) - \tanh\left(\frac{\epsilon - \mu_d}{2T} \right) \right] \delta(\epsilon - \xi_k) \qquad (3.13)$$

3.2.1 Lowest order correction

The diagram corresponding to the lowest order correction of the current is shown in Fig. 3.1. An explanation of the elements used in the diagram is given in table 3.1.

Evaluating the diagram shown in Fig. 3.1 leads to the expression

$$\int \frac{d\epsilon\, d\omega_1\, d\omega_2}{(2\pi)^3} \int (dk)_0 (dk')_0 \sum_a \sum_{\mu \neq \nu} \mathrm{tr}\left\{ \gamma^a \mathcal{G}(\epsilon, k) \gamma^\mu \mathcal{K}(\epsilon + \omega_1 - \omega_2, k') \right\} \times \\ \times \mathrm{tr}\left\{ \gamma^a \mathcal{D}(\omega_1) \gamma^\nu \mathcal{D}(\omega_2) \right\}. \qquad (3.14)$$

This integral (3.14) will be solved for different values of a, μ, ν

Let us consider the case $a = 0, \mu = 1, \nu = 0$ as an example. Evaluating the matrix structure of the integrand gives

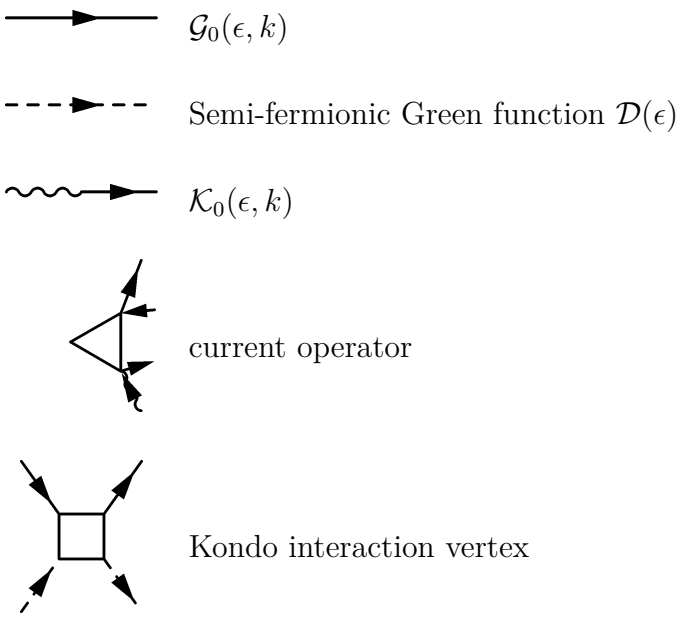

Table 3.1: Elements used in the current diagrams

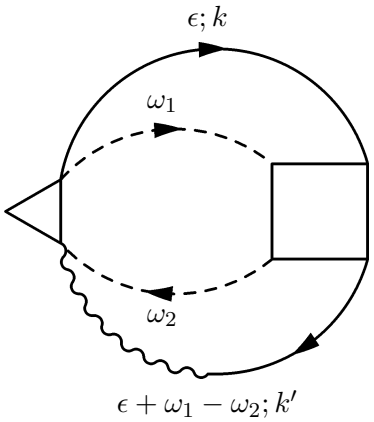

Figure 3.1: Lowest order nonzero contribution to the current through the dot

$$\mathrm{tr}\left\{\mathcal{G}\gamma^1\mathcal{K}\right\} = \mathrm{tr}\left\{ \begin{pmatrix} \mathcal{G}^R & \mathcal{G}^K \\ 0 & \mathcal{G}^A \end{pmatrix} \begin{pmatrix} 0 & 1 \\ 1 & 0 \end{pmatrix} \begin{pmatrix} \mathcal{K}^R & \mathcal{K}^K \\ 0 & \mathcal{K}^A \end{pmatrix} \right\} \tag{3.15}$$

$$= \mathrm{tr}\left\{\mathcal{G}^K\mathcal{K}^R + \mathcal{G}^A\mathcal{K}^K\right\} \tag{3.16}$$

$$= \mathrm{tr}\left\{\mathcal{G}^A\mathcal{K}^K\right\} \tag{3.17}$$

since $\mathcal{K}^R = 0$ because of $\eta_k^s = \eta_k^d$, as mentioned above. The trace over the semi-fermionic Green function $\mathcal{D}$ gives

$$\mathrm{tr}\left\{\mathcal{D}\mathcal{D}\right\} = \mathrm{tr}\left\{\mathcal{D}^R\mathcal{D}^R + \mathcal{D}^A\mathcal{D}^A\right\} \tag{3.18}$$

Using (3.17), (3.18) and the definitions (3.7) – (3.13), Eq. (3.14) expands to

$$\begin{aligned} &\int \frac{d\epsilon\, d\omega_1\, d\omega_2}{(2\pi)^3} \int (dk)_0 (dk')_0 \frac{1}{\epsilon - \xi_k - i0} (-2\pi i) \frac{T^s T^d}{T_0^2} \times \\ &\qquad \times \left[\tanh\left(\frac{\epsilon + \omega_1 - \omega_2 - \mu_s}{2T}\right) - \tanh\left(\frac{\epsilon + \omega_1 - \omega_2 - \mu_d}{2T}\right)\right] \times \\ &\times \delta(\epsilon + \omega_1 - \omega_2 - \xi_{k'}) \left[\frac{1}{\omega_1 + io}\frac{1}{\omega_2 + io} + \frac{1}{\omega_1 - io}\frac{1}{\omega_2 - io}\right] \mathrm{tr}\left\{\mathsf{P}^2\right\}. \end{aligned} \tag{3.19}$$

In the following we express the Fermi levels of the source and drain reservoirs through the transport voltage V by

$$\mu_s = \frac{1}{2}eV \tag{3.20}$$

$$\mu_d = -\frac{1}{2}eV. \tag{3.21}$$

Carrying out the integrations under the assumption that transport voltage is larger then the temperature energy scale $eV/2 > T$ and using the approximation (see Fig. 3.2)

$$\int d\epsilon \left[\tanh\left(\frac{\epsilon + \mu}{2T}\right) - \tanh\left(\frac{\epsilon - \mu}{2T}\right)\right] \approx \int_{-2T}^{2T} d\epsilon \left[\frac{\epsilon + \mu}{2T} - \frac{\epsilon - \mu}{2T}\right] = 4\mu. \tag{3.22}$$

expression (3.14) finally yields

$$\pi\nu_0^2 \frac{T^s T^k}{T^2} \left(\frac{1}{2} + 2b_1^2\right) eV. \tag{3.23}$$

The term inside the brackets results from the trace

$$\mathrm{tr}\left\{\mathsf{P}^2\right\} = \mathrm{tr}\begin{pmatrix} \frac{1}{2} & b_1 \\ b_1 & \frac{1}{2} \end{pmatrix}^2 = \frac{1}{2} + 2b_1^2$$

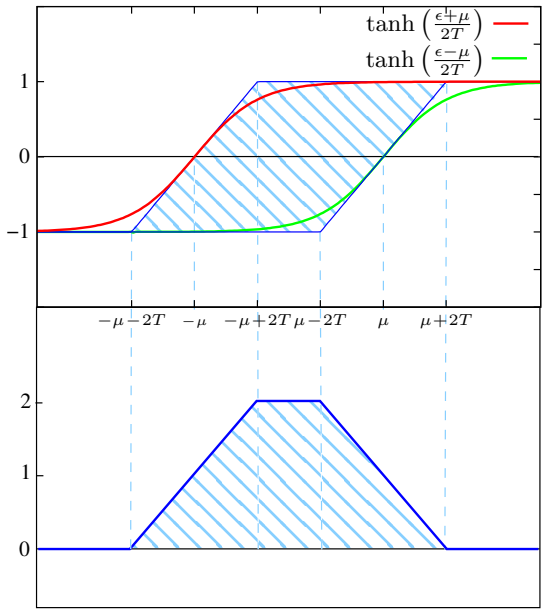

Figure 3.2: Approximation by linearizing the tangens hyperbolicus. The hatched area corresponds to the integral in Eq. 3.22. Upper figure: The exact values of the tangens hyperbolicus are lined in red and green, the linearization in blue. Lower figure: The difference between the linearized tangens hyperbolicus, the hatched area equals 4μ. In the limit $T \to 0$ the approximation gets exact.

where b_1 enters through the averaging over the wave vectors, like described in Sec. 2.3.2.

Other cases of a, μ and ν contribute in a similar way and eventually we end up with

$$j(V) = 40\pi e^2 V \nu_0^2 \frac{(T^s)^2 (T^d)^2}{T_0^4} \sum_{\lambda,\mu,\nu} J_{\lambda\mu\nu}^2 \left(\frac{1}{2} + 2b_1^2\right) \tag{3.24}$$

3.3 Results

The result for the current through the double dot system $j(V)$, Eq. (3.24),

$$j(V) = 40\pi e^2 V \nu_0^2 \frac{(T^s)^2 (T^d)^2}{T_0^4} \sum_{\lambda,\mu,\nu} J_{\lambda\mu\nu}^2 \left(\frac{1}{2} + 2b_1^2\right)$$

consists of three different factors:

- The prefactor, mainly containing the density of states in the reservoirs ν_0, the transport voltage V and the tunneling amplitudes T^s and T^d between the double dots and the source and drain reservoirs,
- the sum of the squares of the coupling constants $\sum_{\lambda,\mu,\nu} J^2_{\lambda\mu\nu}$
- and a factor containing the mixing parameter $\frac{1}{2} + 2b_1^2$

Let us take a closer look at the role of the last two factors. The sum over the coupling constants $\sum_{\lambda,\mu,\nu} J^2_{\lambda\mu\nu}$ obviously represents the spin and orbital Kondo effect, as these quantities are generated during the renormalization group transformation. It is important to note that the coupling constants also depend on the mixing parameter b_1: $J_{\lambda\mu\nu} = J_{\lambda\mu\nu}(b_1)$.

3.3.1 Comparison to the double slit experiment

To elucidate the role of the factor $\frac{1}{2} + 2b_1^2$, let us remind of the physical meaning of the mixing parameter b_1. As explained in Sec. 2.3.2 the limiting cases $b_1 = 0$ and $b_1 = \frac{1}{2}$ correspond to the physical situations of separate reservoirs for each dot, respectively a common reservoir for both dots.

Let us ignore for a moment the Kondo correlations in the system. For $b_1 = 0$, the system splits into two completely decoupled current channels. Each channel consists of a source, a quantum dot and a drain. The partial currents through the now non-interacting reservoir-dot systems would simply add to a total current j_0. This situation is depicted in Fig. 3.3.

In the other limiting case, $b_1 = \frac{1}{2}$, which corresponds to common source and drain reservoirs to the double dot, the resulting geometry of the setup can be interpreted as an analogon to the double slit experiment: In the classical case the intensity I caused by the amplitudes $A_1 = A_2 = A$ of the single slits sum up to

$$I_c = |A_1|^2 + |A_2|^2 = 2|A|^2.$$

In the quantum mechanical case of constructive interference we have

$$I_q = |A_1 + A_2|^2 = |A_1|^2 + |A_2|^2 + 2|A_1 A_2| = 4|A|^2 = 2I_c.$$

Due to single particle interference effects the intensity in the central maximum appears by a factor two larger than the expected value of a classical calculation. If we take a look at the factor $\frac{1}{2} + 2b_1^2$ we find the same behavior. For $b_1 = 0$ this factor gives $\frac{1}{2}$, a value of $b_1 = \frac{1}{2}$ results in $\frac{1}{2} + 2b_1^2 = 1$, reproducing the factor two of the interference effect in the double slit experiment. Compared to the situation $b_1 = 0$, we would expect a total current of $2j_0$ for $b_1 = \frac{1}{2}$. This situation is sketched in Fig. 3.4. Decreasing b_1 from this value

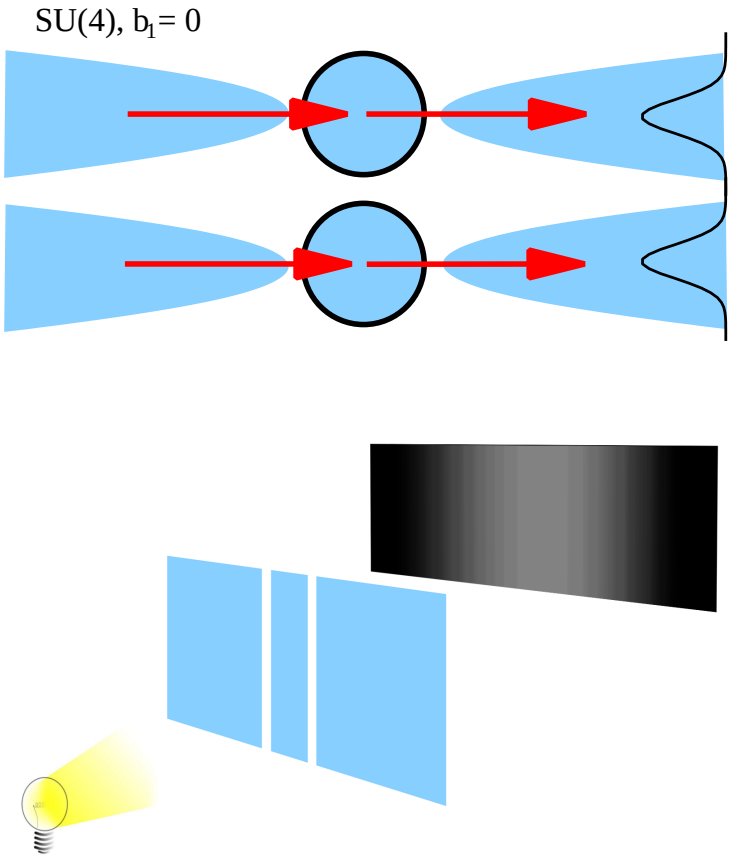

Figure 3.3: Origin of the $\frac{1}{2} + 2b_1^2$ term in the expression for the total current for the limiting case $b_1 = 0$. Separated reservoirs result in a simple addition of the partial currents through the upper and lower dot. This corresponds to a double-slit experiment, in which *no* interference effects are observed. Both partial intensities simply add up to a total intensity.

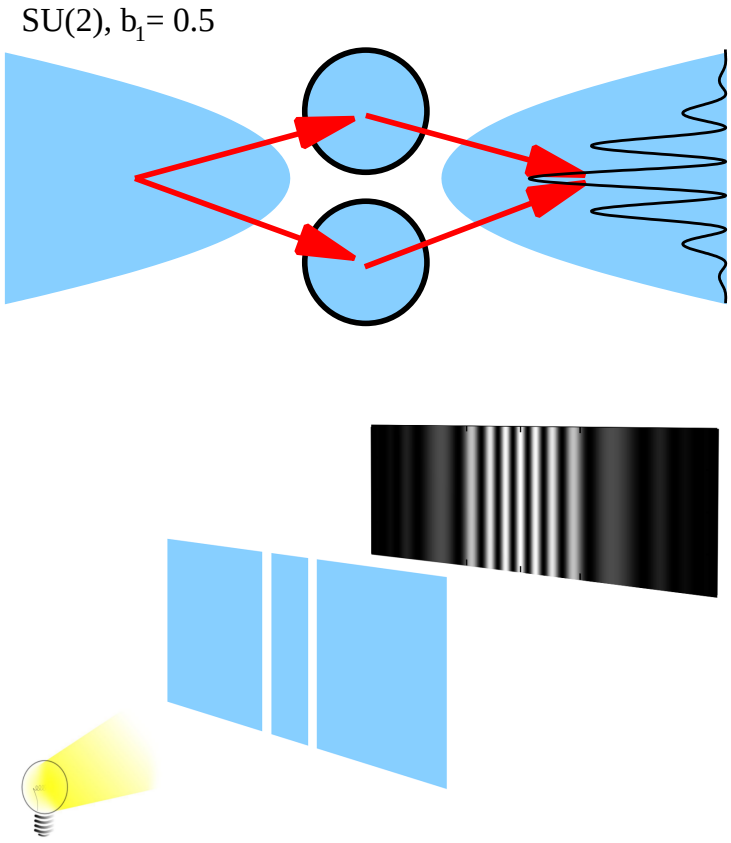

Figure 3.4: $b_1 = \frac{1}{2}$, meaning common reservoirs, gives rise to a single-particle interference term. In case of a constructive interference, as in the central maximum of the the interference pattern of a quantum mechanical double-slit experiment, this results in doubling the Intensity, compared to the case without interference.

we can gradually suppress the interference effect, returning to the classical value j_0.

Now let us take into account again that the coupling constants $J_{\lambda\mu\nu}$ also depend on the mixing parameter b_1. The different setups also show different Kondo correlations. A value of the mixing parameter $b_1 = 0$ means strong orbital fluctuations and therefore the SU(4) Kondo effect, while these fluctuations are suppressed at $b_1 = \frac{1}{2}$, reducing the system to a SU(2) Kondo effect. As the coupling constants $J_{\lambda\mu\nu}$ also enter the total current (3.24) the Kondo correlations will also affect the conductance through the dot and cause deviations from the quadratic b_1 behavior, predicted by the factor $\frac{1}{2} + 2b_1^2$.

3.3.2 Temperature dependence

Far away from the Kondo temperature $T \gg T_K$ the deviations due to Kondo correlations surely will be small and one would expect the quadratic b_1 dependency. Approaching T_K the correlations will gain in significance and close to T_K they will dominate the current through the double dot.

This behavior can be seen in Fig. 3.6 to 3.9. These Figures depict the results of calculations in which the temperature is taken into account by aborting the flow of the coupling constants before they diverge at the critical energy Λ_c.

To justify this approach let us remind of the principle of the renormalization group analysis: The renormalization of the system by integration out an energy shell led to the flow equations, which describe the behavior of the coupling constants as a function of an energy cutoff Λ. As the energy cutoff runs down the coupling constants increase and finally grow above the limits where they can be treated perturbativly. In fact they diverge at a finite critical energy Λ_c which we associate with the Kondo temperature T_K.

In this meaning the flow of the coupling constants can be physically interpreted as cooling the system down to T_K, as we can associate the running energy cutoff Λ during the renormalization with a corresponding running temperature $T(\Lambda)$. The values of the coupling constants can be taken as their values above the Kondo temperature. This approach is certainly not an exact consideration of the temperature, but the results are good enough to demonstrate the deviations from the quadratic behavior, if not taken too far away from or too close to the Kondo temperature. In the first case the system is simply not governed by Kondo physics, in the second the perturbative approach behind the scaling analysis breaks together.

The calculations have been done using two different methods:

1. The critical energy $\Lambda_{c,SU(4)}$ has been calculated at the SU(4) point.

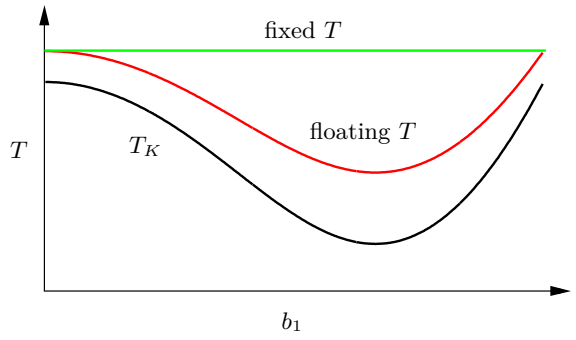

Figure 3.5: Sketch of the temperature behavior for the two methods used

Using a parameter $p < 1$ an abortion energy $\Lambda_a = \exp(-p\, l_{c,SU(4)})$ is calculated, where $l_{c,SU(4)})$ is the critical running logarithmic energy scale[1], at wich the renormaization calculations diverge. The parameter p is an exponential measure of how close the system is to the Kondo temperature, which it reaches for $p = 1$. This abortion energy Λ_a is held constant during the calculations for different values of the mixing parameter b_1. These results are labeled "fixed" in the graphs, as this can be interpreted as a constant temperature for all values of b_1.

2. Like in the first approach a parameter p is defined, but this time the abortion energy is recalculated for each value of the mixing parameter b_1 by $\Lambda_a = \exp(-p\, l_{c,SU(4)}(b_1))$. This is done to keep the system in a constant distance to the Kondo temperature, and therefore having it in the same regime for all values of b_1. These results are labeled as "floating"

The situation with a fixed abortion energy corresponds to a fixed temperature during the b_1 sweep. This would probably the experimentally relevant situation for systems undergoing such a transition from a SU(4) to a SU(2) Kondo-effect.

Tracking the the Kondo-temperature during the b_1 sweep with a floating abortion energy is on the other hand theoretically interesting, since we keep the system at a constant relative distance to the Kondo-temperature.

These two situations are sketched in Fig. 3.5 As one can see in Fig. 3.6 for temperatures far away from the Kondo temperature both methods show

[1]The author apologizes for the ambiguity in the use of the letter Λ for the real and the logarithimic energy scale in this and the previous chapter.

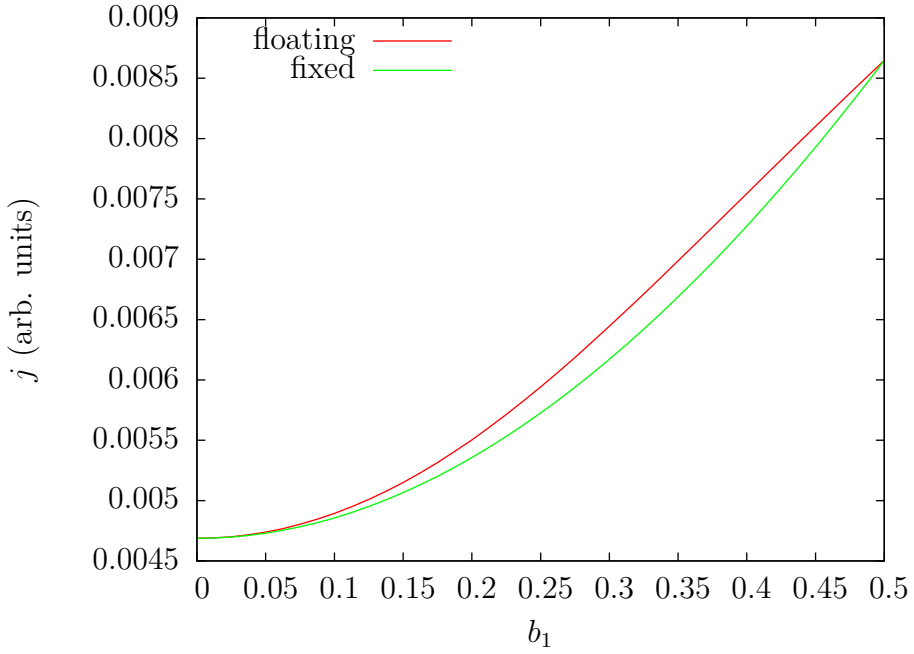

Figure 3.6: Current dependency on b_1 far away from the Kondo temperature, $p = 0.60$, good agreement to the parabolic behaviour due to the $\frac{1}{2} + 2b_1^2$ term.

good agreement with the expected parabolic behavior. The current increases monotonously with b_1 corresponding to the increase in intensity in the double slit experiment due to single-particle interference effects.

In Fig. 3.7 p is increased to 0.854. The calculations for floating temperature start to show distinct deviations from the quadratic behaviour, while those for fixed temperature still are in good agreement with it. As expected the results differ most in the regions where the abortion energy Λ_c differs most for both methods, namely in the vicinity of $b_{1,\mathrm{min}}$, where the Kondo temperature reaches its minimum.

This trend continues for $p = 0.931$, shown in Fig. 3.8. Now the results for floating temperature are governed by the Kondo correlations which destroys the monotonic increase of the single-particle interference term. The suppression of the pseudo-spin correlations for larger values of b_1 leads to a suppression of the current. As for large values of p also the differences between both calculation methods enhances, the values for fixed temperature develop a minimum and those for floating temperatures a maximum to keep their large difference at $b_{1,\mathrm{min}}$.

Finally, for $p = 0.990$ the parabolic b_1 behavior has completely vanished. The Kondo correlations now completely determine the current characteristics.

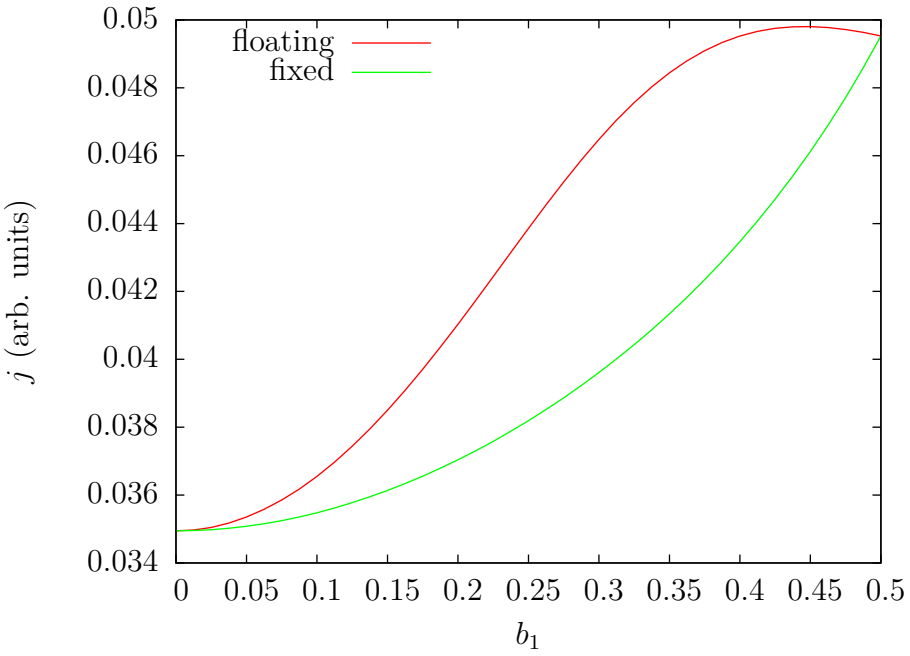

Figure 3.7: Current dependency on b_1 for $p = 0.854$

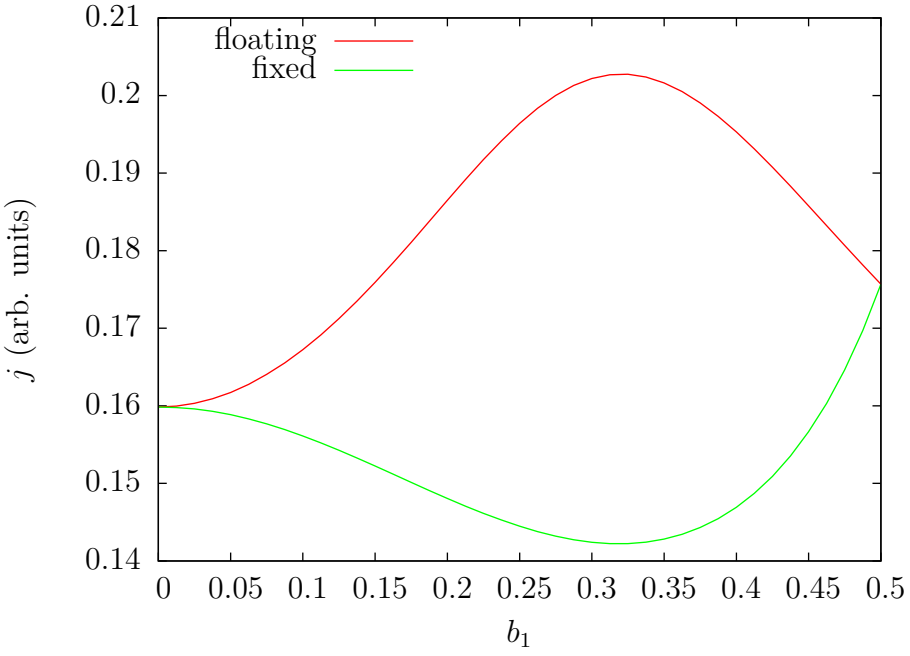

Figure 3.8: Current dependency on b_1 for $p = 0.931$

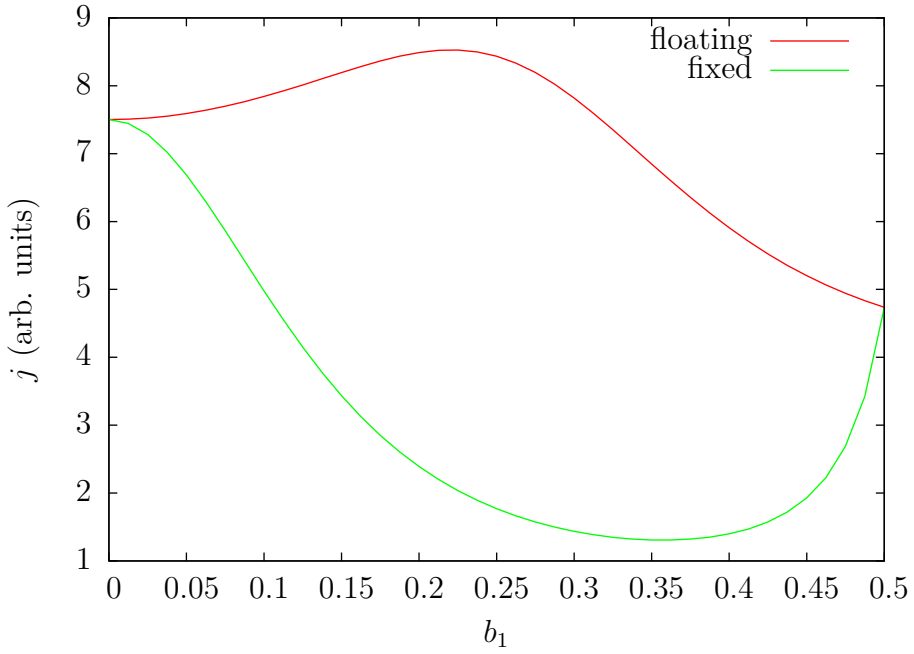

Figure 3.9: Current dependency on b_1 close to the Kondo temperature, $p = 0.990$

The suppression of the orbital Kondo effect pushes the current below its value at the SU(4) point. The difference for both methods increases further as the coupling constants $J_{\mu\lambda\nu}$ get closer to the divergence at T_K. This also marks the breakdown of the perturbative calculations, and therefore these results close to the Kondo temperature should be treated with care.

These results are summarized in Fig. 3.10. Here is the dependency of j on b_1 and p combined in one graph. To illustrate the qualitative behavior, the current is normalized to $j(b_1 = 0)$ for constant values of p. The graph would otherwise be dominated by the enormous increase of the coupling constants as p goes to 1, resulting in a divergence when the Kondo-temperature is eventually reached. The previous graphs displayed in Fig. 3.6–3.9 are qualitatively cuts parallel to the b_1 axis at different values of p.

The parameter p is increased from 0.6 to 0.99 from back to front in this illustration. Again one can clearly see that both start with basically the same parabolic behavior for temperatures far away from the Kondo-temperature, developing the characteristic minimum (respectively maximum) for the different cases of the keeping the temperature constant during the b_1 sweep (respectively tracking the Kondo-temperature).

fixed floating

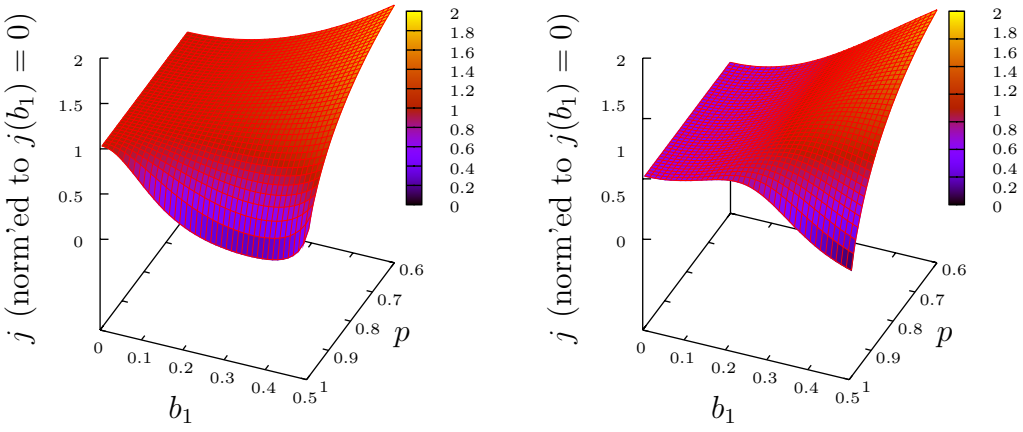

Figure 3.10: Current dependency on b_1 and p, normalized for each p to $j(b_1 = 0)$

Chapter 4

Conclusion

In this work we have considered the transition from a SU(4) spin and orbital Kondo effect to a SU(2) spin Kondo effect in a double quantum dot system connected in parallel to metallic reservoirs with spin and orbital degenerate ground state. The transition is driven by fluctuations of the orbital degree of freedom, described by a mixing parameter b_1. $b_1 = 0$ means asymmetric coupling of the different electronic modes in the reservoir to just one of the dots and thereby strong fluctuations, causing the additional orbital Kondo effect, while $b_1 = 0.5$ strictly symmetric coupling of the electronic modes in the reservoirs to both dots and therefor suppression of the orbital fluctuations, leaving us with a purely SU(2) spin Kondo system.

Although a greatly enhanced Kondo effect is predicted for the SU(4) configuration, we found the Kondo temperature T_K to be exactly the same for both symmetry points. The reason for this behavior is the decomposition of the common reservoirs for both dots into separate reservoirs for each dot in the case of strong fluctuations, resulting an halved density of states, which exactly compensates the enhancement of the Kondo effect in the SU(4) geometry.

In the intermediate regime ($0 < b_1 < 0.5$) between the defined symmetry points we found a diminished Kondo temperature, reaching a minimum at $b_1 \approx 0.33$. This can be understood in the picture of transport channels. No fluctuations ($b_1 = 0.5$) means that the antisymmetric ground state in the double dot system is completely decoupled from the reservoirs. But driving the system just a bit out of this symmetry point (b_1 slightly below 0.5) means a small, but non-vanishing probability for an electron to tunnel through the antisymmetric transport channel. These events have a destructive effect on the spin Kondo effect: The weak coupling suppresses the spin Kondo effect for this channel itself, the Coulomb blockade blocks the transport though the strong coupling symmetric channel, the weak coupling causes a long lifetime

of these states. Decreasing b_1 further enhances the orbital Kondo effect, which eventually restores the Kondo temperature $T_K^{\mathrm{SU(2)}}$ in the SU(4) point for $b_1 = 0$.

Although in our system the Kondo temperature for both symmetries is exactly the same, $T_K^{\mathrm{SU(2)}} = T_K^{\mathrm{SU(4)}}$, they are easily distinguishable by their behaviour in an external Zeeman field. We studied the impact of an in plane Zeeman field and found the expected behavior: While in the SU(4) point the spin Kondo effect is suppressed by the external field, resulting in the reduced Kondo temperature of a spin Kondo system, the suppression of the spin Kondo effect in the SU(2) point leaves us with a system without any Kondo correlations.

In the second part we calculated the differential conductance through the double dot as a function of the mixing parameter b_1. It turned out that the conductance is subject to the interplay of two opposing effects. First, the single particle coherence is increased with b_1. In the picture of a double slit experiment this means that the interference terms cause a quadratic increase of the differential conductance with b_1. Contrariwise we lose the pseudo spin Kondo correlations of the orbital Kondo effect with increasing b_1.

We calculated the differential conductance through the double dot as a function of b_1 and different temperatures for two scenarios: A constant ratio of the temperature and the Kondo temperature of the system (which is also a function of b_1), which emphasizes the interplay of the two factors for different regimes, and the experimental important case of a fixed temperature for the whole b_1 sweep. In both cases we found that far away from the Kondo temperature the increase of the single particle coherence is the dominant effect. Approaching T_K we found increasing strong deviations from the quadratic b_1 behaviour caused by the Kondo effect, leading to a similar non-monotonous behaviour as for T_K. Close to the Kondo temperature the differential conductance is still non-monotonous, but as the differential conductance for the SU(2) point is below that of the SU(4) point, we are clearly in a regime where the suppression of the orbital Kondo effect plays the dominant role.

Appendix A

Mathematica programs used for the decompositon of the Kondo Hamiltionian

■ Definitions

■ Definition of tensor product (CircleTimes) and matrix product (CenterDot)

```
ClearAll[CircleTimes, CenterDot];

SumIndexNr = 1;
```

assign associative law to matrix– and tensor product

```
SetAttributes[CircleTimes, Flat];
SetAttributes[CircleTimes, OneIdentity];
SetAttributes[CircleTimes, Listable];
SetAttributes[CenterDot, Flat];
SetAttributes[CenterDot, OneIdentity];
SetAttributes[CenterDot, Listable];

Default[CircleTimes] = 1;
Default[CenterDot] = 1;
```

matrix product of Pauli matrices σ[i], i=0,...,3, where σ[0]=IdentityMatrix[2]

```
CenterDot[σ[n_], σ[m_]] := δ[m, n] σ[0] + δ[n, 0] β[m, 0] σ[m] + δ[m, 0] β[n, 0] σ[n]
     + i ϵ[n, m, C[SumIndexNr]] σ[C[SumIndexNr++]];
```

defining a 'normal ordering' of the non–commutative matrix products

```
CenterDot[b_, a_] :=
  CenterDot[a, b] /; (b[[0]] === σ && FreeQ[a, σ] && FreeQ[a, CircleTimes]);
CenterDot[b_, a_] := CenterDot[a, b] /;
    (b[[0]] === CircleTimes && FreeQ[a, CircleTimes]);
```

distributive law considering normal ordering

```
CenterDot[a_, b_] := Plus @@ (CenterDot[List @@ a, b]) /; (a[[0]] === Plus);
CenterDot[b_, a_] := CenterDot[a, b] /; (b[[0]] =!= Plus && a[[0]] === Plus);
```

extract scalar factors from matrix products, considering normal ordering

```
CenterDot[a_, b_] :=
  Times[DeleteCases[a, _σ], CenterDot[CenterDot @@ Cases[a, _σ], b]] /;
    (a[[0]] === Times && Count[a, _σ] ≠ 0);
CenterDot[b_, a_] :=
  CenterDot[a, b] /; (b[[0]] =!= Times && a[[0]] === Times && Count[a, _σ] ≠ 0);
CenterDot[a_, b_] := Times[DeleteCases[a, _CircleTimes],
     CenterDot[CenterDot @@ Cases[a, _CircleTimes], b]] /;
    (a[[0]] === Times && Not[FreeQ[a, _CircleTimes]]);
CenterDot[b_, a_] := CenterDot[a, b] /;
    (b[[0]] =!= Times && a[[0]] === Times && Not[FreeQ[a, _CircleTimes]]);
```

(a ⊗ b).(c ⊗ d) → (a.c) ⊗ (b.d), where '.' denotes the matrix product

```
CenterDot[a_, b_] := Inner[CenterDot, List @@ a, List @@ b, CircleTimes] /;
    (a[[0]] === CircleTimes && b[[0]] === CircleTimes);
```

in tensor products reorder Pauli matrices to the right

```
CircleTimes[b_, a_, c_.] := CircleTimes[a, b, c] /;
    (b[[0]] === σ && FreeQ[a, σ]);
```

distributive law considering normal ordering

```
CircleTimes[a_, b_] := Plus @@ (CircleTimes[List @@ a, b]) /;
    (a[[0]] === Plus);
CircleTimes[b_, a_] := CircleTimes[a, b] /;
    (b[[0]] =!= Plus && a[[0]] === Plus);
```

extract scalar factors from tensor products, considering normal ordering

```
CircleTimes[a_, b_] :=
  Times[DeleteCases[a, _σ], CircleTimes[CircleTimes @@ Cases[a, _σ], b]] /;
    (a[[0]] === Times && Not[FreeQ[a, _σ]]);
CircleTimes[b_, a_] := CircleTimes[a, b] /;
    (b[[0]] =!= Times && a[[0]] === Times && Not[FreeQ[a, _σ]]);
```

■ Definition of Kronecker delta and Levi−Civita tensor

the Kronecker delta

```
SetAttributes[δ, Orderless];
δ[a_Integer, b_Integer] := KroneckerDelta[a, b];
δ[a_, a_] := 1;
δ[a_, b_]^:= δ[a, b];
δ[0, _λ] := 0;
```

define the tensor β as 1−δ

```
SetAttributes[β, Orderless];
β[a_Integer, b_Integer] := 1 - KroneckerDelta[a, b];
β[a_, a_] := 0;
β[a_, b_]^:= β[a, b];
β[0, _λ] := 1;
```

the Levi−Civita tensor

```
ϵ[a_Integer, b_Integer, c_Integer] := Signature[{a, b, c}] /; (a ≠ 0 && b ≠ 0 && c ≠ 0);
ϵ[a_, b_, c_] := 0 /; (a == b || a == c || b == c);
ϵ[a_, b_, c_] := 0 /; (a == 0 || b == 0 || c == 0);
ϵ[b_, a_, c_] := -ϵ[a, b, c] /; ! OrderedQ[{b, a}];
ϵ[a_, c_, b_] := -ϵ[a, b, c] /; ! OrderedQ[{c, b}];
```

■ various simplification rules

```
β[0, a_Symbol] * ϵ[i_, j_, k_] ^:= ϵ[i, j, k] /; (a[[0]] =!= λ && (a == i || a == j || a == k));

δ[0, a_] * β[0, a_] ^:= 0;
```

```
R_ β[0, a_Symbol] * δ[a_Symbol, b_Symbol] ^:= (1 - δ[0, a]) * (1 - δ[0, b]) * δ[a, b]
     (R /. {β[0, a] → 1, β[0, b] → 1});

δ[0, a_Symbol] * δ[a_Symbol, b_Symbol] ^:= δ[0, a] * δ[0, b];
```

```
Off[General::spell1];
ϵd[a_, b_, c_λ] * ϵd[c_λ, d_, e_] ^:=
  (δ[a, d] * δ[b, e] - δ[a, e] * δ[b, d]) β[0, a] β [0, b];
ϵd[a_, b_, c_λ] * ϵd[d_, c_λ, e_] ^:=
  -(δ[a, d] * δ[b, e] - δ[a, e] * δ[b, d]) β[0, a] β [0, b];
ϵd[a_, b_, c_λ] * ϵd[d_, e_, c_λ] ^:= (δ[a, d] * δ[b, e] - δ[a, e] * δ[b, d]) β[0, a] β [0, b];
ϵd[a_, c_λ, b_] * ϵd[c_λ, d_, e_] ^:=
  -(δ[a, d] * δ[b, e] - δ[a, e] * δ[b, d]) β[0, a] β [0, b];
ϵd[a_, c_λ, b_] * ϵd[d_, c_λ, e_] ^:= (δ[a, d] * δ[b, e] - δ[a, e] * δ[b, d]) β[0, a] β [0, b];
ϵd[a_, c_λ, b_] * ϵd[d_, e_, c_λ] ^:=
  -(δ[a, d] * δ[b, e] - δ[a, e] * δ[b, d]) β[0, a] β [0, b];
ϵd[c_λ, a_, b_] * ϵd[c_λ, d_, e_] ^:= (δ[a, d] * δ[b, e] - δ[a, e] * δ[b, d]) β[0, a] β [0, b];
ϵd[c_λ, a_, b_] * ϵd[d_, c_λ, e_] ^:=
  -(δ[a, d] * δ[b, e] - δ[a, e] * δ[b, d]) β[0, a] β [0, b];
ϵd[c_λ, a_, b_] * ϵd[d_, e_, c_λ] ^:= (δ[a, d] * δ[b, e] - δ[a, e] * δ[b, d]) β[0, a] β [0, b];

δVer[a_, b_λ] * ϵVer[i_, j_, b_λ] ^:= ϵVer[i, j, a];
On[General::spell1];



a_CircleTimes * δVer[b_, c_λ] ^:= (a /. c → b) /; ! FreeQ[a, c];



δVer[a_, λ[b_]] * R_ ^:= (R /. λ[b] → a) β[a, 0];



R1_ β[0, a_Symbol] * δ[a_Symbol, b_Symbol] * R2_. ^:= R1 R2 β[0, a] * β[0, b] * δ[a, b] /;
   (FreeQ[Unevaluated[R1], β[0, b]] && FreeQ[Unevaluated[R2], β[0, b]] && (R1 ≠ 0));

R1_. β[0, a_Symbol] * δ[a_Symbol, b_Symbol] * R2_ ^:= R1 R2 β[0, a] * β[0, b] * δ[a, b] /;
   (FreeQ[R1, β[0, b]] && FreeQ[R2, β[0, b]] && (R1 ≠ 0));
```

- **decomposition of an summand in the Kondo Hamiltonian into a sum of a scalar term and terms proportional to Pauli matrices and a second−order term $\sigma \otimes \sigma$.**

```
PauliExpand[x_] := Module[{CNummer, Ergebnis, Iter, KommutRegeln, Term, Renum},

       KommutRegeln = {
         CenterDot[a_, b_] :↦ a * b /; (FreeQ[a, σ] || FreeQ[b, σ]),
         CircleTimes[a_, b_] :↦ a * b /; (FreeQ[a, σ] || FreeQ[b, σ]),
         CircleTimes[R1_ a_σ, R2_ b_σ] :↦ R1 R2 CircleTimes[a, b]};

       Renum[T_] := Module[{Term, AktN},
             CNummer = 1;
             Term = T;
             While[! FreeQ[Term, C[_]],
                   Term /. {C[n_] :↦ (AktN = n)};
                   Term = Term /. {C[AktN] -> λ[CNummer]};
                   CNummer++;
              ];
             Return[Term];
         ];

       Renum /@ Expand[x //. KommutRegeln]
  ];
```

perform the summation over all different summation indices λ[i], where each λ[i] runs from 1 to 3.

```
Summation[x_] := Module[{SumIndizes},
       SumIndizes = Union[Cases[x, _λ, Infinity]];
       If[SumIndizes == {}, Return[x]];
       SumIndizes = ({#, 1, 3}) & /@ SumIndizes;
       Return[Sum[x, Evaluate[Sequence @@ SumIndizes]]];
  ];
```

rules to ensure the correct order of application the simplification rules defined above

```
EpsilonProd[x_] := Module[{Term},
       Term = x /. ϵ → ϵd;
       Return[Term /. ϵd → ϵ];
  ];

DeltaSum[x_] := Module[{Term},
       Term = x /. {δ → δVer, ϵ → ϵVer};
       Return[Term /. {δVer → δ, ϵVer → ϵ}];
  ];
```

■ Evaluation of the matrix structure of Kondo Hamiltonian

■ Part of the Hamiltonian that is proportional to b_0

```
PauliExpand[(σ[μ] ⊗ σ[ν]) · (σ[μ'] ⊗ σ[ν']) - (σ[μ'] ⊗ σ[ν']) · (σ[μ] ⊗ σ[ν])] // Simplify
```

```
-2 i (σ[λ[1]] ⊗ σ[ν'] β[0, ν'] δ[0, ν] ∈[μ, λ[1], μ'] +
   σ[λ[1]] ⊗ σ[ν] β[0, ν] δ[0, ν'] ∈[μ, λ[1], μ'] + σ[λ[1]] ⊗ σ[0] δ[ν, ν'] ∈[μ, λ[1], μ'] +
   σ[μ'] ⊗ σ[λ[1]] β[0, μ'] δ[0, μ] ∈[ν, λ[1], ν'] +
   σ[μ] ⊗ σ[λ[1]] β[0, μ] δ[0, μ'] ∈[ν, λ[1], ν'] + σ[0] ⊗ σ[λ[1]] δ[μ, μ'] ∈[ν, λ[1], ν'])
```

■ Part of the Hamiltonian that is proportional to b_1

```
Split[Sort[List @@ (DeltaSum /@ Expand[EpsilonProd /@ PauliExpand[
         (σ[x] ⊗ σ[y]) · (σ[1] ⊗ σ[0]) · (σ[w] ⊗ σ[z]) -
          (σ[w] ⊗ σ[z]) · (σ[1] ⊗ σ[0]) · (σ[x] ⊗ σ[y])]]),
   OrderedQ[{(#1 /. {-1 → 1, _β → 1, _δ → 1, _ϵ → 1}),
      (#2 /. {-1 → 1, _β → 1, _δ → 1, _ϵ → 1})}] &],
  ((#1 /. {R_ a_CircleTimes → a}) == (#2 /. {R_ a_CircleTimes → a})) &] // TableForm
```

```
2 i σ[0] ⊗ σ[0] δ[y, z] ∈[1, w, x]
2 i σ[0] ⊗ σ[y] β[0, y] δ[0, z] ∈[1, w, x]
2 i σ[0] ⊗ σ[z] β[0, z] δ[0, y] ∈[1, w, x]
2 i σ[0] ⊗ σ[λ[1]] δ[0, x] δ[1, w] ∈[y, z, λ[1]]            2 i σ[0] ⊗ σ[λ[1]] δ[0, w] δ[1,
-2 i σ[1] ⊗ σ[λ[1]] δ[w, x] ∈[y, z, λ[1]]                  4 i σ[1] ⊗ σ[λ[1]] δ[0, w] δ[0,
2 i σ[w] ⊗ σ[λ[1]] β[0, w] δ[1, x] ∈[y, z, λ[1]]
2 i σ[x] ⊗ σ[λ[1]] β[0, x] δ[1, w] ∈[y, z, λ[1]]
-2 i σ[λ[1]] ⊗ σ[0] δ[0, w] δ[y, z] ∈[1, x, λ[1]]           2 i σ[λ[1]] ⊗ σ[0] δ[0, x] δ[y,
-2 i σ[λ[1]] ⊗ σ[y] β[0, y] δ[0, w] δ[0, z] ∈[1, x, λ[1]]   2 i σ[λ[1]] ⊗ σ[y] β[0, y] δ[0,
-2 i σ[λ[1]] ⊗ σ[z] β[0, z] δ[0, w] δ[0, y] ∈[1, x, λ[1]]   2 i σ[λ[1]] ⊗ σ[z] β[0, z] δ[0,
```

Appendix B

Full Set of Flow Equations

$$
\begin{aligned}
J_{001} = -8(\quad & b_1(J_{003}J_{012} + J_{002}J_{013} + J_{103}J_{112} + J_{102}J_{113} + J_{203}J_{212} + J_{202}J_{213} + J_{303}J_{312} + J_{302}J_{313}) + \\
& b_0(J_{002}J_{003} + J_{012}J_{013} + J_{022}J_{023} + J_{032}J_{033} + J_{102}J_{103} + J_{112}J_{113} + J_{122}J_{123} + J_{132}J_{133} + J_{202}J_{203} + \\
& \quad J_{212}J_{213} + J_{222}J_{223} + J_{232}J_{233} + J_{302}J_{303} + J_{312}J_{313} + J_{322}J_{323} + J_{332}J_{333})) \\
J_{002} = -8(\quad & b_1(J_{003}J_{011} + J_{001}J_{013} + J_{103}J_{111} + J_{101}J_{113} + J_{203}J_{211} + J_{201}J_{213} + J_{303}J_{311} + J_{301}J_{313}) + \\
& b_0(J_{001}J_{003} + J_{011}J_{013} + J_{021}J_{023} + J_{031}J_{033} + J_{101}J_{103} + J_{111}J_{113} + J_{121}J_{123} + J_{131}J_{133} + J_{201}J_{203} + \\
& \quad J_{211}J_{213} + J_{221}J_{223} + J_{231}J_{233} + J_{301}J_{303} + J_{311}J_{313} + J_{321}J_{323} + J_{331}J_{333})) \\
J_{003} = -8(\quad & b_1(J_{002}J_{011} + J_{001}J_{012} + J_{102}J_{111} + J_{101}J_{112} + J_{202}J_{211} + J_{201}J_{212} + J_{302}J_{311} + J_{301}J_{312}) + \\
& b_0(J_{001}J_{002} + J_{011}J_{012} + J_{021}J_{022} + J_{031}J_{032} + J_{101}J_{102} + J_{111}J_{112} + J_{121}J_{122} + J_{131}J_{132} + J_{201}J_{202} + \\
& \quad J_{211}J_{212} + J_{221}J_{222} + J_{231}J_{232} + J_{301}J_{302} + J_{311}J_{312} + J_{321}J_{322} + J_{331}J_{332})) \\
\mathbf{J_{011}} = -8(\quad & b_0(J_{003}J_{012} + J_{002}J_{013} + J_{103}J_{112} + J_{102}J_{113} + J_{203}J_{212} + J_{202}J_{213} + J_{303}J_{312} + J_{302}J_{313}) + \\
& b_1(J_{002}J_{003} + J_{012}J_{013} - J_{022}J_{023} - J_{032}J_{033} + J_{102}J_{103} + J_{112}J_{113} - J_{122}J_{123} - J_{132}J_{133} + J_{202}J_{203} + \\
& \quad J_{212}J_{213} - J_{222}J_{223} - J_{232}J_{233} + J_{302}J_{303} + J_{312}J_{313} - J_{322}J_{323} - J_{332}J_{333})) \\
\mathbf{J_{012}} = -8(\quad & b_0(J_{003}J_{011} + J_{001}J_{013} + J_{103}J_{111} + J_{101}J_{113} + J_{203}J_{211} + J_{201}J_{213} + J_{303}J_{311} + J_{301}J_{313}) + \\
& b_1(J_{001}J_{003} + J_{011}J_{013} - J_{021}J_{023} - J_{031}J_{033} + J_{101}J_{103} + J_{111}J_{113} - J_{121}J_{123} - J_{131}J_{133} + J_{201}J_{203} + \\
& \quad J_{211}J_{213} - J_{221}J_{223} - J_{231}J_{233} + J_{301}J_{303} + J_{311}J_{313} - J_{321}J_{323} - J_{331}J_{333})) \\
\mathbf{J_{013}} = -8(\quad & b_0(J_{002}J_{011} + J_{001}J_{012} + J_{102}J_{111} + J_{101}J_{112} + J_{202}J_{211} + J_{201}J_{212} + J_{302}J_{311} + J_{301}J_{312}) + \\
& b_1(J_{001}J_{002} + J_{011}J_{012} - J_{021}J_{022} - J_{031}J_{032} + J_{101}J_{102} + J_{111}J_{112} - J_{121}J_{122} - J_{131}J_{132} + J_{201}J_{202} + \\
& \quad J_{211}J_{212} - J_{221}J_{222} - J_{231}J_{232} + J_{301}J_{302} + J_{311}J_{312} - J_{321}J_{322} - J_{331}J_{332})) \\
J_{021} = -8(\quad & b_0(J_{003}J_{022} + J_{002}J_{023} + J_{103}J_{122} + J_{102}J_{123} + J_{203}J_{222} + J_{202}J_{223} + J_{303}J_{322} + J_{302}J_{323}) + \\
& b_1(J_{013}J_{022} + J_{012}J_{023} + J_{113}J_{122} + J_{112}J_{123} + J_{213}J_{222} + J_{212}J_{223} + J_{313}J_{322} + J_{312}J_{323})) \\
J_{022} = -8(\quad & b_0(J_{003}J_{021} + J_{001}J_{023} + J_{103}J_{121} + J_{101}J_{123} + J_{203}J_{221} + J_{201}J_{223} + J_{303}J_{321} + J_{301}J_{323}) + \\
& b_1(J_{013}J_{021} + J_{011}J_{023} + J_{113}J_{121} + J_{111}J_{123} + J_{213}J_{221} + J_{211}J_{223} + J_{313}J_{321} + J_{311}J_{323})) \\
J_{023} = -8(\quad & b_0(J_{002}J_{021} + J_{001}J_{022} + J_{102}J_{121} + J_{101}J_{122} + J_{202}J_{221} + J_{201}J_{222} + J_{302}J_{321} + J_{301}J_{322}) + \\
& b_1(J_{012}J_{021} + J_{011}J_{022} + J_{112}J_{121} + J_{111}J_{122} + J_{212}J_{221} + J_{211}J_{222} + J_{312}J_{321} + J_{311}J_{322})) \\
J_{031} = -8(\quad & b_0(J_{003}J_{032} + J_{002}J_{033} + J_{103}J_{132} + J_{102}J_{133} + J_{203}J_{232} + J_{202}J_{233} + J_{303}J_{332} + J_{302}J_{333}) + \\
& b_1(J_{013}J_{032} + J_{012}J_{033} + J_{113}J_{132} + J_{112}J_{133} + J_{213}J_{232} + J_{212}J_{233} + J_{313}J_{332} + J_{312}J_{333})) \\
J_{032} = -8(\quad & b_0(J_{003}J_{031} + J_{001}J_{033} + J_{103}J_{131} + J_{101}J_{133} + J_{203}J_{231} + J_{201}J_{233} + J_{303}J_{331} + J_{301}J_{333}) + \\
& b_1(J_{013}J_{031} + J_{011}J_{033} + J_{113}J_{131} + J_{111}J_{133} + J_{213}J_{231} + J_{211}J_{233} + J_{313}J_{331} + J_{311}J_{333})) \\
J_{033} = -8(\quad & b_0(J_{002}J_{031} + J_{001}J_{032} + J_{102}J_{131} + J_{101}J_{132} + J_{202}J_{231} + J_{201}J_{232} + J_{302}J_{331} + J_{301}J_{332}) + \\
& b_1(J_{012}J_{031} + J_{011}J_{032} + J_{112}J_{131} + J_{111}J_{132} + J_{212}J_{231} + J_{211}J_{232} + J_{312}J_{331} + J_{311}J_{332})) \\
\mathbf{J_{100}} = 8 \quad & b_1(-J_{230}J_{320} - J_{231}J_{321} - J_{232}J_{322} - J_{233}J_{323} + J_{220}J_{330} + J_{221}J_{331} + J_{222}J_{332} + J_{223}J_{333}) \\
\mathbf{J_{101}} = -8(\quad & b_0(J_{003}J_{102} + J_{002}J_{103} + J_{013}J_{112} + J_{012}J_{113} + J_{023}J_{122} + J_{022}J_{123} + J_{033}J_{132} + J_{032}J_{133}) + \\
& b_1(J_{013}J_{102} + J_{012}J_{103} + J_{003}J_{112} + J_{002}J_{113} + J_{231}J_{320} + J_{230}J_{321} - J_{221}J_{330} - J_{220}J_{331})) \\
\mathbf{J_{102}} = -8(\quad & b_0(J_{003}J_{101} + J_{001}J_{103} + J_{013}J_{111} + J_{011}J_{113} + J_{023}J_{121} + J_{021}J_{123} + J_{033}J_{131} + J_{031}J_{133}) + \\
& b_1(J_{013}J_{101} + J_{011}J_{103} + J_{003}J_{111} + J_{001}J_{113} + J_{232}J_{320} + J_{230}J_{322} - J_{222}J_{330} - J_{220}J_{332})) \\
\mathbf{J_{103}} = -8(\quad & b_0(J_{002}J_{101} + J_{001}J_{102} + J_{012}J_{111} + J_{011}J_{112} + J_{022}J_{121} + J_{021}J_{122} + J_{032}J_{131} + J_{031}J_{132}) + \\
& b_1(J_{012}J_{101} + J_{011}J_{102} + J_{002}J_{111} + J_{001}J_{112} + J_{233}J_{320} + J_{230}J_{323} - J_{223}J_{330} - J_{220}J_{333}))
\end{aligned}
$$

$$
\begin{aligned}
J_{110} = 8 \quad & b_0(J_{230}J_{320} + J_{231}J_{321} + J_{232}J_{322} + J_{233}J_{323} - J_{220}J_{330} - J_{221}J_{331} - J_{222}J_{332} - J_{223}J_{333}) \\
J_{111} = -8(\quad & b_1(J_{003}J_{102} + J_{002}J_{103} + J_{013}J_{112} + J_{012}J_{113} - J_{023}J_{122} - J_{022}J_{123} - J_{033}J_{132} - J_{032}J_{133}) + \\
& b_0(J_{013}J_{102} + J_{012}J_{103} + J_{003}J_{112} + J_{002}J_{113} - J_{231}J_{320} - J_{230}J_{321} + J_{221}J_{330} + J_{220}J_{331})) \\
J_{112} = -8(\quad & b_1(J_{003}J_{101} + J_{001}J_{103} + J_{013}J_{111} + J_{011}J_{113} - J_{023}J_{121} - J_{021}J_{123} - J_{033}J_{131} - J_{031}J_{133}) + \\
& b_0(J_{013}J_{101} + J_{011}J_{103} + J_{003}J_{111} + J_{001}J_{113} - J_{232}J_{320} - J_{230}J_{322} + J_{222}J_{330} + J_{220}J_{332})) \\
J_{113} = -8(\quad & b_1(J_{002}J_{101} + J_{001}J_{102} + J_{012}J_{111} + J_{011}J_{112} - J_{022}J_{121} - J_{021}J_{122} - J_{032}J_{131} - J_{031}J_{132}) + \\
& b_0(J_{012}J_{101} + J_{011}J_{102} + J_{002}J_{111} + J_{001}J_{112} - J_{233}J_{320} - J_{230}J_{323} + J_{223}J_{330} + J_{220}J_{333})) \\
J_{120} = 8(\quad & b_1(-J_{230}J_{300} - J_{231}J_{301} - J_{232}J_{302} - J_{233}J_{303} + J_{200}J_{330} + J_{201}J_{331} + J_{202}J_{332} + J_{203}J_{333}) + \\
& b_0(-J_{230}J_{310} - J_{231}J_{311} - J_{232}J_{312} - J_{233}J_{313} + J_{210}J_{330} + J_{211}J_{331} + J_{212}J_{332} + J_{213}J_{333})) \\
J_{121} = -8(\quad & b_1(J_{023}J_{112} + J_{022}J_{113} + J_{013}J_{122} + J_{012}J_{123} + J_{231}J_{300} + J_{230}J_{301} - J_{201}J_{330} - J_{200}J_{331}) + \\
& b_0(J_{023}J_{102} + J_{022}J_{103} + J_{003}J_{122} + J_{002}J_{123} + J_{231}J_{310} + J_{230}J_{311} - J_{211}J_{330} - J_{210}J_{331})) \\
J_{122} = -8(\quad & b_1(J_{023}J_{111} + J_{021}J_{113} + J_{013}J_{121} + J_{011}J_{123} + J_{232}J_{300} + J_{230}J_{302} - J_{202}J_{330} - J_{200}J_{332}) + \\
& b_0(J_{023}J_{101} + J_{021}J_{103} + J_{003}J_{121} + J_{001}J_{123} + J_{232}J_{310} + J_{230}J_{312} - J_{212}J_{330} - J_{210}J_{332})) \\
J_{123} = -8(\quad & b_1(J_{022}J_{111} + J_{021}J_{112} + J_{012}J_{121} + J_{011}J_{122} + J_{233}J_{300} + J_{230}J_{303} - J_{203}J_{330} - J_{200}J_{333}) + \\
& b_0(J_{022}J_{101} + J_{021}J_{102} + J_{002}J_{121} + J_{001}J_{122} + J_{233}J_{310} + J_{230}J_{313} - J_{213}J_{330} - J_{210}J_{333})) \\
J_{130} = -8(\quad & b_1(-J_{220}J_{300} - J_{221}J_{301} - J_{222}J_{302} - J_{223}J_{303} + J_{200}J_{320} + J_{201}J_{321} + J_{202}J_{322} + J_{203}J_{323}) + \\
& b_0(-J_{220}J_{310} - J_{221}J_{311} - J_{222}J_{312} - J_{223}J_{313} + J_{210}J_{320} + J_{211}J_{321} + J_{212}J_{322} + J_{213}J_{323})) \\
J_{131} = -8(\quad & b_1(J_{033}J_{112} + J_{032}J_{113} + J_{013}J_{132} + J_{012}J_{133} - J_{221}J_{300} - J_{220}J_{301} + J_{201}J_{320} + J_{200}J_{321}) + \\
& b_0(J_{033}J_{102} + J_{032}J_{103} + J_{003}J_{132} + J_{002}J_{133} - J_{221}J_{310} - J_{220}J_{311} + J_{211}J_{320} + J_{210}J_{321})) \\
J_{132} = -8(\quad & b_1(J_{033}J_{111} + J_{031}J_{113} + J_{013}J_{131} + J_{011}J_{133} - J_{222}J_{300} - J_{220}J_{302} + J_{202}J_{320} + J_{200}J_{322}) + \\
& b_0(J_{033}J_{101} + J_{031}J_{103} + J_{003}J_{131} + J_{001}J_{133} - J_{222}J_{310} - J_{220}J_{312} + J_{212}J_{320} + J_{210}J_{322})) \\
J_{133} = -8(\quad & b_1(J_{032}J_{111} + J_{031}J_{112} + J_{012}J_{131} + J_{011}J_{132} - J_{223}J_{300} - J_{220}J_{303} + J_{203}J_{320} + J_{200}J_{323}) + \\
& b_0(J_{032}J_{101} + J_{031}J_{102} + J_{002}J_{131} + J_{001}J_{132} - J_{223}J_{310} - J_{220}J_{313} + J_{213}J_{320} + J_{210}J_{323})) \\
J_{200} = 8 \quad & b_1(J_{130}J_{320} + J_{131}J_{321} + J_{132}J_{322} + J_{133}J_{323} - J_{120}J_{330} - J_{121}J_{331} - J_{122}J_{332} - J_{123}J_{333}) \\
J_{201} = -8(\quad & b_0(J_{003}J_{202} + J_{002}J_{203} + J_{013}J_{212} + J_{012}J_{213} + J_{023}J_{222} + J_{022}J_{223} + J_{033}J_{232} + J_{032}J_{233}) + \\
& b_1(J_{013}J_{202} + J_{012}J_{203} + J_{003}J_{212} + J_{002}J_{213} - J_{131}J_{320} - J_{130}J_{321} + J_{121}J_{330} + J_{120}J_{331})) \\
J_{202} = -8(\quad & b_0(J_{003}J_{201} + J_{001}J_{203} + J_{013}J_{211} + J_{011}J_{213} + J_{023}J_{221} + J_{021}J_{223} + J_{033}J_{231} + J_{031}J_{233}) + \\
& b_1(J_{013}J_{201} + J_{011}J_{203} + J_{003}J_{211} + J_{001}J_{213} - J_{132}J_{320} - J_{130}J_{322} + J_{122}J_{330} + J_{120}J_{332})) \\
J_{203} = -8(\quad & b_0(J_{002}J_{201} + J_{001}J_{202} + J_{012}J_{211} + J_{011}J_{212} + J_{022}J_{221} + J_{021}J_{222} + J_{032}J_{231} + J_{031}J_{232}) + \\
& b_1(J_{012}J_{201} + J_{011}J_{202} + J_{002}J_{211} + J_{001}J_{212} - J_{133}J_{320} - J_{130}J_{323} + J_{123}J_{330} + J_{120}J_{333})) \\
J_{210} = 8 \quad & b_0(-J_{130}J_{320} - J_{131}J_{321} - J_{132}J_{322} - J_{133}J_{323} + J_{120}J_{330} + J_{121}J_{331} + J_{122}J_{332} + J_{123}J_{333}) \\
J_{211} = -8(\quad & b_1(J_{003}J_{202} + J_{002}J_{203} + J_{013}J_{212} + J_{012}J_{213} - J_{023}J_{222} - J_{022}J_{223} - J_{033}J_{232} - J_{032}J_{233}) + \\
& b_0(J_{013}J_{202} + J_{012}J_{203} + J_{003}J_{212} + J_{002}J_{213} + J_{131}J_{320} + J_{130}J_{321} - J_{121}J_{330} - J_{120}J_{331})) \\
J_{212} = -8(\quad & b_1(J_{003}J_{201} + J_{001}J_{203} + J_{013}J_{211} + J_{011}J_{213} - J_{023}J_{221} - J_{021}J_{223} - J_{033}J_{231} - J_{031}J_{233}) + \\
& b_0(J_{013}J_{201} + J_{011}J_{203} + J_{003}J_{211} + J_{001}J_{213} + J_{132}J_{320} + J_{130}J_{322} - J_{122}J_{330} - J_{120}J_{332})) \\
J_{213} = -8(\quad & b_1(J_{002}J_{201} + J_{001}J_{202} + J_{012}J_{211} + J_{011}J_{212} - J_{022}J_{221} - J_{021}J_{222} - J_{032}J_{231} - J_{031}J_{232}) + \\
& b_0(J_{012}J_{201} + J_{011}J_{202} + J_{002}J_{211} + J_{001}J_{212} + J_{133}J_{320} + J_{130}J_{323} - J_{123}J_{330} - J_{120}J_{333})) \\
J_{220} = -8(\quad & b_1(-J_{130}J_{300} - J_{131}J_{301} - J_{132}J_{302} - J_{133}J_{303} + J_{100}J_{330} + J_{101}J_{331} + J_{102}J_{332} + J_{103}J_{333}) + \\
& b_0(-J_{130}J_{310} - J_{131}J_{311} - J_{132}J_{312} - J_{133}J_{313} + J_{110}J_{330} + J_{111}J_{331} + J_{112}J_{332} + J_{113}J_{333})) \\
J_{221} = -8(\quad & b_1(J_{023}J_{212} + J_{022}J_{213} + J_{013}J_{222} + J_{012}J_{223} - J_{131}J_{300} - J_{130}J_{301} + J_{101}J_{330} + J_{100}J_{331}) + \\
& b_0(J_{023}J_{202} + J_{022}J_{203} + J_{003}J_{222} + J_{002}J_{223} - J_{131}J_{310} - J_{130}J_{311} + J_{111}J_{330} + J_{110}J_{331})) \\
J_{222} = -8(\quad & b_1(J_{023}J_{211} + J_{021}J_{213} + J_{013}J_{221} + J_{011}J_{223} - J_{132}J_{300} - J_{130}J_{302} + J_{102}J_{330} + J_{100}J_{332}) + \\
& b_0(J_{023}J_{201} + J_{021}J_{203} + J_{003}J_{221} + J_{001}J_{223} - J_{132}J_{310} - J_{130}J_{312} + J_{112}J_{330} + J_{110}J_{332})) \\
J_{223} = -8(\quad & b_1(J_{022}J_{211} + J_{021}J_{212} + J_{012}J_{221} + J_{011}J_{222} - J_{133}J_{300} - J_{130}J_{303} + J_{103}J_{330} + J_{100}J_{333}) + \\
& b_0(J_{022}J_{201} + J_{021}J_{202} + J_{002}J_{221} + J_{001}J_{222} - J_{133}J_{310} - J_{130}J_{313} + J_{113}J_{330} + J_{110}J_{333})) \\
J_{230} = 8(\quad & b_1(-J_{120}J_{300} - J_{121}J_{301} - J_{122}J_{302} - J_{123}J_{303} + J_{100}J_{320} + J_{101}J_{321} + J_{102}J_{322} + J_{103}J_{323}) + \\
& b_0(-J_{120}J_{310} - J_{121}J_{311} - J_{122}J_{312} - J_{123}J_{313} + J_{110}J_{320} + J_{111}J_{321} + J_{112}J_{322} + J_{113}J_{323})) \\
J_{231} = -8(\quad & b_1(J_{033}J_{212} + J_{032}J_{213} + J_{013}J_{232} + J_{012}J_{233} + J_{121}J_{300} + J_{120}J_{301} - J_{101}J_{320} - J_{100}J_{321}) + \\
& b_0(J_{033}J_{202} + J_{032}J_{203} + J_{003}J_{232} + J_{002}J_{233} + J_{121}J_{310} + J_{120}J_{311} - J_{111}J_{320} - J_{110}J_{321})) \\
J_{232} = -8(\quad & b_1(J_{033}J_{211} + J_{031}J_{213} + J_{013}J_{231} + J_{011}J_{233} + J_{122}J_{300} + J_{120}J_{302} - J_{102}J_{320} - J_{100}J_{322}) + \\
& b_0(J_{033}J_{201} + J_{031}J_{203} + J_{003}J_{231} + J_{001}J_{233} + J_{122}J_{310} + J_{120}J_{312} - J_{112}J_{320} - J_{110}J_{322})) \\
J_{233} = -8(\quad & b_1(J_{032}J_{211} + J_{031}J_{212} + J_{012}J_{231} + J_{011}J_{232} + J_{123}J_{300} + J_{120}J_{303} - J_{103}J_{320} - J_{100}J_{323}) + \\
& b_0(J_{032}J_{201} + J_{031}J_{202} + J_{002}J_{231} + J_{001}J_{232} + J_{123}J_{310} + J_{120}J_{313} - J_{113}J_{320} - J_{110}J_{323}))
\end{aligned}
$$

$$
\begin{aligned}
J_{300} = 8 \quad & b_1(-J_{130}J_{220} - J_{131}J_{221} - J_{132}J_{222} - J_{133}J_{223} + J_{120}J_{230} + J_{121}J_{231} + J_{122}J_{232} + J_{123}J_{233}) \\
J_{301} = -8(\quad & b_1(J_{131}J_{220} + J_{130}J_{221} - J_{121}J_{230} - J_{120}J_{231} + J_{013}J_{302} + J_{012}J_{303} + J_{003}J_{312} + J_{002}J_{313}) + \\
& b_0(J_{003}J_{302} + J_{002}J_{303} + J_{013}J_{312} + J_{012}J_{313} + J_{023}J_{322} + J_{022}J_{323} + J_{033}J_{332} + J_{032}J_{333})) \\
J_{302} = -8(\quad & b_1(J_{132}J_{220} + J_{130}J_{222} - J_{122}J_{230} - J_{120}J_{232} + J_{013}J_{301} + J_{011}J_{303} + J_{003}J_{311} + J_{001}J_{313}) + \\
& b_0(J_{003}J_{301} + J_{001}J_{303} + J_{013}J_{311} + J_{011}J_{313} + J_{023}J_{321} + J_{021}J_{323} + J_{033}J_{331} + J_{031}J_{333})) \\
J_{303} = -8(\quad & b_1(J_{133}J_{220} + J_{130}J_{223} - J_{123}J_{230} - J_{120}J_{233} + J_{012}J_{301} + J_{011}J_{302} + J_{002}J_{311} + J_{001}J_{312}) + \\
& b_0(J_{002}J_{301} + J_{001}J_{302} + J_{012}J_{311} + J_{011}J_{312} + J_{022}J_{321} + J_{021}J_{322} + J_{032}J_{331} + J_{031}J_{332})) \\
J_{310} = 8 \quad & b_0(J_{130}J_{220} + J_{131}J_{221} + J_{132}J_{222} + J_{133}J_{223} - J_{120}J_{230} - J_{121}J_{231} - J_{122}J_{232} - J_{123}J_{233}) \\
J_{311} = -8(\quad & b_0(-J_{131}J_{220} - J_{130}J_{221} + J_{121}J_{230} + J_{120}J_{231} + J_{013}J_{302} + J_{012}J_{303} + J_{003}J_{312} + J_{002}J_{313}) + \\
& b_1(J_{003}J_{302} + J_{002}J_{303} + J_{013}J_{312} + J_{012}J_{313} - J_{023}J_{322} - J_{022}J_{323} - J_{033}J_{332} - J_{032}J_{333})) \\
J_{312} = -8(\quad & b_0(-J_{132}J_{220} - J_{130}J_{222} + J_{122}J_{230} + J_{120}J_{232} + J_{013}J_{301} + J_{011}J_{303} + J_{003}J_{311} + J_{001}J_{313}) + \\
& b_1(J_{003}J_{301} + J_{001}J_{303} + J_{013}J_{311} + J_{011}J_{313} - J_{023}J_{321} - J_{021}J_{323} - J_{033}J_{331} - J_{031}J_{333})) \\
J_{313} = -8(\quad & b_0(-J_{133}J_{220} - J_{130}J_{223} + J_{123}J_{230} + J_{120}J_{233} + J_{012}J_{301} + J_{011}J_{302} + J_{002}J_{311} + J_{001}J_{312}) + \\
& b_1(J_{002}J_{301} + J_{001}J_{302} + J_{012}J_{311} + J_{011}J_{312} - J_{022}J_{321} - J_{021}J_{322} - J_{032}J_{331} - J_{031}J_{332})) \\
J_{320} = 8(\quad & b_1(-J_{130}J_{200} - J_{131}J_{201} - J_{132}J_{202} - J_{133}J_{203} + J_{100}J_{230} + J_{101}J_{231} + J_{102}J_{232} + J_{103}J_{233}) + \\
& b_0(-J_{130}J_{210} - J_{131}J_{211} - J_{132}J_{212} - J_{133}J_{213} + J_{110}J_{230} + J_{111}J_{231} + J_{112}J_{232} + J_{113}J_{233})) \\
J_{321} = -8(\quad & b_0(J_{131}J_{210} + J_{130}J_{211} - J_{111}J_{230} - J_{110}J_{231} + J_{023}J_{302} + J_{022}J_{303} + J_{003}J_{322} + J_{002}J_{323}) + \\
& b_1(J_{131}J_{200} + J_{130}J_{201} - J_{101}J_{230} - J_{100}J_{231} + J_{023}J_{312} + J_{022}J_{313} + J_{013}J_{322} + J_{012}J_{323})) \\
J_{322} = -8(\quad & b_0(J_{132}J_{210} + J_{130}J_{212} - J_{112}J_{230} - J_{110}J_{232} + J_{023}J_{301} + J_{021}J_{303} + J_{003}J_{321} + J_{001}J_{323}) + \\
& b_1(J_{132}J_{200} + J_{130}J_{202} - J_{102}J_{230} - J_{100}J_{232} + J_{023}J_{311} + J_{021}J_{313} + J_{013}J_{321} + J_{011}J_{323})) \\
J_{323} = -8(\quad & b_0(J_{133}J_{210} + J_{130}J_{213} - J_{113}J_{230} - J_{110}J_{233} + J_{022}J_{301} + J_{021}J_{302} + J_{002}J_{321} + J_{001}J_{322}) + \\
& b_1(J_{133}J_{200} + J_{130}J_{203} - J_{103}J_{230} - J_{100}J_{233} + J_{022}J_{311} + J_{021}J_{312} + J_{012}J_{321} + J_{011}J_{322})) \\
J_{330} = -8(\quad & b_1(-J_{120}J_{200} - J_{121}J_{201} - J_{122}J_{202} - J_{123}J_{203} + J_{100}J_{220} + J_{101}J_{221} + J_{102}J_{222} + J_{103}J_{223}) + \\
& b_0(-J_{120}J_{210} - J_{121}J_{211} - J_{122}J_{212} - J_{123}J_{213} + J_{110}J_{220} + J_{111}J_{221} + J_{112}J_{222} + J_{113}J_{223})) \\
J_{331} = -8(\quad & b_0(-J_{121}J_{210} - J_{120}J_{211} + J_{111}J_{220} + J_{110}J_{221} + J_{033}J_{302} + J_{032}J_{303} + J_{003}J_{332} + J_{002}J_{333}) + \\
& b_1(-J_{121}J_{200} - J_{120}J_{201} + J_{101}J_{220} + J_{100}J_{221} + J_{033}J_{312} + J_{032}J_{313} + J_{013}J_{332} + J_{012}J_{333})) \\
J_{332} = -8(\quad & b_0(-J_{122}J_{210} - J_{120}J_{212} + J_{112}J_{220} + J_{110}J_{222} + J_{033}J_{301} + J_{031}J_{303} + J_{003}J_{331} + J_{001}J_{333}) + \\
& b_1(-J_{122}J_{200} - J_{120}J_{202} + J_{102}J_{220} + J_{100}J_{222} + J_{033}J_{311} + J_{031}J_{313} + J_{013}J_{331} + J_{011}J_{333})) \\
J_{333} = -8(\quad & b_0(-J_{123}J_{210} - J_{120}J_{213} + J_{113}J_{220} + J_{110}J_{223} + J_{032}J_{301} + J_{031}J_{302} + J_{002}J_{331} + J_{001}J_{332}) + \\
& b_1(-J_{123}J_{200} - J_{120}J_{203} + J_{103}J_{220} + J_{100}J_{223} + J_{032}J_{311} + J_{031}J_{312} + J_{012}J_{331} + J_{011}J_{332}))
\end{aligned}
$$

Appendix C

Flow Equations for $\nu = 0$ and $\nu \neq 0$

$\boxed{\mu = 0}$

$$
\begin{aligned}
J_{00\nu} = -8(&b_1(2J_{00\nu}J_{01\nu} + 2J_{10\nu}J_{11\nu} + 2J_{20\nu}J_{21\nu} + 2J_{30\nu}J_{31\nu}) \\
&+ b_0(J_{00\nu}^2 + J_{01\nu}^2 + J_{02\nu}^2 + J_{03\nu}^2 + J_{10\nu}^2 + J_{11\nu}^2 + J_{12\nu}^2 + J_{13\nu}^2 \\
&\quad + J_{20\nu}^2 + J_{21\nu}^2 + J_{22\nu}^2 + J_{23\nu}^2 + J_{30\nu}^2 + J_{31\nu}^2 + J_{32\nu}^2 + J_{33\nu}^2)) \\
J_{01\nu} = -8(&b_0(2J_{00\nu}J_{01\nu} + 2J_{10\nu}J_{11\nu} + 2J_{20\nu}J_{21\nu} + 2J_{30\nu}J_{31\nu}) \\
&+ b_1(J_{00\nu}^2 + J_{01\nu}^2 - J_{02\nu}^2 - J_{03\nu}^2 + J_{10\nu}^2 + J_{11\nu}^2 - J_{12\nu}^2 - J_{13\nu}^2 \\
&\quad + J_{20\nu}^2 + J_{21\nu}^2 - J_{22\nu}^2 - J_{23\nu}^2 + J_{30\nu}^2 + J_{31\nu}^2 - J_{32\nu}^2 - J_{33\nu}^2)) \\
J_{02\nu} = -8(&b_0(2J_{00\nu}J_{02\nu} + 2J_{10\nu}J_{12\nu} + 2J_{20\nu}J_{22\nu} + 2J_{30\nu}J_{32\nu}) \\
&+ b_1(2J_{01\nu}J_{02\nu} + 2J_{11\nu}J_{12\nu} + 2J_{21\nu}J_{22\nu} + 2J_{31\nu}J_{32\nu})) \\
J_{03\nu} = -8(&b_0(2J_{00\nu}J_{03\nu} + 2J_{10\nu}J_{13\nu} + 2J_{20\nu}J_{23\nu} + 2J_{30\nu}J_{33\nu}) \\
&+ b_1(2J_{01\nu}J_{03\nu} + 2J_{11\nu}J_{13\nu} + 2J_{21\nu}J_{23\nu} + 2J_{31\nu}J_{33\nu}))
\end{aligned}
$$

$\boxed{\mu = 1}$

$$
\begin{aligned}
J_{100} &= 8b_1(-J_{230}J_{320} - 3J_{23\nu}J_{32\nu} + J_{220}J_{330} + 3J_{22\nu}J_{33\nu}) \\
J_{10\nu} &= -8(b_0(2J_{00\nu}J_{10\nu} + 2J_{01\nu}J_{11\nu} + 2J_{02\nu}J_{12\nu} + 2J_{03\nu}J_{13\nu}) \\
&\quad + b_1(2J_{01\nu}J_{10\nu} + 2J_{00\nu}J_{11\nu} + J_{23\nu}J_{320} + J_{230}J_{32\nu} - J_{22\nu}J_{330} - J_{220}J_{33\nu})) \\
J_{110} &= 8b_0(J_{230}J_{320} + 3J_{23\nu}J_{32\nu} - J_{220}J_{330} - 3J_{22\nu}J_{33\nu}) \\
J_{11\nu} &= -8(b_1(2J_{00\nu}J_{10\nu} + 2J_{01\nu}J_{11\nu} - 2J_{02\nu}J_{12\nu} - 2J_{03\nu}J_{13\nu}) \\
&\quad + b_0(2J_{01\nu}J_{10\nu} + 2J_{00\nu}J_{11\nu} - J_{23\nu}J_{320} - J_{230}J_{32\nu} + J_{22\nu}J_{330} + J_{220}J_{33\nu})) \\
J_{120} &= 8(b_1(-J_{230}J_{300} - 3J_{23\nu}J_{30\nu} + J_{200}J_{330} + 3J_{20\nu}J_{33\nu}) \\
&\quad + b_0(-J_{230}J_{310} - 3J_{23\nu}J_{31\nu} + J_{210}J_{330} + 3J_{21\nu}J_{33\nu})) \\
J_{12\nu} &= -8(b_1(2J_{02\nu}J_{11\nu} + 2J_{01\nu}J_{12\nu} + J_{23\nu}J_{300} + J_{230}J_{30\nu} - J_{20\nu}J_{330} - J_{200}J_{33\nu}) \\
&\quad + b_0(2J_{02\nu}J_{10\nu} + 2J_{00\nu}J_{12\nu} + J_{23\nu}J_{310} + J_{230}J_{31\nu} - J_{21\nu}J_{330} - J_{210}J_{33\nu})) \\
J_{130} &= -8(b_1(-J_{220}J_{300} - 3J_{22\nu}J_{30\nu} + J_{200}J_{320} + 3J_{20\nu}J_{32\nu}) \\
&\quad + b_0(-J_{220}J_{310} - 3J_{22\nu}J_{31\nu} + J_{210}J_{320} + 3J_{21\nu}J_{32\nu})) \\
J_{13\nu} &= -8(b_1(2J_{03\nu}J_{11\nu} + 2J_{01\nu}J_{13\nu} - J_{22\nu}J_{300} - J_{220}J_{30\nu} + J_{20\nu}J_{320} + J_{200}J_{32\nu}) \\
&\quad + b_0(2J_{03\nu}J_{10\nu} + 2J_{00\nu}J_{13\nu} - J_{22\nu}J_{310} - J_{220}J_{31\nu} + J_{21\nu}J_{320} + J_{210}J_{32\nu}))
\end{aligned}
$$

$\boxed{\mu = 2}$

$$
\begin{aligned}
J_{200} &= 8b_1(J_{130}J_{320} + 3J_{13\nu}J_{32\nu} - J_{120}J_{330} - 3J_{12\nu}J_{33\nu}) \\
J_{20\nu} &= -8(b_0(2J_{00\nu}J_{20\nu} + 2J_{01\nu}J_{21\nu} + 2J_{02\nu}J_{22\nu} + 2J_{03\nu}J_{23\nu}) \\
&\quad + b_1(2J_{01\nu}J_{20\nu} + 2J_{00\nu}J_{21\nu} - J_{13\nu}J_{320} - J_{130}J_{32\nu} + J_{12\nu}J_{330} + J_{120}J_{33\nu})) \\
J_{210} &= 8b_0(-J_{130}J_{320} - 3J_{13\nu}J_{32\nu} + J_{120}J_{330} + 3J_{12\nu}J_{33\nu}) \\
J_{21\nu} &= -8(b_1(2J_{00\nu}J_{20\nu} + 2J_{01\nu}J_{21\nu} - 2J_{02\nu}J_{22\nu} - 2J_{03\nu}J_{23\nu}) \\
&\quad + b_0(2J_{01\nu}J_{20\nu} + 2J_{00\nu}J_{21\nu} + J_{13\nu}J_{320} + J_{130}J_{32\nu} - J_{12\nu}J_{330} - J_{120}J_{33\nu})) \\
J_{220} &= -8(b_1(-J_{130}J_{300} - 3J_{13\nu}J_{30\nu} + J_{100}J_{330} + 3J_{10\nu}J_{33\nu}) \\
&\quad + b_0(-J_{130}J_{310} - 3J_{13\nu}J_{31\nu} + J_{110}J_{330} + 3J_{11\nu}J_{33\nu})) \\
J_{22\nu} &= -8(b_1(2J_{02\nu}J_{21\nu} + 2J_{01\nu}J_{22\nu} - J_{13\nu}J_{300} - J_{130}J_{30\nu} + J_{10\nu}J_{330} + J_{100}J_{33\nu}) \\
&\quad + b_0(2J_{02\nu}J_{20\nu} + 2J_{00\nu}J_{22\nu} - J_{13\nu}J_{310} - J_{130}J_{31\nu} + J_{11\nu}J_{330} + J_{110}J_{33\nu})) \\
J_{230} &= 8(b_1(-J_{120}J_{300} - 3J_{12\nu}J_{30\nu} + J_{100}J_{320} + 3J_{10\nu}J_{32\nu}) \\
&\quad + b_0(-J_{120}J_{310} - 3J_{12\nu}J_{31\nu} + J_{110}J_{320} + 3J_{11\nu}J_{32\nu})) \\
J_{23\nu} &= -8(b_1(2J_{03\nu}J_{21\nu} + 2J_{01\nu}J_{23\nu} + J_{12\nu}J_{300} + J_{120}J_{30\nu} - J_{10\nu}J_{320} - J_{100}J_{32\nu}) \\
&\quad + b_0(2J_{03\nu}J_{20\nu} + 2J_{00\nu}J_{23\nu} + J_{12\nu}J_{310} + J_{120}J_{31\nu} - J_{11\nu}J_{320} - J_{110}J_{32\nu}))
\end{aligned}
$$

$\boxed{\mu = 3}$

$$
\begin{aligned}
J_{300} &= 8b_1(-J_{130}J_{220} - 3J_{13\nu}J_{22\nu} + J_{120}J_{230} + 3J_{12\nu}J_{23\nu}) \\
J_{30\nu} &= -8(b_1(J_{13\nu}J_{220} + J_{130}J_{22\nu} - J_{12\nu}J_{230} - J_{120}J_{23\nu} + 2J_{01\nu}J_{30\nu} + 2J_{00\nu}J_{31\nu}) \\
&\quad + b_0(2J_{00\nu}J_{30\nu} + 2J_{01\nu}J_{31\nu} + 2J_{02\nu}J_{32\nu} + 2J_{03\nu}J_{33\nu})) \\
J_{310} &= 8b_0(J_{130}J_{220} + 3J_{13\nu}J_{22\nu} - J_{120}J_{230} - 3J_{12\nu}J_{23\nu}) \\
J_{31\nu} &= -8(b_0(-J_{13\nu}J_{220} - J_{130}J_{22\nu} + J_{12\nu}J_{230} + J_{120}J_{23\nu} + 2J_{01\nu}J_{30\nu} + 2J_{00\nu}J_{31\nu}) \\
&\quad + b_1(2J_{00\nu}J_{30\nu} + 2J_{01\nu}J_{31\nu} - 2J_{02\nu}J_{32\nu} - 2J_{03\nu}J_{33\nu})) \\
J_{320} &= 8(b_1(-J_{130}J_{200} - 3J_{13\nu}J_{20\nu} + J_{100}J_{230} + 3J_{10\nu}J_{23\nu}) \\
&\quad + b_0(-J_{130}J_{210} - 3J_{13\nu}J_{21\nu} + J_{110}J_{230} + 3J_{11\nu}J_{23\nu})) \\
J_{32\nu} &= -8(b_0(J_{13\nu}J_{210} + J_{130}J_{21\nu} - J_{11\nu}J_{230} - J_{110}J_{23\nu} + 2J_{02\nu}J_{30\nu} + 2J_{00\nu}J_{32\nu}) \\
&\quad + b_1(J_{13\nu}J_{200} + J_{130}J_{20\nu} - J_{10\nu}J_{230} - J_{100}J_{23\nu} + 2J_{02\nu}J_{31\nu} + 2J_{01\nu}J_{32\nu})) \\
J_{330} &= -8(b_1(-J_{120}J_{200} - 3J_{12\nu}J_{20\nu} + J_{100}J_{220} + 3J_{10\nu}J_{22\nu}) \\
&\quad + b_0(-J_{120}J_{210} - 3J_{12\nu}J_{21\nu} + J_{110}J_{220} + 3J_{11\nu}J_{22\nu})) \\
J_{33\nu} &= -8(b_0(-J_{12\nu}J_{210} - J_{120}J_{21\nu} + J_{11\nu}J_{220} + J_{110}J_{22\nu} + 2J_{03\nu}J_{30\nu} + 2J_{00\nu}J_{33\nu}) \\
&\quad + b_1(-J_{12\nu}J_{200} - J_{120}J_{20\nu} + J_{10\nu}J_{220} + J_{100}J_{22\nu} + 2J_{03\nu}J_{31\nu} + 2J_{01\nu}J_{33\nu}))
\end{aligned}
$$

Appendix D

Example C Program to Integrate the the Flow Equations

```
#include <stdio.h>
#include <math.h>

int
main (void)                                                    main
{

  double J0, b0, b1, J0n, J10, J1n, Jp0, Jpn, J01n, J100, J10n, TK0;

  double l, dl, dJ0n, dJ10, dJ1n, dJp0, dJpn, dJ01n, dJ100, dJ10n, lerror, A;  10

  double error;

  int first = 1;

  int n;

  J0 = 0.05;

  // init                                                        20
  b0 = 0.5;

  A = 8.0;
```

```
for (b1 = 0.0; b1 < 0.4999; b1 = b1 + 0.001)
  {
    n = 0;

    J0n = J0;
    J10 = J0;
    J1n = J0;
    Jp0 = J0;
    Jpn = J0;
    J01n = 0;
    J100 = 0;
    J10n = 0;

    l = 0.0;
    error = 1E3;
    lerror = 1E−10;
    dl = 1E−5;
    while (dl > lerror)
      {
      again:

        dJ0n =
          A * (b1 * (2 * J0n * J01n + 2 * J1n * J10n) +
               b0 * (J0n * J0n + J1n * J1n + 2 * Jpn * Jpn + J01n * J01n +
                     J10n * J10n)) * dl;
        dJ10 = A * b0 * (Jp0 * Jp0 + 3 * Jpn * Jpn) * dl;
        dJ1n =
          A * (b1 * (2 * J1n * J01n + 2 * J0n * J10n) +
               b0 * (2 * J0n * J1n + 2 * Jp0 * Jpn + 2 * J01n * J10n)) * dl;
        dJp0 =
          A * (b0 * (J10 * Jp0 + 3 * J1n * Jpn) +
               b1 * (Jp0 * J100 + 3 * Jpn * J10n)) * dl;
        dJpn =
          A * (b0 * (J1n * Jp0 + 2 * J0n * Jpn + J10 * Jpn) +
               b1 * (2 * Jpn * J01n + Jpn * J100 + Jp0 * J10n)) * dl;
        dJ01n =
          A * (b0 * (2 * J0n * J01n + 2 * J1n * J10n) +
               b1 * (J0n * J0n + J1n * J1n − 2 * Jpn * Jpn + J01n * J01n +
                     J10n * J10n)) * dl;
        dJ100 = −A * b1 * (Jp0 * Jp0 + 3 * Jpn * Jpn) * dl;
        dJ10n =
```

```
            A * (b0 * (2 * J1n * J01n + 2 * J0n * J10n) +
                 b1 * (2 * J0n * J1n - 2 * Jp0 * Jpn + 2 * J01n * J10n)) * dl;

          if ((fabs (dJ0n) > error) || (fabs (dJ10) > error)
              || (fabs (dJ1n) > error) || (fabs (dJp0) > error)                    70
              || (fabs (dJpn) > error) || (fabs (dJ10n) > error)
              || (fabs (dJ100) > error) || (fabs (dJ10n) > error))
            {
              dl = dl / 2;
              goto again;
            }

          if (dl < lerror)
            {
              if (first == 1)                                                      80
                {
                  TK0 = exp (-J0 * l);
                  first = 0;
                }

              printf
                ("%f\t%f\t%f\t%f\t%f\t%f\t%f\t%d\t%f\t%f\t%f\t%f\t%f\t%f\t%f\t%f\t%f\n",
                 b1, l, J0 * l, exp (-J0 * l), TK0, J0, n, J0n, J10, J1n, Jp0,
                 Jpn, J01n, J100, J10n);
            }                                                                      90

          J0n = J0n + dJ0n;
          J10 = J10 + dJ10;
          J1n = J1n + dJ1n;
          Jp0 = Jp0 + dJp0;
          Jpn = Jpn + dJpn;
          J01n = J01n + dJ01n;
          J100 = J100 + dJ100;
          J10n = J10n + dJ10n;
          l = l + dl;                                                              100

          n++;
        }
    }
  return 0;
}
```

Danksagungen

Mein herzlicher Dank gilt Frau Prof. Dr. Daniela Pfannkuche. Sie nahm sich stets die Zeit meine Fragen ausführlich zu beantworten und motivierte mich Optimismus und der Schaffung eines idealen Arbeitsumfeldes.

Herrn Dr. Alexander Chudnovskiy gilt mein besonderer Dank für die geduldige und intensive Betreuung dieser Arbeit, sowie viele und ausführliche hilfreiche Diskussionen.

Herrn Prof. Dr. Potthoff möchte ich für die freundliche Übernahme des Zweitgutachtens danken.

Allen Mitarbeitern unserer Arbeitsgruppe danke ich für ein angenehmes Arbeitsklima: Besonders genannt seien hier Daniel Becker, mit dem ich das Mathematica-Programm zusammen entwickelt habe, Frank Deuretzbacher und Karel Vyborny für inspirierende Diskussionen und das Korrekturlesen dieser Arbeit. Für Korrekturen danke ich ebenfalls Yvette Salthouse.

Schließlich danke ich meiner Familie und Katrin Malessa für die Unterstützung und den Rückhalt.

Bibliography

[1] W. J. de Haas, J. de Boer, and G. van de Berg, Physica **1** (1934).

[2] J. Kondo, Progress of Theoretical Physics **32**, 37 (1964).

[3] P. W. Anderson, Phys. Rev. **124**, 41 (1961).

[4] J. R. Schreiffer and P. A. Wolff, Phys. Rev. **149**, 491 (1966).

[5] P. Anderson, J. Phys. C: Solid St. Phys. **3**, 2436 (1970).

[6] F. D. M. Haldane, Phys. Rev. Lett. **40**, 416 (1978).

[7] D. Goldhaber-Gordon *et al.*, Nature **391**, 156 (1998).

[8] S. M. Cronenwetta, T. H. Oosterkamp, and L. P. Kouwenhoven, Science **281**, 540 (1998).

[9] A. A. Abrikosov, *Fundamentals Of The Theory Of Metals* (North-Holland, 1987).

[10] A. A. Abrikosov, Physics **2**, 5 (1965).

[11] K. Wilson, Rev. Mod. Phys. **47**, 773 (1975).

[12] J. Nygård, D. H. Cobden, and P. E. Lindelof, Nature **408**, 342 (2000).

[13] W. Liang, M. P. Shores, M. Bockrath, J. R. Long, and H. Park, Nature **417**, 725 (2002).

[14] S. Sasaki, S. Amaha, N. Asakawa, M. Eto, and S. Tarucha, Phys. Rev. Lett. **93**, 017205.

[15] M. Pustilnik, Y. Avishai, and K. Kikoin, Phys. Rev. Lett **84**, 1756 (2000).

[16] M. Eto and Y. V. Nazarov, Phys. Rev. Lett **85**, 1306 (2000).

[17] U. Wilhelm, J. Schmid, J. Weis, and K. v. Klitzing, Physica E **14**, 385.

[18] P. Jarillo-Herrero *et al.*, Nature **404**, 484 (2005).

[19] G. Zaránd, A. Brataas, and D. Goldhaber-Gordon, Solid State Commun. **126**, 466.

[20] M. M. Y. Q. Li, D. Shi, and F. Zhang, Phys. Rev. Lett **81**, 3527.

[21] G. Zaránd, Phys. Rev. B **52** (1995).

[22] L. Borda, G. Zarand, W. Hofstetter, B. I. Halperin, and J. von Delft, Phys. Rev. Lett **90**, 026602 (2003).

[23] M.-S. Choi, R. Lopez, and R. Aguado, Phys. Rev. Lett. **95**, 067204 (2005).

[24] A. W. Holleitner, R. H. Blick, A. K. Huettel, K. Eberl, and J. P. Kotthaus, Science **297**, 70 (2002).

[25] A. W. Holleitner, A. Chudnovskiy, D. Pfannkuche, K. Eberl, and R. H. Blick, Phys. Rev. B **70**, 075204 (2004).

[26] R. López *et al.*, Phys. Rev. B **71**, 115312 (2005).

[27] D. Bezecny, Pseudo-spin kondo effect in a double quantum dot system, Master's thesis, Universität Hamburg, 2005.

[28] M. Kiselev, H. Feldman, and R. Opperman, Eur. Phys. J. B **22**, 53 (2001).

[29] V. Popov and D. Fedotov, Zh. Eksp. Teor. Fiz **94**, 138 (1988).

[30] D. Jacob, B. Wunsch, and D. Pfannkuche, Phys. Rev. B **70**, 081314 (2004).

[31] A. Kamenev, Many-body theory of non-equilibrium systems, in *Les Houches Summer School on Nanoscopic Quantum Transport*, pp. 1–70, 2005, arXiv:cond-mat/0412296.